

UCSF

UC San Francisco Electronic Theses and Dissertations

Title

Serotonergic modulation of fast-spiking interneurons in medial prefrontal cortex

Permalink

<https://escholarship.org/uc/item/3833j8dd>

Author

Athilingam, Jegath

Publication Date

2018

Peer reviewed|Thesis/dissertation

**Serotonergic modulation of fast-spiking
interneurons in medial prefrontal cortex**

by

Jegath Athilingam

DISSERTATION

Submitted in partial satisfaction of the requirements for the degree of

DOCTOR OF PHILOSOPHY

In

Neuroscience

in the

GRADUATE DIVISION

of the

Copyright 2018

by

Jegath Athilingam

DEDICATIONS AND ACKNOWLEDGEMENTS

I have such enormous gratitude for the people in my life that have supported me along the journey to earning my doctoral degree. First and foremost, I was privileged to have not one but two brilliant mentors - Dr. Vikaas Sohal and Dr. Kevin Bender. I cannot thank Vikaas and Kevin enough for allowing me to pursue a project of my own design and follow it wherever it took me. Some people would never sign up to have two different bosses to please but I would not have had it any other way. Vikaas has the brilliant ability to both break down seemingly large tasks into their simple components while also continually keeping in mind how scientific findings fit into the larger base of literature. As a psychiatrist, he also possesses magical powers to make graduate students feel better when their experiments fail. From Kevin's mentorship, I learned scientific rigor and the importance of paying attention to detail. His constant encouragement and enthusiasm for my project was invaluable to my success and his lighthearted and approachable nature made the whole experience enjoyable. I would also like to thank the other members of my thesis committee, Dr. Alexandra Nelson and Dr. Massimo Scanziani, for their invaluable feedback, insight, and understanding throughout my graduate school career and also Pat Veitch and Lucita Nacionales, the neuroscience program administrative rock stars who were always just an email away.

Due to being a part of two labs, I also had the pleasure of having double the number of awesome labmates! The Bender Lab's tight knit lab culture was one of the most supportive work environments I could imagine working in. I would particularly like to thank Ken Burke, a fellow grad student who I have sometimes jokingly referred to as my third PI as he has always been there to dive deep into conversations about my

project and offer feedback and ideas. Our postdoctoral fellow, Roy Ben-Shalom also deserves recognition for training me in computational modeling and for being a generally warm presence in the lab. I'd also like to thank Perry Spratt for saving me hours of labor in manually scoring mouse behavior by letting me use his nifty MATLAB program and also for his sweet companionship through my PhD. The Sohal lab has also been such a fun-loving place to work. From happy hours to march madness competitions to lab olympics, it was so nice to have some play to balance out the work. I would particularly like to thank Sarah Robinson and Margaret Cunniff, who started in the Sohal lab around the same time as me and have been great buddies throughout my time there. I would also like to recognize Dr. Celia Kjaerby, my fellow Serotonin Superstar, with whom I worked on Chapter 3 of this dissertation, and Dr. Audrey Brumback, another postdoctoral fellow who was always there to lend an ear and give me advice. Of course no labs run without amazing lab managers - Tosha Patel and Caroline Keeshen also deserve a word of thanks for always making sure I had mice and supplies to get my work done.

I'm also grateful to have gone through this graduate school journey with such an amazing cohort of classmates. I'd particularly like to shout out the absolutely amazing lady scientists in my class - Yelena Kulik, Ally Girasole, Margaret Cunniff, Claire Tang, Racheli Wer Berger, Jenna Whippen, and Alex Clemente - and Ryan Morrill, who has always been a close friend and great concert buddy. A word of recognition also goes to the program cohort two years senior to me who started graduate school when I was a lab tech and always made me feel like an adopted member of their class.

Outside of graduate school, I have been lucky to have other amazing friends to provide emotional support or a much needed break from the daily grind of doing science. I met Hannah Peckler and Alayna Liptak when we were all lab technicians at the Gallo Research Center before I started graduate school and they have seriously been my rock throughout grad school - I genuinely don't know what I would have done without my almost-daily lunches with Alayna or our regular trio hangouts. They are some of the most supportive and loving women I have ever met and I am so lucky to have them in my life. I am also convinced that I have the best group of college friends that could possibly exist and want to thank them for always staying in touch, coming to friend reunions, and making time in their lives to attend my thesis defense - Lisa Eash, Ravdeep Jaidka, Chelsea Bokman, Gabe Sulkes, Tracey Geronimo, Laura Gomez-Nichols, Geoff Squire. I also want to thank Kathryn "Scoob" Mulholland, my former roomie and fellow dog mom, for being hands down the best thing I've ever found on craigslist.

Of course, I also have to thank my family for their continued support throughout my entire life. My brothers, Paul and Bala Athilingam, have always believed in me even when I have been unsure about my future and should take credit for introducing me to craft beers. The biggest thank you of them all goes to my parents for bringing me to America when I was just a tiny baby. My entire life, they have told me that they brought me here for a better life and, most importantly, a chance to have good education. I know that by accomplishing my doctorate, I have fulfilled their highest hopes and dreams. I specifically want to further acknowledge my mom, Ponrathi Athilingam, who has been a role model and inspiration to me my entire life. She grew up in poverty in India at a time

when girls were not really allowed to pursue education. Nevertheless, she persisted, went to school, and now has attained many higher education degrees. Her story continues to inspire me I will always strive to be as loving, dedicated, driven, and passionate as she is. She has always pushed me to be the best that I can be and is, quite honestly, the best mom that anyone could ever hope for.

And finally, I cannot overstate my gratitude for my partner, Kyle Geronimo, and our sweet dog, Wolfgang. First my roommate and then my partner, Kyle has been by my side from the very beginning of this whole doctoral journey - from studying for the GRE and submitting applications to rotations, grant applications, my qualifying exam, failed experiments, both good and bad paper reviews, paper publishing, and finally now my graduation. He's been there to celebrate every mile stone and to listen to me whine about every setback. He has been patient through late work nights and I know it cannot have been easy to date a super busy graduate student. Most importantly, he has always been there to bring levity and laughter to my life and to be my adventure buddy. Lastly, I have to shout out our little fluffball, Wolfgang. His silly little personality and cuddly friendship has been a constant source of stress relief and joy throughout graduate school.

AUTHOR CONTRIBUTIONS

The text of Chapter 2 of this thesis is largely a reprint of the material as it originally appeared in eLife (Athilingam et al., 2017). Jegath Athilingam, with guidance from co-mentors Vikaas Sohal and Kevin Bender, designed the experiments. Jegath Athilingam performed most of the experiments except for immunohistochemistry, which was performed by Caroline Keeshen, and the iontophoresis and glutamate uncaging experiments, which were performed with assistance from Kevin Bender. Computational modeling was performed by Jegath Athilingam analyzed and visualized all data and wrote the initial manuscript draft. Vikaas Sohal and Kevin bender helped revise the manuscript and supervised the entire project.

The text of Chapter 3 of this thesis is largely a reprint of the material as it originally appeared in Cell Reports (Kjaerby, Athilingam et al., 2016). Celia Kjaerby and Vikaas Sohal designed experiments and wrote the manuscript. Jegath Athilingam measured postsynaptic effects of the 5HT1B agonist CP 93129 and assisted with experiments measuring the effects of CP 93129 on prefrontal LFP. Celia Kjaerby performed most other experiments except for strontium experiments (performed by Sarah Robinson) and control (no drug) experiments for callosal inputs (Jillian lafrati). Celia Kjaerby analyzed and visualized all data.

The text of Chapters 4 and 5 is unpublished and contains preliminary data collected, analyzed, and visualized by Jegath Athilingam. Kevin Bender and Vikaas Sohal supervised the projects in these chapters.

The text of Chapter 6 of this thesis is largely a reprint of the material as it originally appeared in ACS Chemical Neuroscience (Cabrera et al., 2017). Ricardo

Cabrero and Beatrice Garcia-Acosta synthesized the chemical with help from Roberto Etchenique. Jegath Athilingam performed electrophysiological experiments with supervision from Kevin Bender and Kira Poskanzer. All authors analyzed data and helped to write the manuscript.

References

Athilingam, J., Ben-Shalom, R., Keeshen, C., Sohal, V.S., Bender, K.J. 2017. Serotonin enhances excitability and gamma frequency temporal integration in prefrontal fast-spiking interneurons. *eLife*.

Cabrera, R., Filevich, O., Acosta, B. G., Athilingam, J., Bender, K. J., Poskanzer, K. E., et al. (2017). A visible light-sensitive caged serotonin. *ACS Chemical Neuroscience*, 8(5), 1036-1042.

Kjaerby, C., Athilingam, J., Robinson, S. E., lafrati, J., & Sohal, V. S. (2016). Serotonin 1B receptors regulate prefrontal function by gating callosal and hippocampal inputs. *Cell Reports*, 17(11), 2882-2890.

ABSTRACT

The prefrontal cortex (PFC) functions to integrate information from the internal and external world in order to flexibly guide behavior. As the most recently evolved brain region, the PFC is implicated in a range of psychiatric disorders such as depression, anxiety, and schizophrenia. The circuitry within the PFC consists of a diversity of excitatory and inhibitory neurons and each neuronal subtype represents a unique locus for action by neuromodulators, such as dopamine and serotonin. The serotonergic system is heavily implicated in mood and emotion and is the target of many modern psychiatric drugs. Despite this, we have a limited understanding of the actions of serotonin on the diverse cell types in the PFC. In this dissertation, I describe the actions of serotonin (5HT) on interneurons and excitatory inputs arriving from discrete brain regions and suggest how this may relate to behavior and disease. I find that 5HT increases the excitability of fast-spiking interneurons but not somatostatin-expressing interneurons by reducing conductance through potassium channels, leading to enhanced summation of gamma frequency inputs. Furthermore, this causes an increase in gamma-frequency inhibitory events in downstream pyramidal cells, a finding which may contribute to my observation that serotonergic signaling reduces low frequency oscillatory power without changing in gamma power *in vivo*. I also describe how serotonin may act at multiple loci within the prefrontal circuit to reduce anxiety behavior. By both presynaptically suppressing ventral hippocampal inputs and increasing inhibition, 5HT may reduce theta oscillations and attenuate anxiety behavior. These findings may have wide implications for our understanding of psychiatric disorders.

TABLE OF CONTENTS

1. Introduction.....	1
1.1 The prefrontal cortex is critical for cognition	1
1.2 Diversity of cell types in the prefrontal cortical circuit	1
1.3 Role of fast-spiking interneurons in mediating prefrontal network activity	3
1.4 Modulation of prefrontal behaviors and circuitry by serotonin	4
1.5 Prefrontal serotonin and interneurons in psychiatric disorders.....	5
1.6 References	8
2. Serotonin enhances excitability and gamma frequency temporal integration in prefrontal fast-spiking interneurons	12
2.1 Abstract	12
2.2 Introduction.....	12
2.3 Methods.....	14
2.31 Electrophysiology.....	14
2.32 Viral injection for expression of ChR2 or fluorescent reporter	16
2.33 ChR2 stimulation	17
2.34 Electrical stimulation	17
2.35 Two-photon imaging, glutamate uncaging, and 5HT iontophoresis..	17
2.36 Computational Modeling	19
2.37 Immunohistochemistry	20
2.38 Statistical Analysis	21
2.4 Results.....	21
2.41 Activating 5HT _{2A} receptors increases FSI intrinsic excitability	21
2.42 5HT decreases inward-rectifying potassium channel function.....	24
2.43 5HT enhances the temporal integration of inputs at gamma frequencies	28
2.44 Computational models reproduce frequency-specific enhancement of summation by 5HT.....	29
2.45 FSIs preferentially spike in response to gamma frequency inputs with 5HT.....	31
2.5 Discussion	33

2.51 5HT increases FSI excitability by altering intrinsic properties.....	33
2.52 5HT promotes temporal summation of inputs arriving at gamma frequency by prolonging EPSP decay	34
2.53 Implications for serotonergic regulation of prefrontal circuit activity .	35
2.54 Clinical Relevance	37
2.6 Figures.....	38
2.7 References	56
3. Serotonin 1B Receptors Regulate Prefrontal Function by Gating Callosal and Hippocampal Inputs.....	61
3.1 Abstract	61
3.2 Introduction.....	61
3.3 Methods.....	65
3.31 Slice electrophysiology and optogenetics.....	65
3.32 Drug infusion.....	66
3.33 Local field potential recording	66
3.34 Behavior.....	66
3.4 Results.....	67
3.41 Serotonin suppresses synaptic input to prefrontal pyramidal neurons in a projection-specific manner	67
3.42 Serotonin suppresses synaptic input through the 5-HT1B receptor .	68
3.43 Serotonin suppresses synaptic input via presynaptic inhibition.....	70
3.44 Local infusion of a 5-HT1B receptor agonist into mPFC reduces innate anxiety.....	72
3.45 Local infusion of a 5-HT1B receptor agonist suppresses mPFC theta power	73
3.5 Discussion	74
3.51 Serotonin acts presynaptically through 5-HT1B receptors	74
3.52 Serotonin targets specific cells and synapses within the mPFC.....	75
3.53 Serotonin regulates the flow of anxiety-related information through the mPFC	76
3.6 Conclusion	77

3.7 Figures.....	79
3.8 References	91
4. Input-specific modulation of excitatory synapses onto prefrontal FSIs.....	96
4.1 Introduction.....	96
4.2 Methods.....	97
4.21 Electrophysiology.....	97
4.22 Viral injection for expression of ChR2.....	98
4.23 ChR2 stimulation	99
4.3 Results.....	99
4.31 5HT suppresses callosal and hippocampal inputs to FSIs presynaptically	99
4.32 5HT increases FSI firing in response to all inputs	100
4.4 Discussion	101
4.5 Figures.....	102
4.6 References	104
5. Serotonergic modulation of prefrontal oscillations and behavior.....	105
5.1 Introduction.....	105
5.2 Methods.....	106
5.21 Stereotaxic surgery for viral injections and implants.....	106
5.22 In vivo DREADD activation	108
5.23 Photometry recording and analysis	108
5.24 Local field potential recording and analysis	109
5.25 Behavioral assays.....	109
5.3 Results.....	111
5.31 Gq activation in FSIs increases FSI activity.....	111
5.32 Gq activation in FSIs attenuates power of low-frequency oscillations	112
5.33 Gq activation in FSIs rescues cognitive flexibility deficits in mice that model key aspects of schizophrenia	112
5.34 Gq activation in FSIs increases novel object exploration time and reduces immobility in forced swim test	113

5.4 Discussion	114
5.41 Serotonergic effects increase FSI activity in vivo and reduce the power of low-frequency oscillations while leaving gamma power intact .	114
5.42 Serotonergic effects in FSIs may rescue cognitive flexibility deficits in a mouse model of schizophrenia	115
5.43 Serotonergic effects in FSIs may mediate anxiety behavior	115
5.5 Figures.....	117
5.6 References	121
6. A visible light-sensitive caged serotonin.....	123
6.1 Abstract	123
6.2 Introduction	123
6.3 Methods	126
6.31 Syntheses	126
6.32 Spectroscopic Measurements and Photolysis	127
6.33 Voltammetry	127
6.34 Electrophysiology Slice Preparation	128
6.35 Serotonin Uncaging & Patch Clamp Electrophysiology	128
6.4 Results and Discussion	129
6.5 Conclusion	133
6.6 Figures.....	135
6.7 References	138
7. Concluding remarks.....	143

LIST OF FIGURES

Figure 2.1	Serotonin alters intrinsic properties to increase FSI excitability	38
Figure 2.2	5HT reduces conductance through inward rectifying potassium channels	40
Figure 2.3	Decreasing dendritic K ⁺ conductance elicits change in tau of synaptic responses in a compartmental model	41
Figure 2.4	Local 5HT iontophoresis at FSI dendrites increases FSI firing	42
Figure 2.5	5HT promotes integration of synaptic inputs in a frequency-specific manner	43
Figure 2.6	Modeling indicates that changing tau and reducing K ⁺ conductance can modulate temporal summation	44
Figure 2.7	Mimicking 5HT effects elicits preferential firing to gamma frequency inputs in FSIs.....	45
Figure 2.8	Mimicking 5HT effects in FSIs produces gamma frequency events in pyramidal neurons.....	46
Figure 2.9	Supplement to Figure 1. Modulation of FSI intrinsic properties by 5HT	47
Figure 2.10	Supplement to Figure 1. Dose response for 5HT.....	48
Figure 2.11	Supplement to Figure 1. 5HT does not change membrane potential or input resistance of SOM interneurons	48
Figure 2.12	Supplement to Figure 3. 5HT-induced dendritic depolarization reduces synaptic driving force in compartmental model	49
Figure 2.13	Supplement to Figure 4. Dendritic 5HT iontophoresis depolarizes neuron sufficiently to induce observed change in firing rate.....	50
Figure 2.14	Supplement to Figure 5. Broad 5HT iontophoresis over the slice produces 5HT effects	51
Figure 2.15	Supplement to Figure 6. Model is robust to changes in synaptic parameters	52
Figure 2.16	Supplement to Figure 6. Background synaptic noise does not change summation enhancement	53
Figure 2.17	Supplement to Figure 7. CNO has no effect on FSIs not expressing DREADD.....	54

Figure 2.18 Supplement to Figure 7. 5HT2A agonist increases probability of FSI firing in response to gamma frequency inputs	54
Figure 3.1 Serotonin suppresses afferent input to mPFC layer V pyramidal neurons from the contralateral mPFC and vHPC, but not MD thalamus.....	79
Figure 3.2 Serotonin suppresses callosal and ventral hippocampal input to mPFC through the 5-HT1B receptor.....	81
Figure 3.3 5-HT1B receptors increase the paired pulse ratio and reduce the frequency of asynchronous unitary events elicited by stimulation of callosal or vHPC terminals	83
Figure 3.4 Intra-mPFC infusion of a 5-HT1B receptor agonist reduces innate anxiety and mPFC theta power	85
Figure 3.5 Supplemental Figure. Tetrodotoxin blocks EPSCs induced by Chr2-expressing terminals	86
Figure 3.6 Supplemental Figure. No effect of 5-HT1A or 5-HT7 receptor activation on evoked callosal or ventral hippocampal EPSCs.....	87
Figure 3.7 Supplemental Figure. 5-HT and the 5-HT1B receptor agonist, CP 93129, reduces the frequency of asynchronous unitary events without affecting amplitude, rise time or decay time	88
Figure 3.8 Supplemental Figure. Effect of 5-HT1B receptors on intrinsic properties in layer V pyramidal neurons and on open field enter zone exploration.....	90
Figure 4.1 Serotonin modulates excitatory synapses in a projection-specific Manner	102
Figure 4.2 5HT increases FSI firing in response to synaptic stimulation regardless of input.....	102
Figure 5.1 Chemogenetic activation of Gq-coupled receptors in FSIs increases FSI activity and reduces low frequency oscillations.....	117
Figure 5.2 Gq-DREADD activation could attenuate cognitive flexibility deficits in a mouse model of schizophrenia.....	118
Figure 5.3 Gq-DREADD activation of prefrontal FSIs may reduce anxiety behavior ..	119
Figure 5.4 Gq-DREADD activation of FSIs has no effect on locomotion or social	

Interaction.....	120
Figure 6.1 Coordination reaction schematic.....	126
Figure 6.2 ¹ H-NMR spectra	126
Figure 6.3 Subset of UV-Vis spectra	127
Figure 6.4 Progression of the UV-Vis spectra during a photolysis reaction against absorbed photons.....	127
Figure 6.5 Cyclic voltammogram of [Ru(bpy) ₂ PMe ₃ (5HT)] ²⁺	128
Figure 6.6 Validation of Ruby-5HT in mouse cortical neurons	128

CHAPTER 1 INTRODUCTION

1.1 The prefrontal cortex is critical for cognition

The prefrontal cortex (PFC) is a brain region located in the frontal lobe that is responsible for higher-order cognitive functions, emotional processing, and social cognition. Our earliest observation of prefrontal cortical function was the famous clinical case of Phineas Gage, a railroad worker whose left frontal lobe was destroyed after an explosion caused an iron rod to penetrate his skull. Though Gage apparently recovered and retained most mental faculties such as movement control and normal learning ability, his friends and relatives noticed a marked change in his personality. Once a gentle and responsible man, Gage was now irrational, crude, capricious, and disrespectful (Damasio et al., 1994). The case of Phineas Gage has been supported with numerous other studies suggesting that the PFC is important for coordinating complex goal-directed behaviors such as working memory (Euston et al., 2012), cognitive flexibility (Dias et al., 1996), and emotion regulation (Ray & Zald, 2012). Furthermore, due to its reciprocal connections with essentially all cortical and subcortical structures, the PFC is well poised to function as a master integrator of information and exert 'top down' control over this extensive range of brain processes (Miller, 2000).

1.2 Diversity of cell types in the prefrontal cortical circuit

To achieve these higher order cognitive functions, proper functioning of the prefrontal cortex necessitates the organized activity of many neurons firing together. The local circuitry within the PFC boasts a diversity of different neuronal cell types with

a robust diversity of firing properties and synaptic connections. This complex circuitry facilitates a broad range of neuronal firing patterns that can flexibly mediate this wide range of cognitive behaviors. Most broadly, neurons can be classified by their actions on their downstream synaptic partners. Excitatory neurons release glutamate and depolarize their downstream targets while inhibitory interneurons release GABA and hyperpolarize postsynaptic cells. Both excitatory pyramidal cells and inhibitory GABAergic interneurons come in multiple different flavors. Pyramidal neurons can be broadly divided based on their projection targets into intratelencephalic (IT) neurons that project to other parts of the telencephalon (e.g. cortex, striatum, amygdala) and pyramidal tract (PT) neurons that project subcortically (e.g. thalamus, brain stem, spinal cord) (Harris & Shepherd, 2015).

Approximately 80% of GABAergic interneurons can be classified into three main non-overlapping categories based on their expression of different proteins: parvalbumin (PV), somatostatin (SOM), and vasoactive intestinal peptide (VIP) (Rudy et al., 2011). These interneuron subtypes exhibit distinct firing properties and synaptic connectivity profiles. PV interneurons comprise 40% of all interneurons and exhibit characteristic “fast-spiking” properties (Kawaguchi et al., 1987), resulting in their nickname as fast-spiking interneurons (FSIs). FSIs have a low input resistance, fast membrane time constant, and synapse on the axon initial segment (chandelier cells) or the soma and proximal dendrites (basket cells) of pyramidal neurons. SOM interneurons, which synapse on the distal dendrites of pyramidal neurons, display regular adapting firing patterns and a low-threshold to spike (Rudy et al., 2011). Lastly, VIP interneurons, which often display a bursting firing phenotype followed by depolarization block, are

thought to make synapses on PV and SOM interneurons, mediating a disinhibitory role in the cortical microcircuit (Pi et al., 2013).

1.3 Role of fast-spiking interneurons in mediating prefrontal network activity

Fast-spiking interneurons (FSIs) that express the calcium-binding protein parvalbumin (PV) are the most numerous of interneurons and play a critical role in regulating the network activity of the cortical circuit. With abundant reciprocal connections and highly divergent synapses on the somata of pyramidal cells, FSIs are able to precisely control the timing of spike discharge of large numbers of cortical neurons (Bartos et al., 2007, Busaki & Wang, 2012). Specifically, due to coordinated inhibitory conductances in downstream pyramidal neurons, the spiking of pyramidal neurons is more likely to occur in the period following the offset of inhibition. This population activity can be recorded as oscillations in the local field potential (LFP) and is observed in the gamma frequency range (30-90 Hz). This frequency range emerges due to the ~10-30 ms time constant of GABA-A-mediated inhibition. Critically, this time window also corresponds to the membrane time constant of pyramidal neurons and the time window for synaptic plasticity (Harris et al., 2003). Furthermore, the coordinated synchronous firing of peer pyramidal neurons allows for more efficient discharge of downstream neurons (Busaki & Wang, 2012). This type of network activity, specifically in the gamma frequency range (30-90Hz), has been suggested to be important for information encoding (Buzsaki & Chrobak, 1995) and information transfer (Sohal et al., 2009).

Gamma oscillations are established by FSIs (Cardin et al., 2009), and excitatory inputs that drive spiking in FSIs can trigger gamma rhythms in prefrontal cortex (Sohal

et al., 2009). Synaptic inputs onto FSIs also excite their downstream pyramidal cells, resulting in short latency excitation followed by delayed disynaptic inhibition in those neurons. This feedforward inhibition produces periodic membrane potential fluctuations in principal cells, creating a temporal integration window where inputs arriving within the duration of a gamma cycle are able to summate to produce spiking. Therefore, feedforward inhibition and gamma oscillations promote coincidence detection in pyramidal neurons (Pouille & Scanziani, 2001). Consequently, any manipulation of FSI activity could regulate temporal integration and gamma oscillations. In Chapter 2, I will discuss how simple neuromodulation of FSI passive membrane properties is able to robustly influence synaptic temporal integration. In Chapter 5, I will focus on implications of FSI neuromodulation on prefrontal oscillations and behavior.

1.4 Modulation of prefrontal behaviors and circuitry by serotonin

Due to dense innervation by subcortical afferents from the median and dorsal raphe nuclei (Azmitia & Segal, 1978), prefrontal activity is subject to potent modulation by the neurotransmitter serotonin (5HT). Consistently, serotonergic depletion is known to impair performance in prefrontal-mediated tasks such as reversal learning (Clarke et al., 2004, Clarke et al., 2005), decision-making (Koot et al., 2012), and emotional processing (Robinson et al., 2013). Pharmacological studies have further implicated prefrontal serotonin receptors in working memory (Williams et al., 2002), impulsivity (Carli et al., 2006), and strategy switching (Baker et al., 2011). In Chapter 3, we describe how serotonin may regulate anxiety behavior via presynaptic effects on ventral hippocampal projections to PFC. In Chapter 5, I describe how serotonergic effects in FSIs may play a role in cognitive flexibility and anxiety.

Both fast-spiking interneurons and pyramidal cells in PFC express 5HT receptors, predominantly of the 5HT1A, 5HT2A, and 5HT2C variety (Santana et al., 2004). The 5HT1A receptor is $G_{i/o}$ coupled resulting in neuronal inhibition while the 5HT2 receptors are excitatory through coupling to G_q . Distinct subsets of pyramidal neurons express one or both of the 1A and 2A receptors, leading to inhibition, excitation, or biphasic inhibition and excitation (Avesar & Gullledge, 2012). On the other hand, serotonergic regulation of prefrontal interneurons is less well understood. Some reports indicate that 5HT can increase the frequency of spontaneous inhibitory postsynaptic potentials (Zhou & Hablitz, 1999) and may increase spiking of FSIs (Zhong & Yan, 2011). However, others report distinct subpopulations of FSIs that are excited and inhibited by electrical stimulation of the raphe (Puig et al., 2010). This same group also indicated that systemic 5HT antagonists are able regulate the power of gamma oscillations (Puig et al., 2010). Despite these initial studies, there has been no rigorous and thorough investigation of serotonergic modulation of FSI function in PFC. In Chapter 2, I will thoroughly characterize the effects of 5HT on FSIs. Furthermore, in Chapter 4, I will characterize the effects of 5HT on synaptic inputs from three critical brain regions that project to the PFC: contralateral PFC, mediodorsal (MD) thalamus, and ventral hippocampus (vHPC).

1.5 Prefrontal serotonin and interneurons in psychiatric disorders

Importantly, prefrontal dysfunction is implicated in the etiology of many major psychiatric disorders, such as schizophrenia and depression. Moreover, most effective treatments for these disorders regulate serotonergic transmission. Selective serotonin reuptake inhibitors (SSRIs) remain the most commonly used and effective medicine for

depression and new second-generation antipsychotics block the 5HT2A receptor with high affinity. These drugs tend to produce the best improvement of cognitive symptoms while reducing extrapyramidal side effects (Meltzer & Massey, 2011) and classic hallucinogens such as lysergic acid diethylamide (LSD) actually activate that same receptor (Marek & Aghajanian, 1996).

Notably, impairments in FSI function and gamma rhythms may also be involved in the pathology of schizophrenia (Uhlhaas & Singer, 2010, Lewis et al., 2012, Gonzalez-Burgos et al., 2015). Postmortem studies indicate that patients with schizophrenia have reduced levels of the GABA synthesis enzyme GAD67 in interneurons as well as reduced levels of PV (Hashimoto et al., 2003). With potentially dysfunctional FSIs, it is no surprise that one of the most common biological observations in patients with schizophrenia is a deficit in gamma band oscillatory power (Cho et al., 2003, Minzenberg et al., 2010). Interestingly, increasing prefrontal FSI activity in a mouse model of interneuron dysfunction was able to rescue deficits in both gamma oscillations and cognitive flexibility (Cho et al., 2015).

Despite these clear connections, the relationship between serotonergic signaling in FSIs, prefrontal oscillations, and psychiatric disorders is not currently understood. This work takes critical strides into furthering our understanding of these links. In Chapter 3, we find a link between a subtype of serotonin receptor in PFC and anxiety behavior. In Chapter 5, I suggest that eliciting serotonergic signaling in FSIs may help to rescue cognitive deficits in a mouse model of schizophrenia.

The work in this dissertation aims to examine the role of serotonin signaling in modulating individual neurons and network activity in the prefrontal cortex as it may relate to psychiatric disorders. Chapter 2 deeply investigates the cellular mechanisms of serotonergic modulation of prefrontal FSIs (Athilingam et al., 2017). Using patch-clamp electrophysiology, optogenetics, two-photon microscopy guided glutamate uncaging, and computational modeling, we find that serotonin reduces the conductance of inward-rectifying potassium channels leading to depolarization and increased input resistance and excitability. Furthermore, we find an increase in the decay time of excitatory postsynaptic potentials leading to an enhancement of temporal summation in the gamma frequency range. Finally, we suggest that this enhancement in gamma frequency summation leads to an increased probability of spiking of FSIs in response to gamma frequency inputs and results in gamma frequency inhibition in downstream pyramidal neurons.

The work in Chapter 3 was done largely in collaboration with a postdoctoral fellow in the Sohal lab, Celia Kjaerby and examines the modulation of distinct synaptic inputs onto pyramidal neurons by serotonin (Kjaerby et al., 2016). Dr. Kjaerby found that serotonin suppresses hippocampal and callosal inputs via presynaptic 5HT1B receptors with no effect on thalamic inputs. Together, we discovered that activation of 5HT1B receptors in PFC *in vivo* suppresses anxiety behavior and corresponding theta oscillations.

In Chapter 4, I replicate Dr. Kjaerby's findings in FSIs and show that serotonin reduces hippocampal and callosal inputs while not affecting thalamic inputs. I further demonstrate that despite these presynaptic effects, the postsynaptic depolarization

caused by 5HT in FSIs (characterized in Chapter 2) outweighs presynaptic suppressive effects and results in 5HT eliciting an increase in FSI firing to all inputs.

In Chapter 5, I investigate the effects of serotonergic signaling in FSIs on prefrontal network oscillations and behavior *in vivo*. Specifically, I find that activating serotonergic signaling pathways in FSIs reduces the power of oscillations in all frequency bands except for the gamma frequency range. I also find that this manipulation increases novelty seeking and reduces helplessness behavior in a depression assay. Lastly, I find that this manipulation may be able to rescue deficits in cognitive flexibility in a mouse model of schizophrenia.

In Chapter 6, I helped to validate a novel caged-5HT compound that can be used in future studies to elicit serotonin activation in a temporally controlled manner (Cabrera et al., 2017).

And finally in Chapter 7, I synthesize the findings from this dissertation and draw conclusions as to what this work contributes to the general body of knowledge about how serotonin affects prefrontal circuits and behavior and what questions remain for future study.

1.6 References

Avesar, D., & Gullledge, A. T. (2011). Selective serotonergic excitation of callosal projection neurons. *Frontiers in Neural Circuits*, 6, 12.

Azmitia, E. C., & Segal, M. (1978). An autoradiographic analysis of the differential ascending projections of the dorsal and median raphe nuclei in the rat. *Journal of Comparative Neurology*, 179(3), 641-667.

Baker, P. M., Thompson, J. L., Sweeney, J. A., & Ragozzino, M. E. (2011). Differential effects of 5-HT(2A) and 5-HT(2C) receptor blockade on strategy-switching. *Behavioural Brain Research*, 219(1), 123-131.

Bartos, M., Vida, I., & Jonas, P. (2007). Synaptic mechanisms of synchronized gamma oscillations in inhibitory interneuron networks. *Nature Reviews Neuroscience*, 8(1), 45-56.

Buzsaki, G., & Chrobak, J. J. (1995). Temporal structure in spatially organized neuronal ensembles: A role for interneuronal networks. *Current Opinion in Neurobiology*, 5(4), 504-510.

Buzsaki, G., & Wang, X. (2012). Mechanisms of gamma oscillations. *Neuroscience*,

Cabrera, R., Filevich, O., Acosta, B. G., Athilingam, J., Bender, K. J., Poskanzer, K. E., et al. (2017). A visible light-sensitive caged serotonin. *ACS Chemical Neuroscience*, 8(5), 1036-1042.

Cardin, J. A., Carlan, M., Meletis, K., Knoblich, U., Zhang, F., Deisseroth, K., et al. (2009). Driving fast-spiking cells induces gamma rhythm and controls sensory responses. *Nature*, 459(7247), 663-667.

Carli, M., Baviera, M., Invernizzi, R. W., & Balducci, C. (2006). Dissociable contribution of 5-HT_{1A} and 5-HT_{2A} receptors in the medial prefrontal cortex to different aspects of executive control such as impulsivity and compulsive perseveration in rats. *Neuropsychopharmacology : Official Publication of the American College of Neuropsychopharmacology*, 31(4), 757-767.

Cho, K. A., Hoch, R., Lee, A., Patel, T., Rubenstein, J. R., & Sohal, V. (2015). Gamma rhythms link prefrontal interneuron dysfunction with cognitive inflexibility in *Dlx5/6*^{-/-} mice. *Neuron*, 85(6), 1332-1343.

Cho, R. Y., Konecky, R. O., & Carter, C. S. (2006). Impairments in frontal cortical gamma synchrony and cognitive control in schizophrenia. *Proceedings of the National Academy of Sciences of the United States of America*, 103(52), 19878-19883.

Clarke, H. F., Dalley, J. W., Crofts, H. S., Robbins, T. W., & Roberts, A. C. (2004). Cognitive inflexibility after prefrontal serotonin depletion. *Science (New York, N.Y.)*, 304(5672), 878-880.

Clarke, H. F., Walker, S. C., Crofts, H. S., Dalley, J. W., Robbins, T. W., & Roberts, A. C. (2005). Prefrontal serotonin depletion affects reversal learning but not attentional set shifting. *The Journal of Neuroscience : The Official Journal of the Society for Neuroscience*, 25(2), 532-538.

Damasio, H., Grabowski, T., Frank, R., Galaburda, A., & Damasio, A. (1994). The return of phineas gage: Clues about the brain from the skull of a famous patient. *Science*, 264(5162), 1102-1105.

Dias, R., Robbins, T. W., & Roberts, A. C. (1996). Primate analogue of the Wisconsin card sorting test: Effects of excitotoxic lesions of the prefrontal cortex in the marmoset. *Behavioral Neuroscience*, 110(5), 872-886.

Euston, D. R., Gruber, A. J., & McNaughton, B. L. (2012). The role of medial prefrontal cortex in memory and decision making. *Neuron*, 76(6)

Gonzalez-Burgos, G., Cho, R. Y., & Lewis, D. A. (2015). Alterations in cortical network oscillations and parvalbumin neurons in schizophrenia. *Biological Psychiatry*,

Harris, K. D., Csicsvari, J., Hirase, H., Dragoi, G., & Buzsaki, G. (2003). Organization of cell assemblies in the hippocampus. *Nature*, 424(6948), 552-556.

Harris, K. D., & Shepherd, G. M. G. (2015). The neocortical circuit: Themes and variations. *Nature Neuroscience*, 18(2), 170-181.

Hashimoto, T., Volk, D. W., Eggen, S. M., Mirnics, K., Pierri, J. N., Sun, Z., et al. (2003). Gene expression deficits in a subclass of GABA neurons in the prefrontal cortex of subjects with schizophrenia. *The Journal of Neuroscience : The Official Journal of the Society for Neuroscience*, 23(15), 6315-6326.

Kawaguchi, Y., Katsumaru, H., Kosaka, T., Heizmann, C. W., & Hama, K. (1987). Fast spiking cells in rat hippocampus (CA1 region) contain the calcium-binding protein parvalbumin. *Brain Research*, 416(2), 369-374.

Kjaerby, C., Athilingam, J., Robinson, S. E., Iafrati, J., & Sohal, V. S. (2016). Serotonin 1B receptors regulate prefrontal function by gating callosal and hippocampal inputs. *Cell Reports*, 17(11), 2882-2890.

Koot, S., Zoratto, F., Cassano, T., Colangeli, R., Laviola, G., Bos, R. v. d., et al. (2012). Compromised decision-making and increased gambling proneness following dietary serotonin depletion in rats. *Neuropharmacology*, 62(4), 1640-1650.

Lewis, D. A., Curley, A. A., Glausier, J. R., & Volk, D. W. (2012). Cortical parvalbumin interneurons and cognitive dysfunction in schizophrenia. *Trends in Neurosciences*, 35(1), 57-67.

Marek, G. J., & Aghajanian, G. K. (1996). LSD and the phenethylamine hallucinogen DOI are potent partial agonists at 5-HT_{2A} receptors on interneurons in rat piriform cortex. *The Journal of Pharmacology and Experimental Therapeutics*, 278(3), 1373-1382.

Meltzer, H., & Massey, B. (2011). The role of serotonin receptors in the action of atypical antipsychotic drugs. *Current Opinion in Pharmacology*,

Miller, E. K. (2000). The prefrontal cortex and cognitive control. *Nature Reviews Neuroscience*, 1(1), 59-65.

Minzenberg, M. J., Firl, A. J., Yoon, J. H., Gomes, G. C., Reinking, C., & Carter, C. S. (2010). Gamma oscillatory power is impaired during cognitive control independent of medication status in first-episode schizophrenia. *Neuropsychopharmacology*, 35(13), npp2010150.

Pi, H. J., Hangya, B., Kvitsiani, D., Sanders, J. I., Huang, Z. J., & Kepecs, A. (2013). Cortical interneurons that specialize in disinhibitory control. *Nature*, 503(7477), 521-524.

Pouille, F., & Scanziani, M. (2001). Enforcement of temporal fidelity in pyramidal cells by somatic feed-forward inhibition. *Science (New York, N.Y.)*, 293(5532), 1159-1163.

Puig, M. V., Watakabe, A., Ushimaru, M., Yamamori, T., & Kawaguchi, Y. (2010). Serotonin modulates fast-spiking interneuron and synchronous activity in the rat prefrontal cortex through 5-HT_{1A} and 5-HT_{2A} receptors. *The Journal of Neuroscience*, 30(6), 2211-2222.

Ray, R. D., & Zald, D. H. (2011). Anatomical insights into the interaction of emotion and cognition in the prefrontal cortex. *Neuroscience and Biobehavioral Reviews*, 36(1), 479-501.

Rudy, B., Fishell, G., Lee, S., & Hjerling-Leffler, J. (2011). Three groups of interneurons account for nearly 100% of neocortical GABAergic neurons. *Developmental Neurobiology*, 71(1), 45-61.

Santana, N., Bortolozzi, A., Serrats, J., Mengod, G., & Artigas, F. (2004). Expression of Serotonin_{1A} and Serotonin_{2A} receptors in pyramidal and GABAergic neurons of the rat prefrontal cortex. *Cerebral Cortex*, 14(10), 1100-1109.

Sohal, V. S., Zhang, F., Yizhar, O., & Deisseroth, K. (2009). Parvalbumin neurons and gamma rhythms enhance cortical circuit performance. *Nature*, 459(7247), 698-702.

Uhlhaas, P. J., & Singer, W. (2010). Abnormal neural oscillations and synchrony in schizophrenia. *Nature Reviews Neuroscience*, 11(2), 100-113.

Williams, G., & Rao, S. (2002). The physiological role of 5-HT_{2A} receptors in working memory.

Zhong, P., & Yan, Z. (2011). Differential regulation of the excitability of prefrontal cortical fast-spiking interneurons and pyramidal neurons by serotonin and fluoxetine. *Plos One*, 6(2), e16970.

Zhou, F. M., & Hablitz, J. J. (1999). Activation of serotonin receptors modulates synaptic transmission in rat cerebral cortex. *Journal of Neurophysiology*, 82(6), 2989-2999.

CHAPTER 2

SEROTONIN ENHANCES EXCITABILITY AND GAMMA FREQUENCY TEMPORAL INTEGRATION IN PREFRONTAL FAST-SPIKING INTERNEURONS

2.1 ABSTRACT

The medial prefrontal cortex plays a key role in higher order cognitive functions like decision making and social cognition. These complex behaviors emerge from the coordinated firing of prefrontal neurons. Fast-spiking interneurons (FSIs) control the timing of excitatory neuron firing via somatic inhibition and generate gamma (30-100 Hz) oscillations. Therefore, factors that regulate how FSIs respond to gamma-frequency input could affect both prefrontal circuit activity and behavior. Here, we show that serotonin (5HT), which is known to regulate gamma power, acts via 5HT_{2A} receptors to suppress an inward-rectifying potassium conductance in FSIs. This leads to depolarization, increased input resistance, enhanced spiking, and slowed decay of excitatory postsynaptic potentials (EPSPs). Notably, we found that slowed EPSP decay preferentially enhanced temporal summation and firing elicited by gamma frequency inputs. These findings show how changes in passive membrane properties can affect not only neuronal excitability but also the temporal filtering of synaptic inputs.

2.2 INTRODUCTION

The prefrontal cortex (PFC) organizes higher order cognitive functions ranging from decision making to social cognition (Euston et al., 2012, Dias et al., 1996, Ray and Zald, 2011). These complex behaviors emerge from the coordinated firing of PFC neurons, resulting in neuronal oscillations (Buzsáki and Chrobak, 1995). Synchronized oscillations of neuronal activity in the gamma frequency range (30-100 Hz) play a key

role in information encoding (Buzsáki and Chrobak, 1995) and prefrontal gamma oscillations influence the performance of tasks related to cognitive flexibility and attention (Cho et al., 2015; Kim et al., 2016). The neuromodulator serotonin (5HT) has been shown to regulate gamma power in motor cortex (Puig et al., 2010), suggesting that it could play a role in regulating task-dependent changes in gamma oscillations. Furthermore, neuropsychiatric disease associated with deficits in PFC gamma synchrony, including schizophrenia and depression, are currently treated with medications that have high affinity for serotonin receptors (Meltzer and Massey, 2011). Overall, this suggests that serotonergic modulation of gamma oscillations is important for prefrontal function; however, the cellular mechanisms by which 5HT modulates gamma oscillations remain elusive.

Gamma oscillations are orchestrated by cortical fast-spiking interneurons (FSIs; Cardin et al., 2009; Sohal et al., 2009, Bartos et al., 2007, Bartos et al., 2002, Galarreta and Hestlin, 2001). In contrast to neighboring excitatory cells, FSIs resonate intrinsically in the 30-50 Hz range (Bracci et al., 2003; Fellous et al., 2001; Pike et al., 2000). In turn, FSIs are more likely to generate action potentials in response to gamma-modulated sinusoidal waveforms (Pike et al., 2000), suggesting that action potential generation in FSIs may favor gamma frequency input. This process may be regulated by 5HT. Indeed, 5HT can increase FSI intrinsic excitability, as measured at the soma (Weber and Andrade, 2010; Zhou and Hablitz, 1999; Zhong and Yan, 2011), but whether this also changes how FSIs encode synaptic input is not known.

Here, we used patch clamp electrophysiology, glutamate uncaging, optogenetic stimulation, and compartmental modeling to investigate how serotonergic modulation of

FSIs can regulate the integration of synaptic inputs, particularly at gamma frequencies. We found that 5HT enhances the excitability of FSIs due to a depolarization caused by a suppression of inward-rectifying potassium channels. Furthermore, we found that this reduction of potassium conductance in FSI dendrites increases the time constant of synaptic potentials, leading to a selective enhancement of temporal summation of gamma frequency inputs. This made FSIs more likely to fire action potentials, specifically in response to gamma-frequency inputs, and resulted in more inhibition in the gamma frequency band in downstream pyramidal neurons. These results suggest that 5HT can play a role in modulating prefrontal circuit activity by enhancing the flow of gamma-frequency information through FSIs via modulation of passive membrane properties.

2.3 METHODS

2.31 Electrophysiology

Coronal brain slices (250 μ m) including medial prefrontal cortex were made from adult mice aging 8 weeks or older. We used the following transgenic mouse lines: PV-Cre (RRID: IMSR_JAX:008069), PV-Cre::Ai14 (RRID:MGI:2176738), and SERT-Cre (RRID: IMSR_JAX:014554). All experiments were conducted in accordance with procedures established by the Institutional Animal Care and Use Committee and Laboratory Animal Resource Center at the University of California, San Francisco. Slicing solution was chilled to 4°C and contained (in mM): 234 sucrose, 26 NaHCO₃, 11 glucose, 10 MgSO₄, 2.5 KCl, 1.25 NaH₂PO₄, 0.5 CaCl₂, bubbled with 5% CO₂/ 95% O₂. Slices were incubated in artificial cerebrospinal fluid (aCSF) at 32°C for 30 minutes

and then at room temperature until recording. aCSF contained (in mM): 123 NaCl, 26 NaHCO₃, 11 glucose, 3 KCl, 2 CaCl₂, 1.25 NaH₂PO₄, 1 MgCl₂, also bubbled with 5% CO₂/ 95% O₂.

Neurons were visualized using differential interference contrast or DODT contrast microscopy on an upright microscope (Olympus). Recordings were made using a Multiclamp 700B (Molecular Devices) amplifier and acquired with either pClamp or IgorPro (iontophoresis & uncaging experiments). Patch pipettes (2-5 M Ω tip resistance) were filled with the following (in mM): 130 KGluconate, 10 KCl, 10 HEPES, 10 EGTA, 2 MgCl₂, 2 MgATP, 0.3 Na₃GTP. For some voltage clamp experiments, a cesium based internal solution was used that contained (in mM): 130 CsCH₄O₃S, 4 NaCl, 2 MgCl₂, 10 EGTA, 10 HEPES, 2 MgATP, 0.5 Na₃GTP. For recordings of inhibitory postsynaptic currents (IPSCs) in pyramidal neurons, a high chloride internal solution was used that contained (in mM): 120 CsCl, 15 CsMeSO₄, 8 NaCl, 0.5 EGTA, 10 HEPES, 2 MgATP, 0.5 Na₃GTP. All recordings were made at 32-34°C. Series resistance was compensated in all current clamp experiments and monitored throughout recordings. Recordings were discarded if R_s changed by >25%.

Fast-spiking interneurons were identified by fluorescent visualization of td-Tomato (PV-Cre::Ai14 mice) or mCherry expressed by Cre-dependent viral injection (AAV5-hSyn-DIO-hM3D(Gq)-mCherry or AAV-DJ-Ef1a-DIO-mCherry, PV-Cre mice) or mCherry driven by the Dlx12b enhancer (AAV5-Dlx12b-mCherry, SERT-Cre mice). All bath-applied drugs (Tocris) were dissolved in water (3, 15, 30, or 100 μ M 5HT, 10 μ M CNQX, 100 μ M DL-AP5, 10 μ M gabazine, 1 μ M CNO, 30 μ M α -methyl-5HT, 2 μ M carbachol) or DMSO (1 μ M MDL100907) before being diluted in aCSF. MNI-Glutamate

(2.5 mM) was dissolved directly in aCSF as powder. Alexa 488 (Invitrogen) was dissolved in water and then diluted to 10 μ M in internal solution. For experiments including iontophoresis, the 5HT or vehicle solutions were made to pH = 4.5 using 10N HCl. The experimenter was not blind to pharmacological treatment.

2.32 Viral injection for expression of ChR2 or fluorescent reporter

Viral injections were performed using standard mouse stereotactical methods. Mice were anesthetized for the duration of the surgery using isoflurane gas. After cleaning, an incision was made in the scalp, the skull was leveled, and small burr holes were drilled over the brain region of interest using a dental drill. Virus was injected through the burr holes using a microinjector (WPI) at a speed of 150 nL/minute and the scalp was closed using sutures or tissue adhesive (Vetbond).

For expression of ChR2 in serotonergic neurons, we injected a Cre-dependent ChR2 virus (AAV5-Ef1a-DIO-ChR2-eYFP, 1 μ L) into the dorsal raphe of SERT-Cre mice (>p40) and waited 5-15 months for trafficking of ChR2 to the axon terminals in mPFC. In these mice, we additionally injected an AAV-Dlx12b-mCherry virus (750 nL) into the mPFC one month before patching to label interneurons for easy identification.

For stimulation of synaptic inputs into mPFC using ChR2, we injected a ChR2 virus driven by the CaMKII promoter (AAV5-CaMKII-ChR2-eYFP, 750 nL) unilaterally into PV-Cre::Ai14 mice and patched FSIs in the opposite hemisphere after waiting 4-5 weeks for expression.

For DREADD activation of fast-spiking interneurons, we injected a Cre-dependent virus expressing the Gq-DREADD (AAV-DJ-Ef1a-DIO-hM3D(Gq) -mCherry,

750 nL) or a control fluorophore (AAV-DJ-Ef1a-DIO-mCherry, 750 nL) into PV-Cre+/- mice and patched from fluorescent cells after waiting 5 weeks for expression.

Dorsal raphe injection coordinates were A/P = -4.55, M/L = 0.0, D/V = -3.0. mPFC injection coordinates were A/P = 1.7, M/L = +/- 0.3, D/V = -2.75

2.33 ChR2 stimulation

We stimulated ChR2 in terminals using 5ms flashes of light generated by a Lambda DG-4 (Sutter Instruments) high-speed optical switch with a 300 W Xenon lamp delivered through a 470 nm excitation filter. For stimulation of 5HT terminals, light flashes were delivered at 10 Hz for 10 seconds through a 40x objective. For stimulation of ChR2 from contralateral PFC, we delivered a train of 10 light flashes at 5 Hz.

2.34 Electrical stimulation

mPFC synapses were stimulated using an IsoFLEX stimulator (AMPI, 200 μ s pulse duration) via a bipolar glass stimulation electrode (Sutter) placed within 100 μ m of the patched cell. A two second stimulus train was delivered where stimulus pulses of varying interstimulus intervals (5, 10, 20, 50, 100 ms) were randomly distributed in the train.

2.35 Two-photon imaging, glutamate uncaging, and 5HT iontophoresis

Neurons were visualized using a two-photon imaging system (Bruker) powered by two femtosecond lasers (Coherent, Ultra II) as previously described (Bender and Trussell, 2009). Internal solution was supplemented with 10 μ M Alexa 488 and dendritic

arbors were visualized with an 880 nm excitation source. For local application of 5HT to specific neuronal subcompartments or minimal 5HT application during uncaging experiments, borosilicate pipettes were filled with 200 mM 5HT in H₂O (pH adjusted to 4.5). Scanning interference contrast images of slice morphology and the iontophoretic pipette were acquired with a photomultiplier tube downstream of a 770 nm longpass filter. The iontophoretic pipette was positioned upstream of the application site, relative to the overall flow of extracellular solution, either directly above the slice, near the recorded somata (within 10 μ m) for uncaging experiments, or in proximity to a dendrite (0-15 μ m). 5HT was applied using a 200 nA pulses (40 nA backing current) for 5 seconds (uncaging) or 50 ms (local iontophoresis) using an ION-100 current generator (Dagan).

To activate putative synaptic sites along FSI dendrites, 4-methoxy-7-nitroindolinyll-caged L-glutamate (MNI-glutamate, 2.5 mM, Tocris) was photolyzed using a 720 nm excitation source (0.5 ms duration, power determined empirically to produce 0.5–5 mV EPSPs at the soma). Five uncaging locations were chosen on a single dendrite spaced 1 μ m apart. Glutamate was uncaged at each location individually and then at all locations together in a burst with varying interstimulus intervals (0.12, 5, 10, 20, 50 ms). The sequence of uncaging events always began at the most distal dendritic location, approaching the soma serially. Results were averaged over 4-7 repetitions at each interstimulus interval before and after iontophoretic 5HT application. Trials in which EPSP failures were noted due to preparation drift, or in which spikes were generated, were discarded from analysis.

2.36 Computational Modeling

Algebraic model

A simple double exponential voltage response (template EPSP) was created using the following equation: $(1/\text{normfac}) * (-\exp(-t/\text{tauslow})) + \exp(-t/\text{taufast})$ where $\text{normfac} = (\text{tauslow}/\text{taufast})^{(\text{taufast}/(\text{taufast}-\text{tauslow}))}$ and t is time. The decay tau (tauslow) was set to either 15 ms (taubaseline) or 23 ms (tau5HT). The template EPSP was convolved 5 times at varying ISIs (0-50 ms). EPSP amplitude was calculated by taking the maximum of the convolved trace.

Compartmental model in NEURON

Our compartmental neuronal model was adapted from a model FSI from the Allen Institute for Brain Science (ID#: 469610831). All channel parameters from this model were translated into NEURON and commands were run in the hoc language. The original model contained only one mechanism for passive conductance (reversal potential $e = -61.6229$). This single passive mechanism was split into two separate mechanisms: K^+ (Kpas , $e_{\text{K}} = -107$ mV) & Na^+ passive (Napas , $e_{\text{Na}} = 53$ mV) and the values of these conductances (g) were altered while maintaining their relative conductances to each other until the resting membrane potential and input resistance of the cell matched experimental values. Dendritic diameter was set to 1.5 μm (Gulyás et al., 1999) and axial resistance (R_{a}) was set to 172 (Nörenberg et al., 2010). Five double exponential synapses ($e_{\text{syn}} = 0$ mV) were either placed at the midpoint of one dendrite (96 μm from soma, 1 μm apart). Synaptic parameters (tau , weight) were modified until the EPSP waveform matched experimental data. In some experiments, background

synaptic noise was inserted as a point process into a subset of dendrites with a stochastic model containing fluctuating excitatory and inhibitory conductances (Michalikova et al. 2016). The level of background noise was varied by scaling total synaptic conductance to match R_{in} values obtained during in vivo whole-cell recordings of cortical FSIs (Pala & Peterson, 2015). Each model was replicated 10 times with random noise. To mimic the effects of 5HT in the model neuron, the conductances of K^+ channels in the soma (K_{pas} , $Kv3.1$, SK) and dendrites (K_{pas} , $Kv3.1$, $Mv2$) were reduced by varying percentages (90-30%) and membrane potential and input resistance (calculated by Ohm's law for a -50pA current step) were measured. Synapses were stimulated in the model alone or at varying intervals (5, 10, 20, 50ms). Tau of the single synaptic response was calculated by fitting an exponential to the decay of the EPSP. EPSP amplitude was calculated by taking the maximum of the voltage response.

2.37 Immunohistochemistry

Brain slices obtained for electrophysiological recording were drop-fixed in 4% paraformaldehyde in phosphate buffered solution overnight, then rinsed with phosphate-buffered saline (PBS), cryopreserved in 30% sucrose solution in PBS, and then re-sectioned at 50 μ m using a freezing stage microtome. Sections were rinsed in PBS and blocked with blocking solution (Fisher B10710) for one hour. Sections were then incubated in primary antibodies diluted in 0.2% TritonX-100 in PBS overnight at 4°C. The following primary antibodies were used: Rabbit anti-5HT (Immunostar 20080; 1:500) and mouse anti-GFP (Invitrogen A11120; 1:500). Sections were then rinsed with PBS and incubated in secondary antibodies (1:250, Invitrogen: Alexa 405 goat anti-

rabbit A31556, Alexa 488 goat anti-mouse A11029) for four hours. Finally, sections were rinsed and mounted (Fisher P36934). Images were obtained using a high speed wide-field microscope (Nikon Ti, with Andor Zyla 5.5 sCMOS) with a 10x/0.45 or 20x/0.75 (60x) Plan Apo objective. Fiji software was used to make adjustments for brightness and contrast. Widefield images were stitched with Fiji.

2.38 Statistical Analysis

All data are shown as mean \pm 1 SEM. We used student's t-test to compare pairs of groups if data were normally distributed (verified using Lillie test). If more than two groups were compared, we used ANOVA with post-hoc tests between groups corrected for multiple comparisons (Tukey). Sample sizes were chosen based on current standards in the field. No power analysis was done.

2.4 RESULTS

2.41 Activating 5HT_{2A} receptors increases FSI intrinsic excitability

To determine if 5HT modulated the intrinsic properties of FSIs, we performed whole-cell patch clamp recordings of fluorescent neurons in PV-Cre::Ai14 mice and applied 5HT (30 μ M). 5HT consistently depolarized FSIs by 6.1 ± 1.1 mV, from -71 ± 1.3 mV to -66 ± 2.2 mV (Figure 2.9B, $p < 0.0048$, paired t-test 5HT vs. baseline, $n=10$; Figure 2.1C, $p = 0.0328$, 5HT $n=10$ vs. time-locked controls $n=8$, post-hoc Tukey comparison after one-way ANOVA with $p = 0.0046$) and increased input resistance by $31.1 \pm 6.0\%$, from 92.9 ± 11.5 M Ω to 121.6 ± 16.9 M Ω (Figure 2.9C, $p = 0.0256$, paired t-test 5HT vs. baseline, $n=10$; Figure 2.1D, $p = 0.0365$ 5HT $n=10$ vs. time-locked

controls $n=8$, post-hoc Tukey comparison after one-way ANOVA with $p = 0.004$). We found this concentration of $30 \mu\text{M}$ to be sub-saturating, eliciting approximately 80% of the maximal response (Figure 2.10). 5HT depolarized FSIs even in the presence of ionotropic glutamatergic ($10 \mu\text{M}$ CNQX, $100 \mu\text{M}$ DL-AP5) and GABAergic ($10 \mu\text{M}$ SR95531) antagonists (Figure 2.1C-D, $p = 0.0427$ for V_m & $p = 0.0496$ for Rin, 5HT + syn block $n=9$ vs. time-locked controls $n=8$, post-hoc Tukey comparison after one-way ANOVAs with $p = 0.0046$ for V_{rest} and $p = 0.0040$ for Rin), but effects were blocked ($n=7$) by the 5HT_{2A} antagonist MDL100907 ($1 \mu\text{M}$, Figure 2.1C-D, $p = 0.0238$ for V_m & $p = 0.0258$ for Rin, 5HT vs. 5HT + 2A antagonist post-hoc Tukey comparison after one-way ANOVAs with $p = 0.0046$ for V_{rest} and $p = 0.0040$ for Rin). Thus, 5HT signals through 2A receptors expressed on FSIs.

Changes in V_m and Rin can change neuronal firing properties. Indeed, 5HT increased spiking in response to somatic current injection (Figure 2.1B; Figure 2.9D, $p = 0.0277$ for treatment factor, 5HT vs. baseline in repeated measures two-way ANOVA for firing rate vs. current curve with current and treatment as factors, $n = 10$; Supplemental Figure 1F, $p = 0.0013$, rheobase, 5HT vs. baseline, paired t-test, $n = 10$). No other changes in intrinsic firing properties were noted after 5HT application (Figure 2.9G-L).

Two broad classes of cortical interneurons arise from the medial (MGE) and caudal (CGE) ganglionic eminences (Rudy et al., 2011). Interneuron classes that arise from the CGE, including CCK and VIP interneurons, have been shown to express 5HT_{3A} receptors exclusively (Lee et al., 2010); however, it is unclear whether the other major MGE-derived class, somatostatin-expressing interneurons (SOM), express

5HT_{2A} receptors. Therefore, we made similar excitability measurements from fluorescently identified SOM⁺ neurons (Figure 2.11). Intrinsic excitability was unaltered by 5HT application ($p = 0.3374$ for V_m & $p = 0.1423$ for R_{in} , paired t-test 5HT vs. baseline, $n=6$). Overall, this indicates that FSIs respond to serotonin in a unique manner.

To determine if activation of endogenous serotonergic fibers could also increase FSI excitability in mPFC, we expressed ChR2 in serotonergic neurons in the dorsal raphe nucleus. A Cre-dependent virus (AAV5-Ef1a-DIO-ChR2-eYFP) was injected into SERT-Cre mice, which express Cre-recombinase under the promoter for the serotonin transporter (Figure 2.1E). Immunohistochemistry confirmed that both ChR2 expressing cells in the DRN and axon terminals in mPFC contained 5HT (Figure 2.1E). After waiting 5+ months for trafficking of ChR2 to prefrontal terminals, whole-cell recordings were made from prefrontal FSIs and serotonergic terminals were stimulated with rhythmic flashes of light (470nm, ~2mW, 5ms flashes, 10Hz for 10 seconds). Endogenous 5HT release increased FSI firing rate from 10.9 ± 3.8 Hz to 29.8 ± 6.8 Hz (Figure 2.1F, $p = 0.0345$, during stimulation vs. before stimulation, paired t-test, $n = 7$). This increase was blocked by the 5HT_{2AR} antagonist MDL100907 (Figure 2.1G, 1 μ M, $p = 0.32$, during stimulation vs. before stimulation, paired t-test, $n = 5$).

Membrane depolarization can increase excitability and, therefore, neuronal firing in response to synaptic inputs. To further investigate effects of 5HT on FSI responses to synaptic inputs (as opposed to somatic current injection), we optogenetically activated glutamatergic inputs from contralateral mPFC while recording from FSIs (Figure 2.1H-I, 470nm, ~2mW, 5ms flashes, 10 flashes at 5Hz). 5HT application increased the number

of spikes elicited by each light flash (Figure 2.1J, $p < 0.0001$ for both treatment and flash number in repeated measures two-way ANOVA, $p < 0.0001$ for the interaction term, $p < 0.05$ for flashes 1-8 5HT vs. baseline post-hoc comparison Bonferroni correction, $n = 9$).

By increasing membrane resistivity, 5HT could affect how synaptic inputs are filtered along FSI dendrites. To test this hypothesis, we delivered single light flashes at lower light power ($\sim 0.5\text{--}1\text{mW}$) and recorded excitatory post-synaptic potentials (EPSPs) before and after 5HT application (Figure 2.1I bottom). Interestingly, EPSP amplitude did not change (Figure 2.1K, $p = 0.1980$, paired t-test 5HT vs. baseline, $n = 7$, Figure 2.1H). However, EPSPs decayed more slowly following 5HT application (Figure 2.1L, decay tau: baseline 10.4 ± 1.2 ms, 5HT: 17.4 ± 3.5 ms, $p = 0.0367$, same analysis, $n = 7$).

2.42 5HT decreases inward-rectifying potassium channel function

5HT could modulate FSI intrinsic properties by regulating membrane ion channels. Specifically, a decrease in the overall potassium conductance, either through a direct effect on the channel or through channel internalization, would explain both of our observations: a depolarization of V_m and an increase in R_{in} . To determine whether 5HT altered K^+ channel function, we made voltage clamp recordings during a membrane potential ramp from -130 mV to -50 mV over 3 seconds. We measured the total whole-cell current throughout the ramp before and after 5HT application (Figure 2.2A top). 5HT decreased the slope of the I-V curve ($p = 0.0370$, paired t-test 5HT vs. baseline, $n = 7$), indicating a decrease in membrane conductance. By subtracting the baseline I-V curve from 5HT, we calculated the I-V curve for the current modulated by

5HT (Figure 2.2A bottom). This current displayed inward rectification and reversed at -99 ± 4.7 mV, very close to the predicted reversal potential for K⁺ in our preparation (-101 mV). Both the 5HT-mediated current ($p = 0.0007$, KGluc + MDL100907 vs. KGluc, post-hoc Tukey multiple comparison test with one-way ANOVA with $p < 0.0001$, Figure 2F) and I-V curve slope change ($p = 0.0401$, same analysis, Figure 2.2E) were abolished ($n=3$) with pre-application of MDL100907 ($1 \mu\text{M}$) (Figure 2.2B).

5HT-sensitive currents reversed at potassium equilibrium and were smaller in the outward direction, suggesting that 5HT modulates an inward rectifying K⁺ channel. To test this, we first repeated voltage ramps using a cesium-based internal solution to block K⁺ channels (Figure 2.2C). Both the 5HT-mediated current ($p < 0.0001$, CsMe vs. KGluc, ANOVA with post-hoc Tukey multiple comparison test, Figure 2.2F) and changes in I-V curve ($p < 0.0069$, same analysis, Figure 2.2E) were absent ($n=6$) in these conditions. Secondly, we switched back to a K-based internal solution and blocked inward-rectifying K⁺ channels using Ba²⁺ (Figure 2.2D) at a concentration that fully blocks Kir ion flux across the entire voltage range of the ramp ($400 \mu\text{M}$, Alagem et al., 2001). Again, both the I-V curve changes ($p < 0.0001$, BaCl₂ vs. KGluc, ANOVA with post-hoc Tukey multiple comparison test, Figure 2.2E) and the 5HT-mediated current ($p = 0.0107$, same analysis, Figure 2.2F) were blocked ($n=5$). Thus, 5HT reduces the conductance of inward rectifying potassium channels in FSIs.

Reducing K⁺ conductance in a compartmental model of a fast-spiking interneuron (Figure 2.3A) also increased V_m and R_{in} (Figure 2.3B); a reduction of g_K by 60-70% across the cell was sufficient to recapitulate our experimental data. However, increased cable filtering and prolonged synaptic decay (τ) is likely due to reduction of

K⁺ channel conductance specifically in the dendrites. Indeed, when K⁺ channel conductance was systematically reduced in different subcompartments (Figure 2.3C soma only, 3D dendrites only, 3E both soma & dendrites), only dendritic reduction of gK resulted in an increase in synaptic time constant (Figure 2.3G). Interestingly, consistent with our experimental observations during optogenetic stimulation of inputs to FSIs (Figure 2.1L), no manipulation of gK affected EPSP amplitude in our model (Figure 2.3F).

This last observation can be understood using a simple computational model as follows. According to Ohm's law, increasing R_{in} might be expected to elicit an increase in EPSP amplitude ($V_{syn} = I_{syn} R_{in}$). However, this could be countered by a decrease in driving force ($V_m - E_{syn}$) if the membrane depolarization from 5HT was sufficiently large. In fact, in our compartmental model, reducing the dendritic gK to mimic the experimentally observed effects of 5HT on somatic V_m and R_{in} caused a decrease in the EPSP amplitude and synaptic current when measured at the dendrite (90% of baseline amplitude, Figure 2.12A-C), indicating that this reduction in driving force dominates the dendritic response to synaptic stimulation. However, due to the increase in R_{in} , the dendritic EPSP also attenuates less as it travels towards the soma such that the EPSP amplitude, measured at the soma, is ultimately unchanged by this manipulation. As such, the effects of reducing dendritic gK on EPSP amplitude and tau should depend on the distance of the synapse from the soma (Figure 2.12D). Indeed, in our model, placing the synapse closer to the soma (< 100 μ m) and reducing dendritic gK to match the observed effects of 5HT on V_m and R_m slightly reduced the somatic EPSP amplitude (Figure 2.12E). By contrast, moving the model synapse further out

along the dendrite (100-150 μm) did not affect the EPSP amplitude, presumably indicating that for a range of dendritic locations, the effects on driving force and EPSP attenuation cancel out. At distances furthest from the soma ($> 150 \mu\text{m}$), somatic EPSP amplitude was increased after reducing gK. We did consistently observe an increase in EPSP tau especially when the model synapse was placed far from the soma (Figure 2.12F). These results from our computational model provide simple intuition as to how 5HT can modulate the EPSP decay without affecting EPSP amplitude.

Since our modeling results suggest that 5HT acts mainly to suppress K⁺ channels located in the dendrites, we decided to test this experimentally by delivering 5HT exclusively to the dendrites using local iontophoresis under two-photon guidance (Figure 2.4A). 5HT significantly increased FSI firing rate when applied immediately adjacent to a dendrite (Figure 2.4B, $p = 0.0013$, before iontophoresis vs. after iontophoresis, paired t-test, $n=9$). By computationally filtering out spikes from our traces, we determined that dendritic iontophoresis of 5HT elicited a 1.19 ± 0.69 mV depolarization of the soma (Figure 2.13A-B). By applying this same filtering technique to spike trains elicited by somatic current injection, we found that a somatic depolarization of 2.63 ± 1.57 mV of FSIs was sufficient to cause an increase in firing rate comparable to that observed by dendritic iontophoresis of 5HT (Figure 2.13C). This effect disappeared when the iontophoretic pipette was withdrawn from the dendrite (Figure 2.4C-D, $p = 0.14$, same analysis, $n=7$). By placing the iontophoretic pipette at varying distances from the dendrite, we determined that 5HT only increased firing rate when the pipette was $< 5 \mu\text{m}$ away (space constant = $3.13 \mu\text{m}$, Figure 2.4E). All iontophoretic sites were $> 30 \mu\text{m}$ from the soma (Figure 2.4F), confirming that effects are due to local

action of 5HT at receptors on the dendrite and not due to diffusion of 5HT to the soma.

2.43 5HT enhances the temporal integration of inputs at gamma frequencies

By prolonging the decay of synaptic potentials, 5HT could enhance the integration of multiple synaptic inputs within FSI dendrites. For example, 5HT could improve summation of a second EPSP that arrives during the period of prolonged decay (~10-20 ms after the first input, Figure 2.11). This suggests that 5HT might promote temporal summation (and spike output) in response to inputs arriving specifically in the 50 to 100 Hz range (i.e., in line with the prolonged decay). To test this, we first mimicked glutamatergic input onto FSI dendrites using 2-photon flash photolysis of caged-glutamate, as this technique allows precise control of the position and timing of synaptic activity. Slices were bathed in MNI-glutamate (2.5 mM), and glutamate was released at five specific sites (~1 μm apart) on FSI dendrites (720 nm 2-photon excitation, 0.5 ms pulses, Figure 2.5A). EPSPs were recorded at the soma before and after 5HT application (applied via iontophoresis directly above the slice for 5 seconds). 5HT delivered in this manner produced increases in membrane potential, input resistance, and firing rate comparable to bath application (Figure 2.14). Consistent with ChR2 synaptic stimulation experiments (Figure 2.1H-L) and compartmental modeling (Figure 2.3), 5HT did not affect single EPSP amplitude (Figure 2.5C, $p = 0.45$, normalized change in amplitude: Post/Pre, one-sample t-test vs. 1, $n = 39$ dendrites, 25 cells). However, 5HT did increase the time constant of the EPSPs from 14.7 ± 0.6 ms to 18.6 ± 1.0 ms (Figure 2.5D, $p = 0.0002$, change in tau: Post – Pre, one-sample t-test vs. 0, $n = 39$ dendrites, 25 cells). As with ChR2 synaptic stimulation, changes in EPSP

decay peaked 10-20 ms after stimulation (Figure 2.5E), suggesting that the summation of synaptic inputs arriving within this time window may be preferentially enhanced by 5HT.

To examine frequency-specific effects of 5HT on temporal summation, we uncaged glutamate at all five sites using varying inter-stimulus intervals (0.12, 5, 10, 20, 50 ms, Figure 2.5F), and measured the amplitude of the last EPSP as well as the total integrated EPSP area. As predicted, 5HT significantly promoted summation, specifically at the 10ms ($p = 0.05$, change in 5th EPSP amplitude: 5HT/Baseline, one-sample t-test vs. 1, $n = 26$ dendrites, 18 cells; $p = 0.0062$, change in area under curve: 5HT/Baseline, one-sample t-test vs. 1, $n = 26$ dendrites, 18 cells, Figure 2.5H) and 20ms intervals ($p < 0.05$, change in 5th EPSP amplitude, same analysis as above, $n = 29$ dendrites, 20 cells, Figure 2.5G; $p = 0.0171$, change in area under curve, same analysis as above, $n = 29$ dendrites, 20 cells, Figure 2.5H). Thus, by slowing the decay of synaptic potentials, 5HT promotes summation of gamma frequency inputs.

2.44 Computational models reproduce frequency-specific enhancement of summation by 5HT

To determine if the change in synaptic decay could fully account for the observed differences in temporal summation, we first used a simple algebraic model to explore the effect of changing the synaptic time constant independent of changes in membrane potential and resistivity. After creating an EPSP template using a double exponential equation, the decay time constant was altered to mimic the effect of 5HT ($\tau_{\text{baseline}} = 15$ ms, $\tau_{\text{5HT}} = 23$ ms) and five template EPSPs were convolved at varying intervals (0

– 50 ms). Consistent with experimental data, changing the tau of the EPSP decay promoted summation of inputs at 10-20 ms intervals more than other frequencies (Figure 2.6B).

We then implemented this change in tau in the FSI compartmental model by reducing g_K in all compartments. To simulate our two-photon uncaging experiment, five model synapses along a single dendrite (1 μm apart, Figure 2.6C) were stimulated using varying interstimulus intervals (Figure 2.6E). A 70% reduction in g_K throughout the neuron changed V_m , R_{in} , and tau by an amount comparable to the experimental effect of 5HT (Figure 2.6D). Furthermore, in the model, the reduction in g_K and resultant change in tau could reproduce the frequency-specific enhancement of summation observed in our uncaging experiments. Specifically, inputs arriving within 10-20 ms were summated preferentially, as compared to higher (0-5 ms ISI) or lower (50 ms ISI) frequencies. Preferential summation at 10-20 ms ISIs was observed even when we varied synaptic strength, synapse placement on the dendritic arbor, or number of synapses recruited (Figure 2.15). While the same general effect was observed when all synapses were clustered onto the soma, we found that peak amplitudes were attenuated, likely due to reductions in driving force from membrane depolarization (Figure 2.15B-C). Next, we included random background synaptic noise to reduce R_{in} and more closely simulate in vivo conditions. For these experiments, we included randomly fluctuating noise conductances that modeled both excitatory and inhibitory conductances on a subset of dendrites and stimulated synapses at baseline and after reducing K^+ conductance by 70%. As expected, inclusion of noise reduced the measured input resistance (Figure 2.16). But even when R_{in} was reduced up to 33%,

summation remained tuned to enhancements for 10 - 20ms (Figure 2.16D). These values encompass those measured in vivo (47 M Ω ; Pala et al., 2015), suggesting that serotonin enhances frequency-specific summation over a broad range of background activity levels.

2.45 FSIs preferentially spike in response to gamma frequency inputs with 5HT

Preferential summation of gamma-frequency inputs could, in turn, promote gamma-specific FSI output. To isolate the intrinsic effect of 5HT in FSIs and avoid any potential off target effects of 5HT modulation at other loci within the prefrontal microcircuit, we took a chemogenetic approach, expressing the Gq-coupled designer receptor hM3D (AAV-DJ-Ef1a-DIO-h3MD(Gq)-mCherry), which is activated by the exogenous ligand clozapine-N-oxide (CNO), or a control fluorophore virus (AAV-DJ-Ef1a-DIO-mCherry) in FSIs using PV-Cre \pm mice. CNO had no effect on Vm or Rin in FSIs expressing only the control fluorophore (Figure 2.17). However, in FSIs expressing the Gq-DREADD receptor, CNO application increased Vm (Figure 2.7C; $p < 0.0001$, paired t-test CNO vs. baseline, $n=7$), Rin (Figure 2.7D; $p = 0.0004$, paired t-test CNO vs. baseline), and spiking (Figure 2.7B) in FSIs, and produced similar changes in Kir function (Figure 2.7E-F), suggesting that hM3D receptors can co-opt signaling pathways downstream of 5HT_{2A} receptors and mimic the effects of 5HT on FSI physiology.

We delivered a train of randomly distributed electrical stimuli (Figure 2.8G-H) using predefined ISIs (5, 10, 20, 50, 100 ms) through a local stimulating electrode. Again, we observed no measurable change in single EPSP amplitude ($p = 0.1285$, paired t-test CNO vs. baseline, $n=7$). Interestingly, CNO application mainly enhanced

EPSPs following ISIs of 10 or 20 ms ($p = 0.0384$ for 10ms and $p = 0.0460$ for 20ms, normalized change in EPSP integral: CNO/baseline, one sample t-test vs. 1, $n = 7$, Figure 2.7H). The increased summation at these frequencies translated into an increase in the probability of firing in response to inputs after 10 ms ISIs. Specifically, CNO increased the percentage of spikes that occurred after stimulation with 10 ms ISI compared to other frequencies ($p < 0.0001$ for treatment in ANOVA, $p = 0.0022$ for 10 ms vs. 20 ms, $p < 0.0001$ for 10 ms vs. 50 ms, $p = 0.0039$ for 10ms vs. 100 ms, post-hoc comparison with Tukey's correction, Figure 2.7I). While the Gq-DREADD activates the same downstream signaling cascades, it is not clear if its localization is similar to that of endogenous 5HT_{2A} receptors. Therefore, we performed similar experiments using a selective 5HT_{2A} agonist α -methyl-5HT (30 μ M). Effects on FSI Vm ($p = 0.0019$, paired t-test baseline vs. α -methyl-5HT, $n=5$) and Rin ($p = 0.0138$, paired t-test baseline vs. α -methyl-5HT, $n=5$) were similar with α -methyl-5HT as with endogenous 5HT and Gq-DREADD activation with CNO (Figure 2.18B-C). As in other experiments, we found that α -methyl-5HT did not change the amplitude ($p = 0.9591$, paired t-test baseline vs. α -methyl-5HT, $n=5$, Figure 2.18D), but did increase the decay time ($p = 0.0328$, paired t-test baseline vs. α -methyl-5HT, $n=5$, Figure 2.18E) of subthreshold EPSPs. Furthermore, we replicated our earlier findings and found that 5HT_{2AR} agonism increased the percentage of spikes that occurred after stimulation with 10 ms and 20 ms ISIs compared to other frequencies ($p < 0.001$ for treatment in ANOVA, $p = 0.002$ for 10 ms vs. 50 ms, $p = 0.0015$ for 10 ms vs. 100 ms, $p = 0.0126$ for 5 ms vs. 20 ms, $p = 0.002$ for 20ms vs. 50 ms & 100 ms post-hoc comparison with Tukey's correction, 6 cells, Figure 2.18D). Thus, serotonergic signaling in FSIs seems to

specifically enhance the ability of these cells to respond to gamma-frequency input.

Due to heavy reciprocal connectivity, FSIs are able to entrain the synchronous firing of neighboring interneurons and pyramidal cells, and an increased probability of firing in response to gamma frequency inputs in FSIs could promote gamma frequency inhibition in the prefrontal cortical microcircuit. Therefore, we recorded spontaneous inhibitory postsynaptic currents (IPSCs) in pyramidal neurons in an “active” slice preparation (2 μ M carbachol) at baseline and after Gq-DREADD activation in FSIs with CNO (Figure 2.8A-B). We found that CNO dramatically increased the number of IPSCs recorded ($p = 0.0433$ paired t-test CNO vs. baseline, 5 cells, Figure 2.8C), indicating an overall increase in inhibition. Interestingly, we also found that the frequency of IPSCs shifted toward inter-event intervals of 10-20 ms (Figure 2.8D), corresponding to an increase in the probability of gamma frequency inhibitory events (Figure 2.8E). Thus, we conclude that 5HT increases gamma frequency inhibition in the prefrontal network.

2.5 DISCUSSION

Here, we provide a detailed examination of how changes to passive membrane properties by a neuromodulator alter temporal integration by a neuron. We find that by closing potassium channels, serotonin not only increases the excitability of FSIs, but also promotes synaptic integration in a frequency-specific manner, leading to preferential enhancement of responses to gamma frequency inputs, both in terms of EPSP summation, spiking, and network inhibition.

2.51 5HT increases FSI excitability by altering intrinsic properties

We described the detailed cellular mechanism through which 5HT modulates FSI activity in the mPFC. Previous slice physiology studies showed that 5HT or a 5HT_{2A} agonist could increase the frequency of spontaneous inhibitory post-synaptic currents (sIPSCs) recorded in pyramidal neurons (Weber and Andrade, 2010; Zhou and Hablitz, 1999) and that 5HT increased firing of FSIs (Weber and Andrade, 2010; Zhong and Yan, 2011). Here, we showed that 5HT increased FSI input resistance, membrane voltage, and AP excitability in response to both somatic current injection (Figure 2.1B, Supplementary Figure 2.1D) and optogenetically-evoked synaptic input (Figure 2.1H-L). These changes in intrinsic properties reflect the reduction of an inward-rectifying potassium conductance in FSIs (Figure 2.2). These data may provide mechanistic insight into a previously observed increase in presynaptic facilitation of inhibitory glycinergic synapses (Mintz et al., 1989). Our results are in contrast to one study that found that 5HT differentially increases or decreases firing of distinct subpopulations of FSIs in vivo (Puig et al., 2010). However, these experiments were performed in a different species (rat) and in a more dorsolateral brain region (M2). Furthermore, systemic 5HT antagonists in that study could have influenced other cells in the network such that the observed effects may not reflect direct actions on FSIs.

2.52 5HT promotes temporal summation of inputs arriving at gamma frequency by prolonging EPSP decay

Compared to neighboring pyramidal cells, which can respond to synaptic input with the generation of dendritic superlinearities (Stuart & Spruston, 2015), FSI dendrites tend to function more as passive filters (Abrahamsson et al., 2012). As such, changes in

passive membrane properties can have significant effects on integration in FSIs. Here, 5HT-mediated suppression of dendritic Kir conductances prolonged the decay of synaptic potentials without changing EPSP amplitude (Figure 2.1K-L, Figure 2.5A-E). This provides a mechanism for promoting the summation of inputs arriving during the period of prolonged decay, and specifically enhancing high gamma frequency (50-100 Hz) inputs, as compared to input at other frequencies. FSIs also exhibit subthreshold resonance around 30 Hz (Bracci et al., 2003; Fellous et al., 2001; Pike et al., 2000) and network models show that this membrane resonance contributes to network gamma oscillations (Moca et al., 2014). Furthermore, FSIs show enhanced firing in response to gamma frequency modulation of sinusoidal current injected into the soma (Pike et al., 2000). However, no studies have explored whether synaptic integration in FSIs also favors gamma frequency inputs. Here, we show that the enhanced temporal integration of gamma frequency inputs elicited by 5HT also translates to a greater probability of FSI spiking by using a Gq-DREADD expressed exclusively in PV cells (Figure 2.7F-I). By enhancing summation of inputs at these frequencies, 5HT could further enhance an intrinsic preference for FSIs to fire at gamma frequencies, and thus regulate the power of gamma oscillations.

2.53 Implications for serotonergic regulation of prefrontal circuit activity

FSIs play a critical role in shaping cortical circuit activity. With abundant reciprocal connections and highly divergent synapses onto principal pyramidal cells, FSIs are able to precisely control the timing of spike discharges of large populations of cortical neurons (Bartos et al., 2007, McBain and Fisahn, 2001, Tamas et al., 2000).

These properties endow FSIs with the ability to orchestrate network oscillations (Cardin et al., 2009; Sohal et al., 2009), specifically in the gamma frequency range, which have been suggested to be important for information encoding (Buzsáki and Chrobak, 1995). A previous study (Puig et al., 2010) found that electrical stimulation of the dorsal raphe of rat both increased and decreased the activity of distinct populations of FSIs in secondary motor cortex via 5HT2A and 5HT1A receptors respectively. Furthermore, this group found that blocking 5HT2ARs decreased the power of gamma oscillations, suggesting that 5HT2AR activation could contribute to increases in gamma oscillatory power. In our preparation, we did not find distinct subpopulations of FSIs with differential responses to 5HT; all recorded FSIs displayed an increase in membrane potential, input resistance, and excitability. Therefore, by regulating the temporal summation of inputs to FSIs and resulting FSI spiking, serotonergic actions on FSI dendrites may provide a substrate for regulating the power or frequency of network oscillatory activity, thereby enhancing information transfer to downstream structures (Sohal et al., 2009). Future studies should examine the effect of 5HT on FSI activity and gamma oscillations in vivo.

Serotonin plays a complex role in prefrontal circuits and has been implicated in a wide array of prefrontal cognitive tasks from rule shifting (Clarke et al., 2007, 2004; Baker et al., 2011) and executive control (Koot et al., 2012; Carli et al., 2006) to working memory (Williams and Rao, 2002) and social cognition (Passamonti et al., 2012). While we focus here on the role of 5HT on FSIs, 5HT receptors are also expressed on pyramidal neurons (Araneda and Andrade, 1991, Avesar and Gullledge, 2012) and 5HT3a-expressing interneurons, including VIP, CCK, and others (Puig and Gullledge, 2011). Thus, it will be interesting in future studies to determine whether serotonergic

regulation of one or all of these populations is important for its behavioral effects.

2.54 Clinical Relevance

Prefrontal dysfunction is etiological to many major psychiatric disorders, including schizophrenia and depression (Drevets et al., 2008). Moreover, current treatments for these disorders often target serotonergic transmission. Selective serotonin reuptake inhibitors (SSRIs) remain the most commonly used treatments for depression (Risch and Nemeroff, 1992; Willner, 1985) and second-generation antipsychotics used in schizophrenia block the 5HT_{2A} receptor with high affinity (Meltzer et al., 2003, Meltzer and Massey, 2011). Classic hallucinogens such as lysergic acid diethylamide (LSD) activate the 5HT_{2A} receptor (Titeler et al., 1988), implicating it in psychosis. Additionally, patients with schizophrenia show lower levels of the 5HT_{2A} receptor in PFC (Arora and Meltzer, 1991; Selvaraj et al., 2014).

Impairments in FSI function and gamma rhythms may also be involved in the pathophysiology of schizophrenia (Gonzalez-Burgos et al., 2010, Gonzalez-Burgos et al., 2015; Lewis et al., 2005; Uhlhaas and Singer, 2010). Previous work from our group showed that optogenetic activation of FSIs at gamma frequency is able to rescue impairments in cognitive flexibility in mice that model key aspects of schizophrenia (Cho et al., 2015). Furthermore, treatment with antipsychotic drugs that act on 5HT receptors can reduce gamma power (Schulz et al., 2012). The precise relationship between 5HT, prefrontal FSIs, and schizophrenia is still unclear. However, the findings of this study may contribute to understanding clinical actions of second-generation antipsychotics through their actions on prefrontal FSIs.

2.6 FIGURES

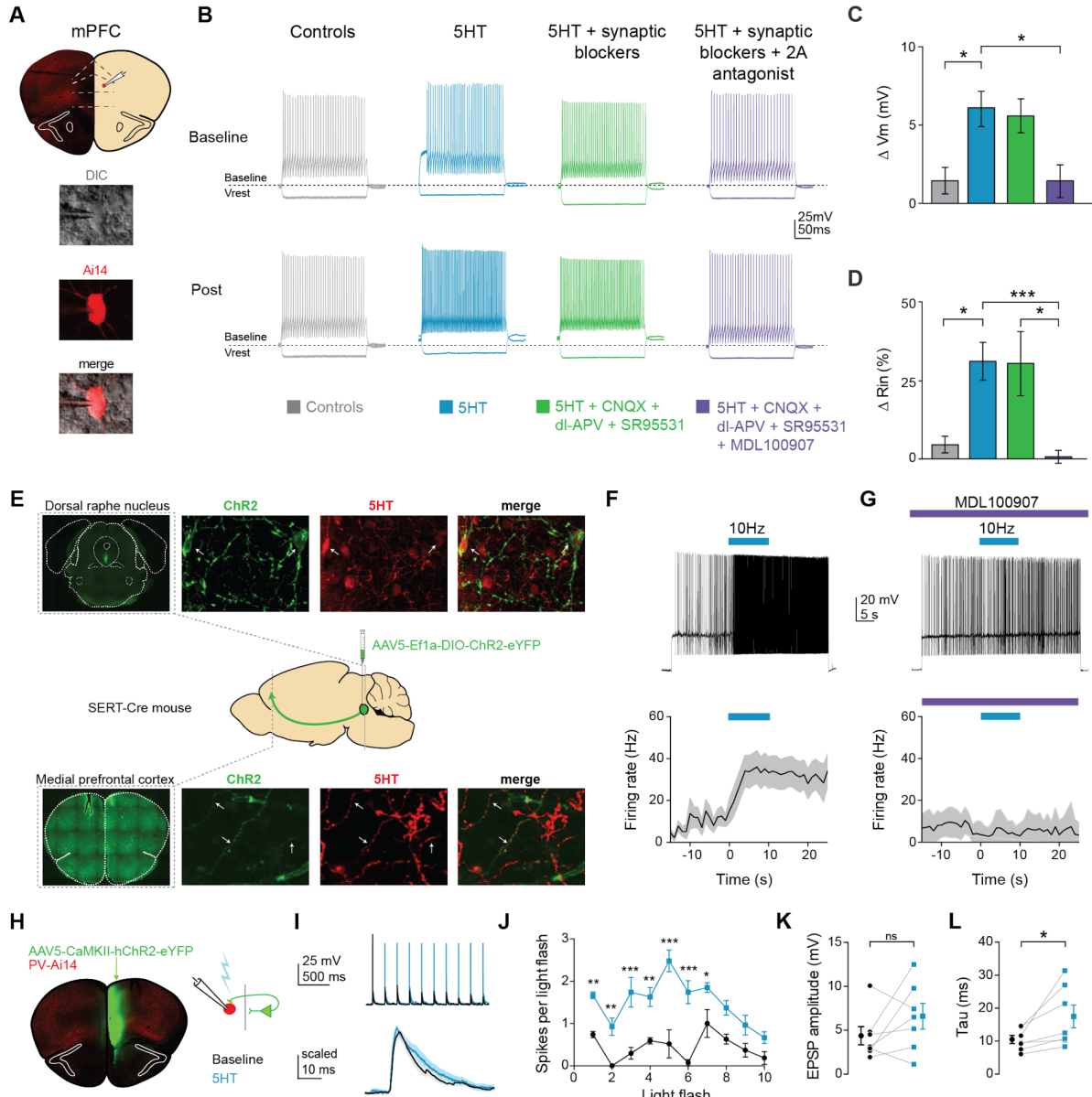


Figure 2.1. Serotonin alters intrinsic properties to increase FSI excitability.

A) Experimental design: we recorded from fast-spiking interneurons labeled in a PV-Cre:: Ai14 in mPFC (top). Images of a recorded neuron in DIC and showing tdTomato expression (bottom). B) Example FSI responses to hyperpolarizing (-200 pA) and depolarizing (50 pA above rheobase) current steps at baseline and after application (Post, 10 min after drug wash in) of 5HT (30 μ M, blue), 5HT + synaptic blockers (10 μ M CNQX, 100 μ M DL-AP5, 10 μ M gabazine, green), 5HT + synaptic blockers + 5HT2A antagonist (1 μ M MDL-100907, purple), or time-locked control aCSF (gray). C-D) Subtracted change in membrane potential (C) and percent change in input resistance (D) after pharmacological manipulations listed above. E) Experimental design: Cre-dependent ChR2 was injected into the dorsal raphe of SERT-Cre mice. Top and bottom rows: Images of ChR2 expression and 5HT immunohistochemistry in dorsal raphe

injection side (top) and mPFC recording site (bottom). Confocal images of ChR2 (green), 5HT immunohistochemistry (red), and merged. Yellow sections indicate overlap. Arrows point to examples of overlap. F) Top: FSIs in mPFC were injected with light depolarizing current to elicit spiking and ChR2 expressing terminals were activated with blue light (10 Hz, 10 s) to release endogenous 5HT (top). Bottom: Peristimulus time histograms of FSI firing rate during current step with ChR2-activated release of 5HT G) These experiments were repeated after washing in a 5HT_{2A} antagonist (1 μ M MDL100907). H) Experimental design: ChR2 was injected into one hemisphere of mPFC and FSIs were patched on the opposite hemisphere. I) Example traces of FSI responses at baseline (black) and after 5HT (blue) in response to activation of synaptic inputs from ChR2-expressing terminals with either a train of blue light pulses (5 Hz, 2 mW, top) or single light flashes (0.5-1 mW, bottom). J) Number of spikes fired in response to each light flash in the stimulus train depicted before and after application of 5HT. K-L) Change in amplitude (K) and decay time constant (τ , L) of synaptic responses before (black) and after 5HT (blue). * $p < 0.05$, ** $p < 0.01$

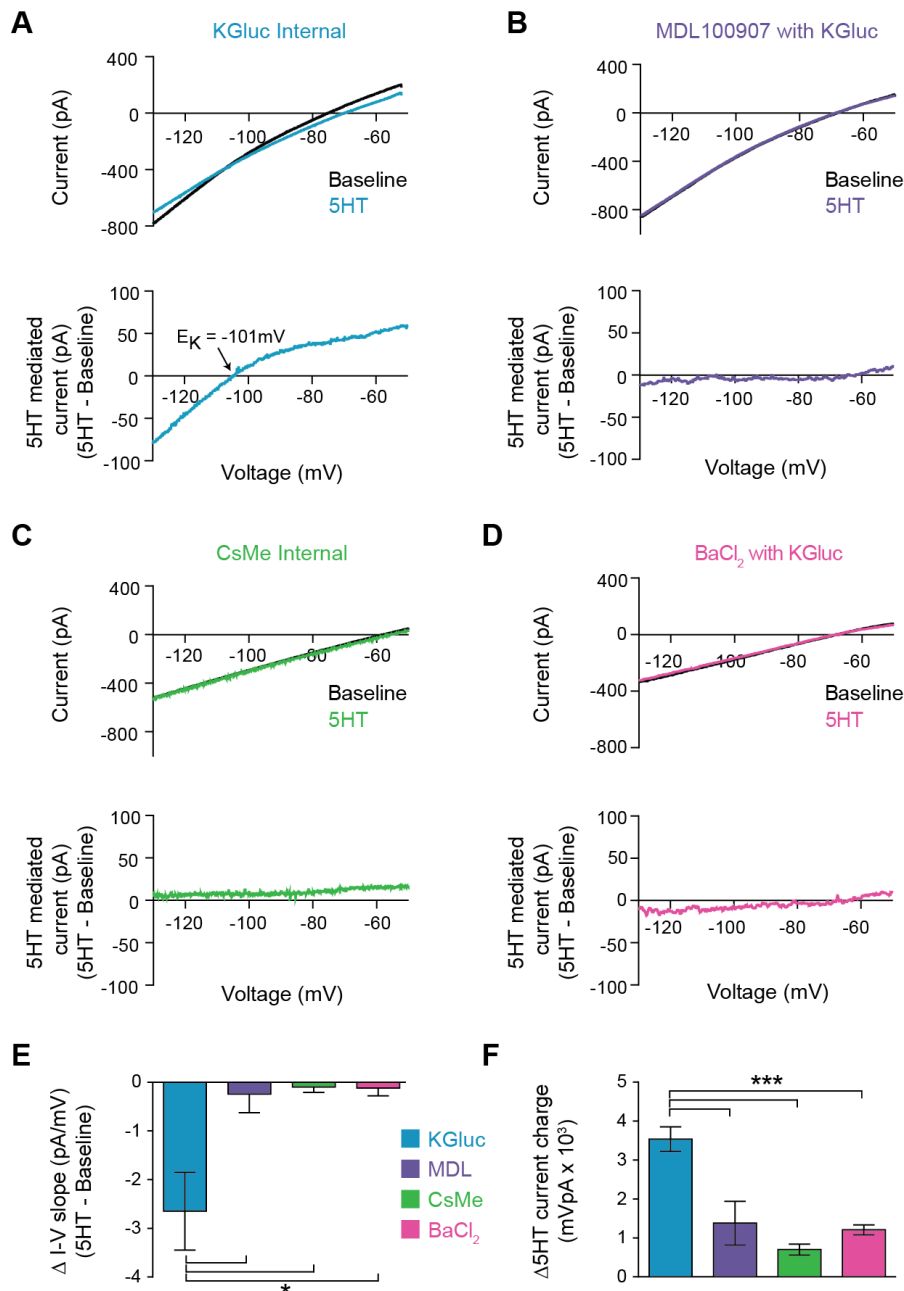


Figure 2.2. 5HT reduces conductance through inward rectifying potassium channels.

A-B) Top: Current recorded during a voltage ramp (3 seconds) from -150mV to -50mV before (black) and after 5HT (blue) using KGluc in the internal solution (A) and with pre-application of the 5HT_{2A} antagonist MDL100907 (1 μ M). Bottom: The raw currents from the I-V curves subtracted from each other to show the current modulated by 5HT. C) Top: Current in response to voltage ramp using CsMe internal solution to block K⁺ channels. Bottom: 5HT mediated current. D) Top: Current in response to same voltage ramp with barium chloride (400 μ M) in the bath solution to block inward-rectifying K⁺ channels. Bottom: 5HT mediated current. E) The change in slope of the I-V curves (change in conductance) from A-D. F) Quantification of charge transfer by 5HT

in above conditions, calculated by taking the integral of bottom traces in A-D. * $p < 0.05$,
 *** $p < 0.005$

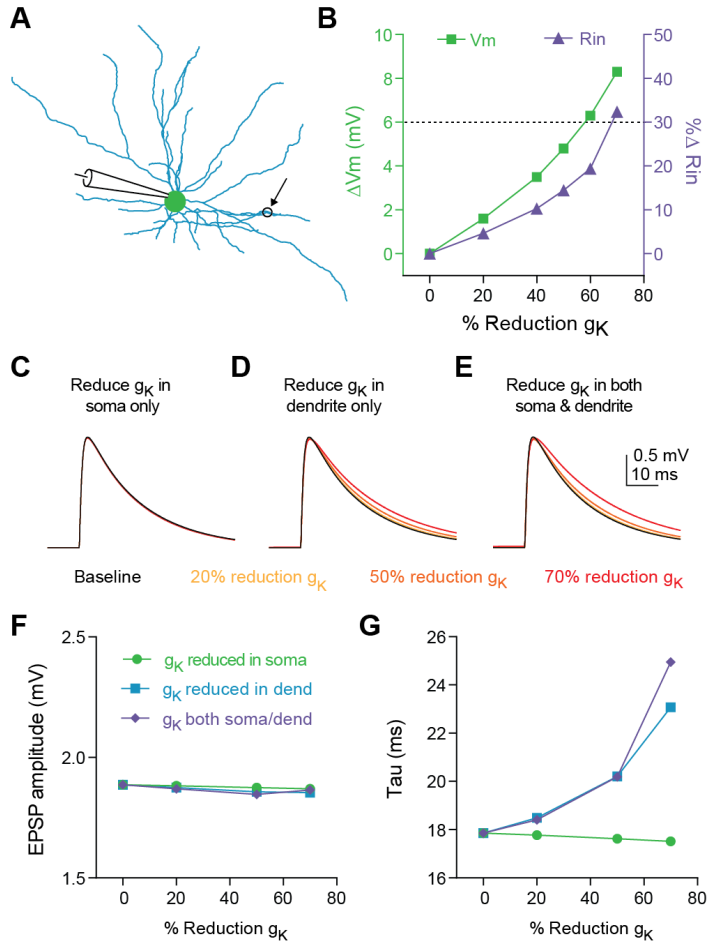


Figure 2.3. Decreasing dendritic K⁺ conductance elicits change in tau of synaptic responses in a compartmental model.

A) Morphology of FSI model. Black circle represents location of synapse. B) Change in membrane potential (left axis) and input resistance (right axis) in response to reducing conductance of K⁺ channels in both the soma and dendrites of model. Dashed black line indicates average effect from experimental data on V_m and R_{in} in response to 5HT application. C-E) Synaptic responses recorded at the model soma after reducing K⁺ conductance by varying amounts (30-80%) only at the soma (C), only at the dendrites (D), or at both the soma and dendrites (E). F-G) EPSP amplitude (F) and synaptic time constant (G) after reducing K⁺ conductance in soma (green), dendrites (purple), or both (blue).

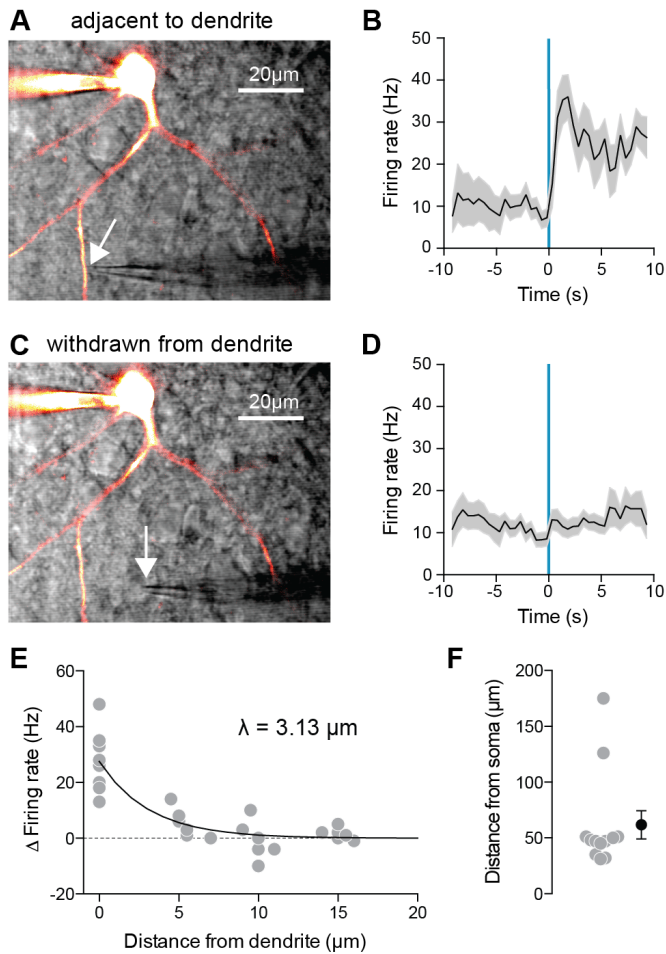


Figure 2.4. Local 5HT iontophoresis at FSI dendrites increases FSI firing.

A,C) Experimental design: Neurons were patched and filled with Alexa-488. 5HT was applied locally to the dendrite using iontophoresis (50 ms) while FSIs were injected with a small amount of depolarizing current to elicit spiking. DIC and overlaid fluorescent images with iontophoretic pipette adjacent to (A) or withdrawn from (C) dendrite. B,D) Firing rate in response to current injection with local 5HT iontophoresis adjacent to dendrite (B) or withdrawn from dendrite (D). E) Change in firing rate with iontophoresis (FR 1 sec before ionto pulse subtracted from FR after ionto pulse) at different distances from the dendrite. Solid black line in exponential fit to data. Space constant is 3.13 μm . F) Distances of iontophoretic sites from the soma.

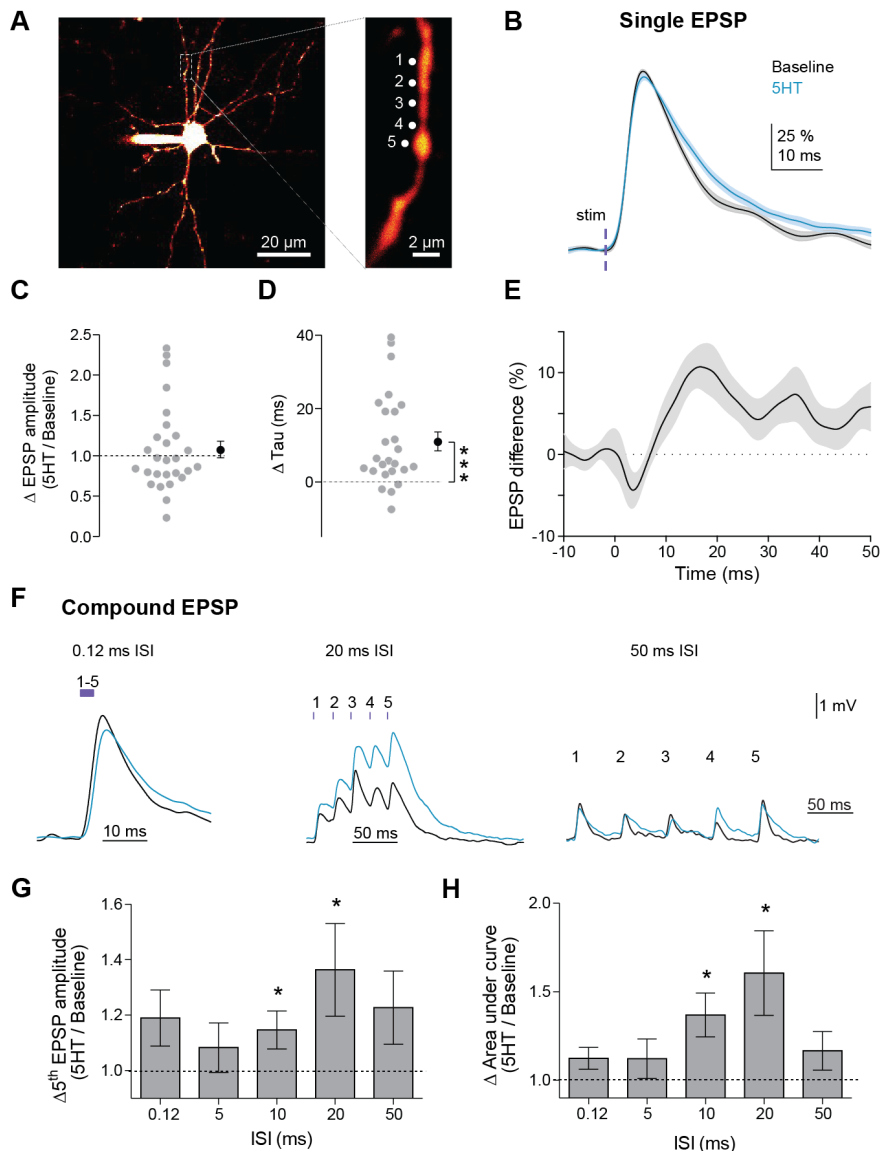


Figure 2.5. 5HT promotes integration of synaptic inputs in a frequency-specific manner.

A) Experimental design: Slices were bathed in a caged glutamate compound (MNI-Glutamate 2.5 mM) that is only biochemically active with photolysis. Glutamate was uncaged at 5 locations (1 μm apart) on a dendrite individually and then at all five together with varying interstimulus intervals (0.12, 5, 10, 20, 50 ms). B) Amplitude-normalized EPSP in response to single uncaging events before (black) and after application of 5HT (blue). C) Ratio of EPSP amplitudes (5HT / baseline) for single uncaging events (averaged per dendrite). Dotted line indicates no change. D) Change in synaptic decay time constant (τ) of single uncaging events (averaged per dendrite) before and after 5HT. Dotted line indicates no change. E) Difference of 5HT and baseline EPSP traces in B. F) Example compound EPSPs in response to uncaging at all five dendritic locations at varying interstimulus intervals (0.12, 20, 50ms). G-H) Ratio

of 5th EPSP amplitude (G, 5HT/Baseline) and charge transfer (H, 5HT/Baseline integral) for different interstimulus intervals. * $p < 0.05$, ** $p < 0.01$

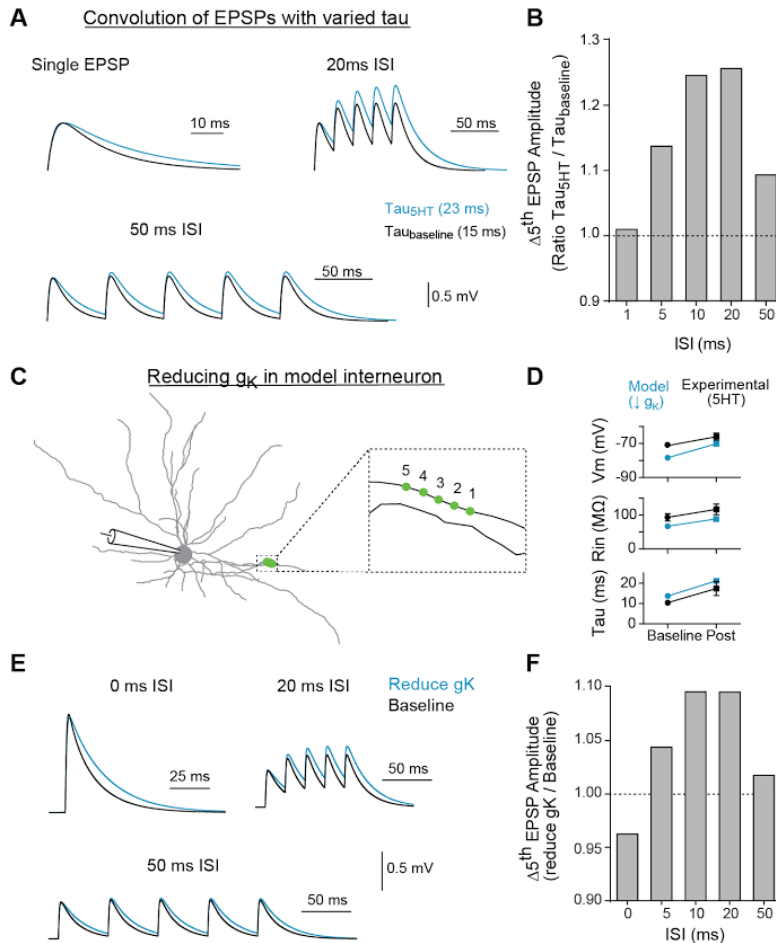


Figure 2.6. Modeling indicates that changing tau and reducing K+ conductance can modulate temporal summation.

A) Experimental design: Single EPSPs were modeled using a double exponential with two different decay constants ($\tau_{baseline} = 15$ ms, $\tau_{5HT} = 23$ ms) to match the change in tau observed with 5HT application. These template EPSPs were convolved five times with varying intervals (ISI). Example traces shown here of single EPSP, 20 ms ISI, and 50ms ISI with baseline tau (black) and 5HT tau (blue). B) The ratio of amplitude of the 5th EPSP (slow tau / fast tau) as a function of interval. C) Morphology of FSI model. Purple circles represent location of synapses. D) Comparisons of model (blue) and experimental (black) intrinsic properties at baseline (circles) and after manipulations (blue = model: reducing g_K by 70%, black = experimental: application of 5HT). E) Synapses in model were stimulated at variable interstimulus intervals (ISI). Example traces for compound EPSPs with 0 ms, 20 ms, and 50 ms ISIs at baseline (black) and after reducing g_K by 70% (blue). F) The ratio of amplitude of the 5th EPSP (reduced g_K / baseline) as a function of ISI.

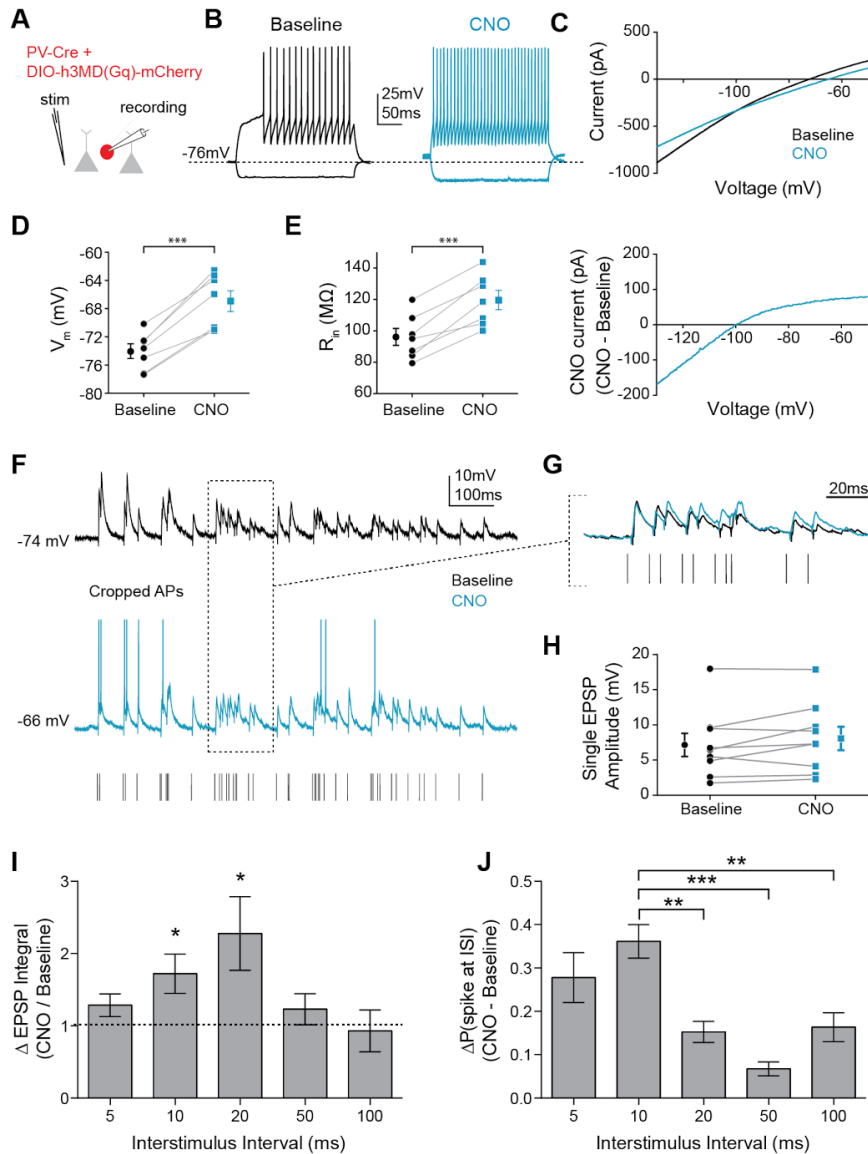


Figure 2.7. Mimicking 5HT effects elicits preferential firing to gamma frequency inputs in FSIs.

A) Experimental design: The Gq-coupled Designer Receptor Exclusively Activated by Designer Drugs (DREADD) was expressed specifically in FSIs using a Cre-dependent virus injected into PV-Cre mice. FSIs were identified with fluorescence for patching. B) Example FSI responses to hyperpolarizing and depolarizing current steps at baseline (black) and after application of CNO to activate the Gq-DREADD (1 μ M, blue). C) Top: Current recorded during a voltage ramp (3 seconds) from -150mV to -50mV before (black) and after CNO (blue). Bottom: The raw currents from the I-V curves subtracted from each other to show the current modulated by CNO. D-E) Changes in membrane potential (D) and input resistance (E) before and after CNO. F) Experimental design: A stimulating electrode was placed in the tissue within 100 μ m of the recorded FSI and a 2 second train of randomly distributed stimulating current pulses (200 μ s) with varied interstimulus intervals (ISIs = 5, 10, 20, 50, 100 ms) was delivered. Example FSI responses to stimulus train at baseline (black) and after application of CNO (blue). G)

Expanded view of subthreshold responses indicated by dotted box in F. H) Change in single EPSP amplitude with CNO I) Normalized change in EPSP integral (CNO / Baseline) with CNO application for different ISIs. J) Change in the percentage of all spikes occurring at each ISI after CNO. * $p < 0.05$, ** $p < 0.01$ *** $p < 0.005$

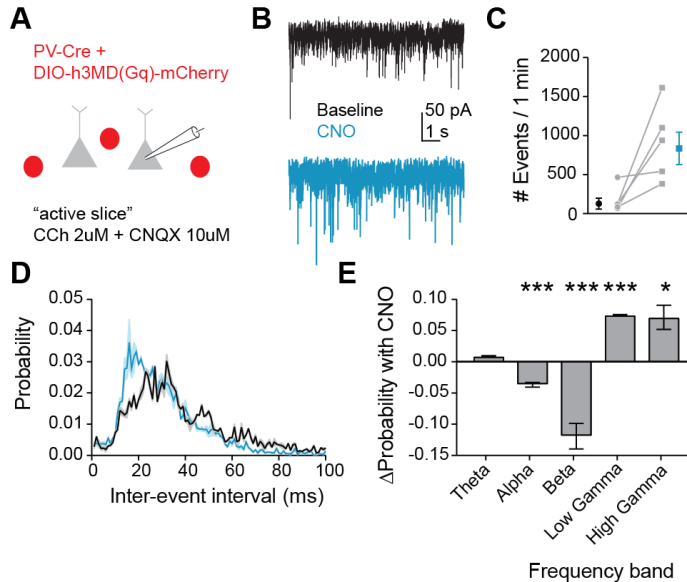


Figure 2.8. Mimicking 5HT effects in FSIs produces gamma frequency events in downstream pyramidal neurons.

A) Experimental design: The Gq-DREADD was expressed specifically in FSIs using a cre-dependent virus injected into PV-Cre mice. Prefrontal slices were bathed in carbachol ($2 \mu\text{M}$) to induce spontaneous background synaptic activity. Non-fluorescent pyramidal neurons were chosen for patching using a high chloride internal solution to elicit inward IPSCs. CNQX ($10 \mu\text{M}$) was included in the bath to block AMPA currents. B) Example traces of spontaneous IPSCs recorded at baseline (black) and after wash-in of CNO (blue). C) Total number of IPSC events in one minute at baseline and after CNO application. D) Probability distribution of inter-event intervals for IPSCs recorded at baseline and after CNO. E) Change in probability of inter-event intervals of different frequency bands. Theta = 48 Hz, alpha = 8-12 Hz, beta = 13-29 Hz, low gamma = 39-59 Hz, high gamma = 61-100 Hz. * $p < 0.05$, ** $p < 0.01$ *** $p < 0.005$

Supplemental Figures

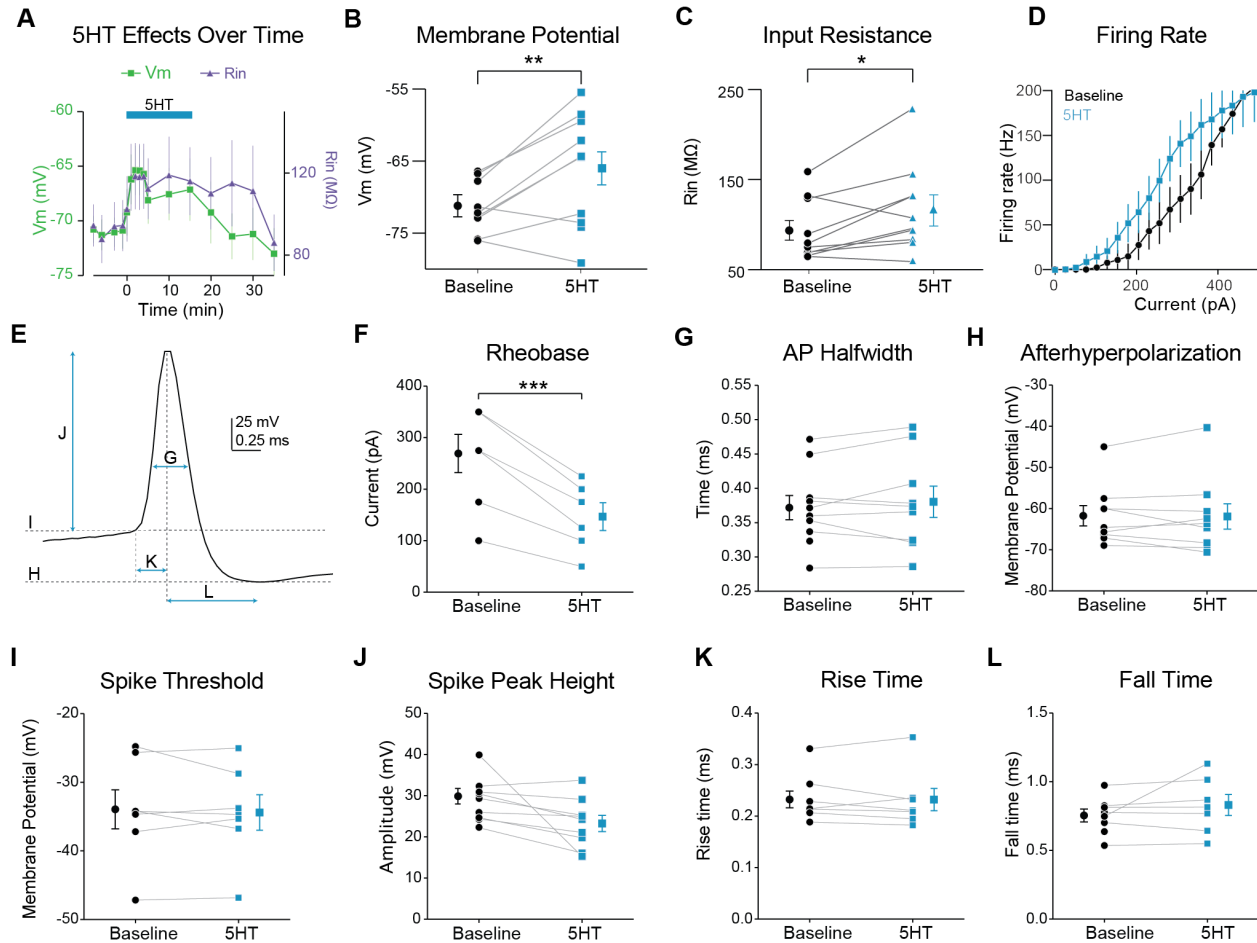


Figure 2.9 – Supplement to Figure 1. Modulation of FSI intrinsic properties by 5HT.

A) Membrane potential (left axis) and input resistance (right axis) over time during application of 5HT. B-C) Membrane potential (B) and input resistance (C) before (averaged -5 min to 0 min) and after (averaged 2 to 7 min) application of 5HT. D) FSI firing rate in response to depolarizing current steps. E) Single action potential (AP) of a recorded FSI. Arrows and dotted lines indicate how measurements were made for the rest of the figure panels. F) Rheobase (minimal current needed to elicit spiking) before (black) and after 5HT (blue). G) AP halfwidth (time for V_m to rise from point halfway between peak and trough to the peak and back to the halfway point) before (black) and after 5HT (blue). H) Afterhyperpolarization (membrane potential of AP trough) before (black) and after 5HT (blue). I) Spike threshold (determined by max of third derivative of membrane potential) before (black) and after 5HT (blue). J) Spike height (difference between peak and threshold) before (black) and after 5HT (blue). K) AP rise time (time from threshold to peak) before (black) and after 5HT (blue). L) AP fall time (time from peak to trough) before (black) and after 5HT (blue). *** $p < 0.005$

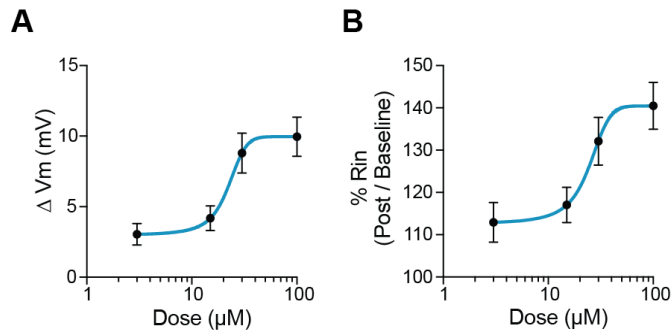


Figure 2.10 – Supplement to Figure 1. Dose response for 5HT

A) Change in membrane potential with various doses of 5HT. 0 mV indicates no change. B) Percentage change in input resistance with various doses of 5HT. 100% indicates no change.

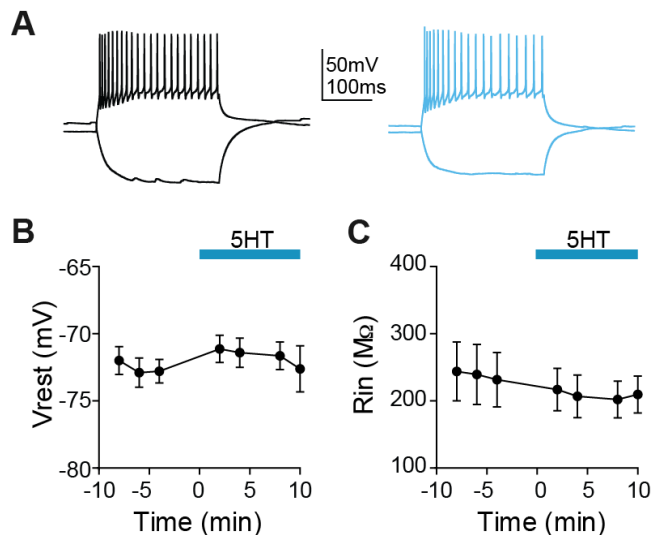


Figure 2.11 – Supplement to Figure 1. 5HT does not change membrane potential or input resistance of SOM interneurons.

A) Experimental design: We recorded from somatostatin (SOM)-expressing interneurons labeled in a SOM-Cre:: Ai14 in mPFC. Example somatostatin (SOM)-expressing interneuron responses to hyperpolarizing and depolarizing current steps at baseline (black) and after application of 5HT (blue).

B-C) Membrane potential B) and input resistance (C) over time during application of 5HT

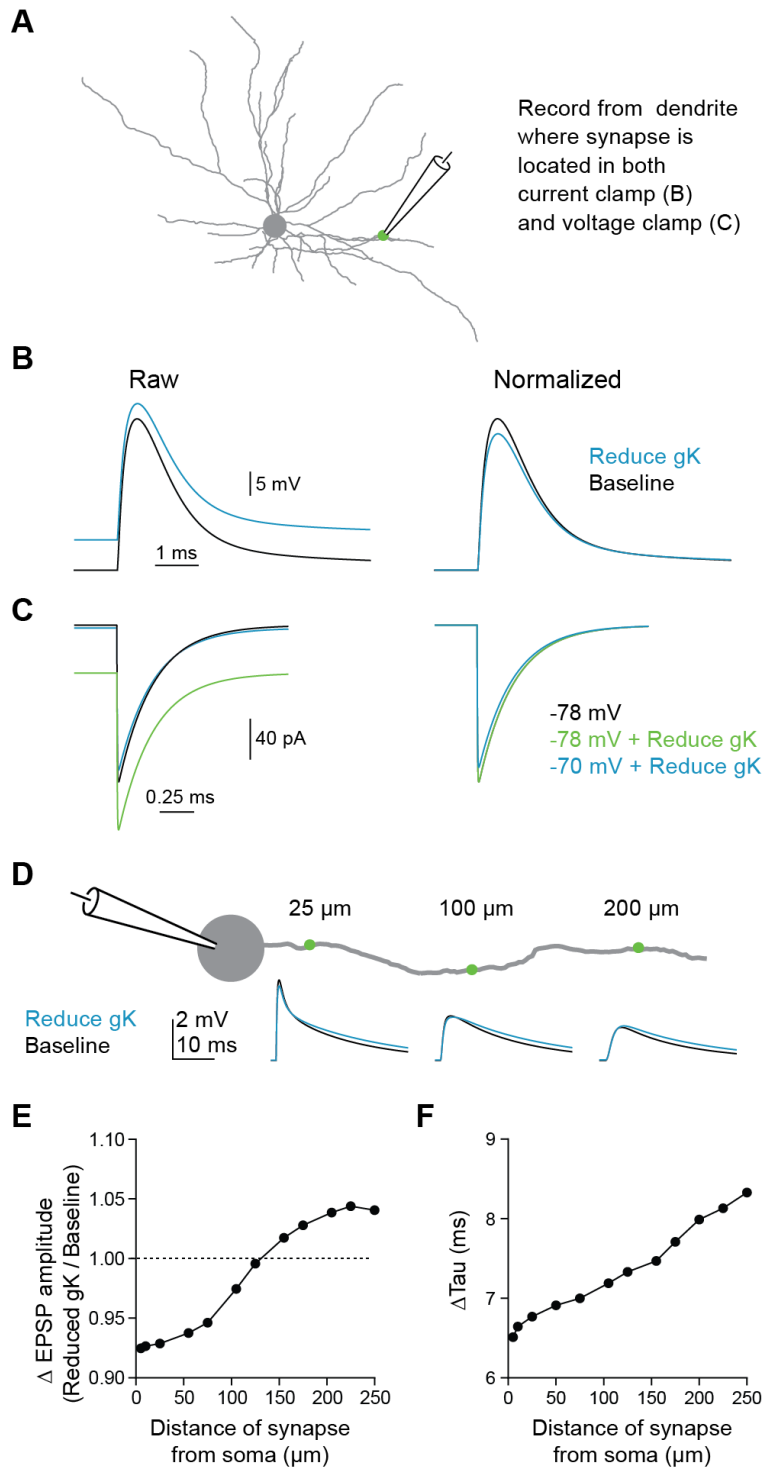


Figure 2.12 – Supplement to Figure 3. 5HT-induced dendritic depolarization reduces synaptic driving force in compartmental model.

A) Experimental design: Synapse was stimulated on dendrite and response was recorded at site of synapse in either voltage clamp or current clamp. B) EPSP traces recorded in current clamp at dendrite at baseline and after reducing gK to mimic 5HT. C) EPSC traces recorded in voltage clamp at dendrite with varying holding potentials and reducing gK. D) Experimental design: Synapse was placed at varying distances

from soma (5-200 μm) on a single dendrite and EPSP was recorded at the soma at baseline and after reducing gK. E-F) Change in EPSP amplitude (D) and tau (D) due to gK reduction as a function of distance from soma are shown.

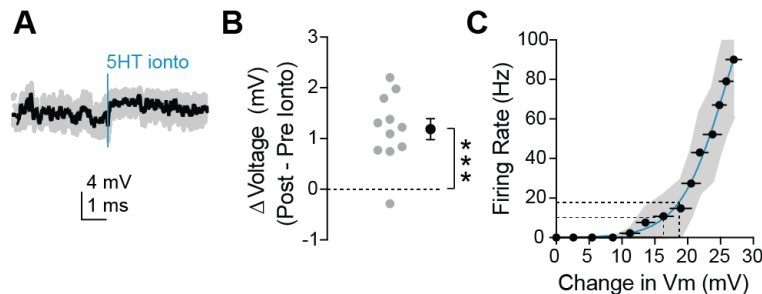


Figure 2.13 – Supplement to Figure 4. Dendritic 5HT iontophoresis depolarizes neuron sufficiently to induce observed change in firing rate.

A) Average membrane potential recorded at the soma during dendritic iontophoresis with spikes removed via median filtering. Blue line indicates time of iontophoresis. B) Change in membrane potential in the 2 seconds preceding and following iontophoresis. C) Number of spikes fired in response to somatic square current injections versus change in membrane potential (computed by removing spikes from traces). Dotted lines on the y-axis indicate the firing rates pre (~ 10 Hz) and post (~ 18 Hz) iontophoresis. Dotted lines on the x-axis display the change in membrane potential required to elicit those firing rates. A depolarization of 2 - 3 mV is sufficient to change an FSI's firing rate from 10 to 18 Hz.

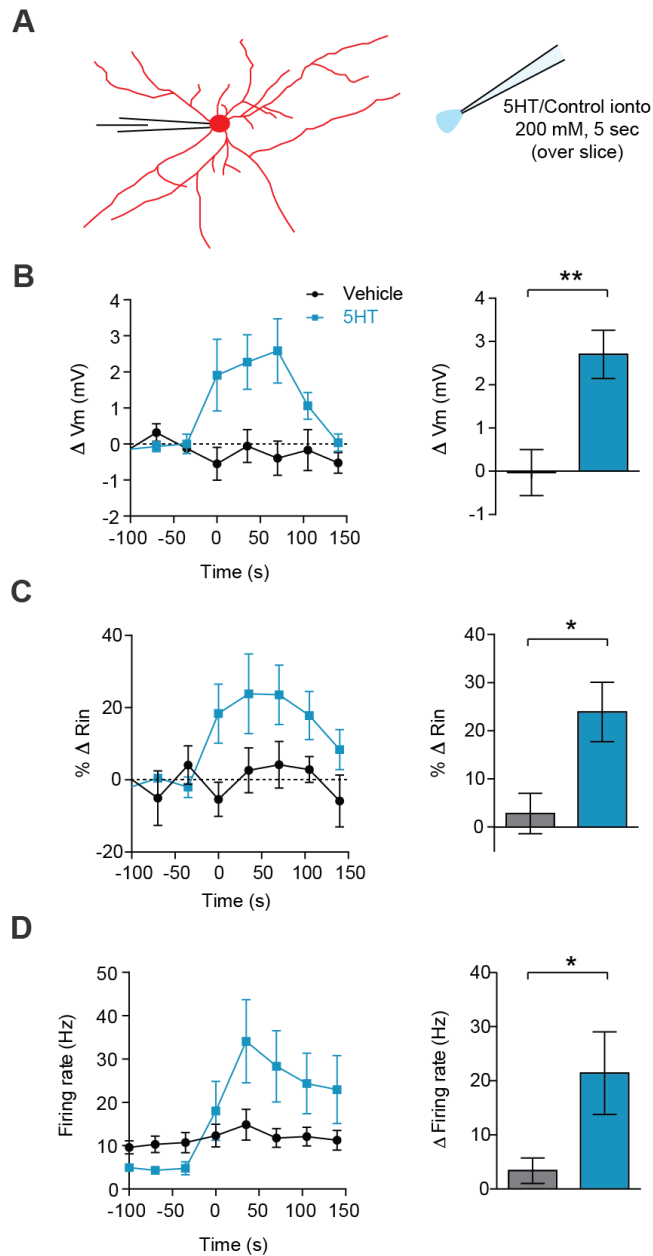


Figure 2.14 – Supplement to Figure 5. Broad 5HT iontophoresis over the slice produces typical 5HT effects.

A) Experimental design: FSIs were patch clamped and an iontophoretic pipette containing 5HT (200 mM, pH = 4.5) or vehicle control solution (aCSF, pH = 4.5) was hovered just above the slice. B-D) Left panels: change in membrane potential (B), input resistance (C), and firing rate (D) in response to iontophoresis (5 sec) of either 5HT (blue) or vehicle control (black) over time. Right panels: Quantification change in parameters before (-100 to 0 sec) or after (0 to 150 sec) iontophoresis. * $p < 0.05$, ** $p < 0.01$

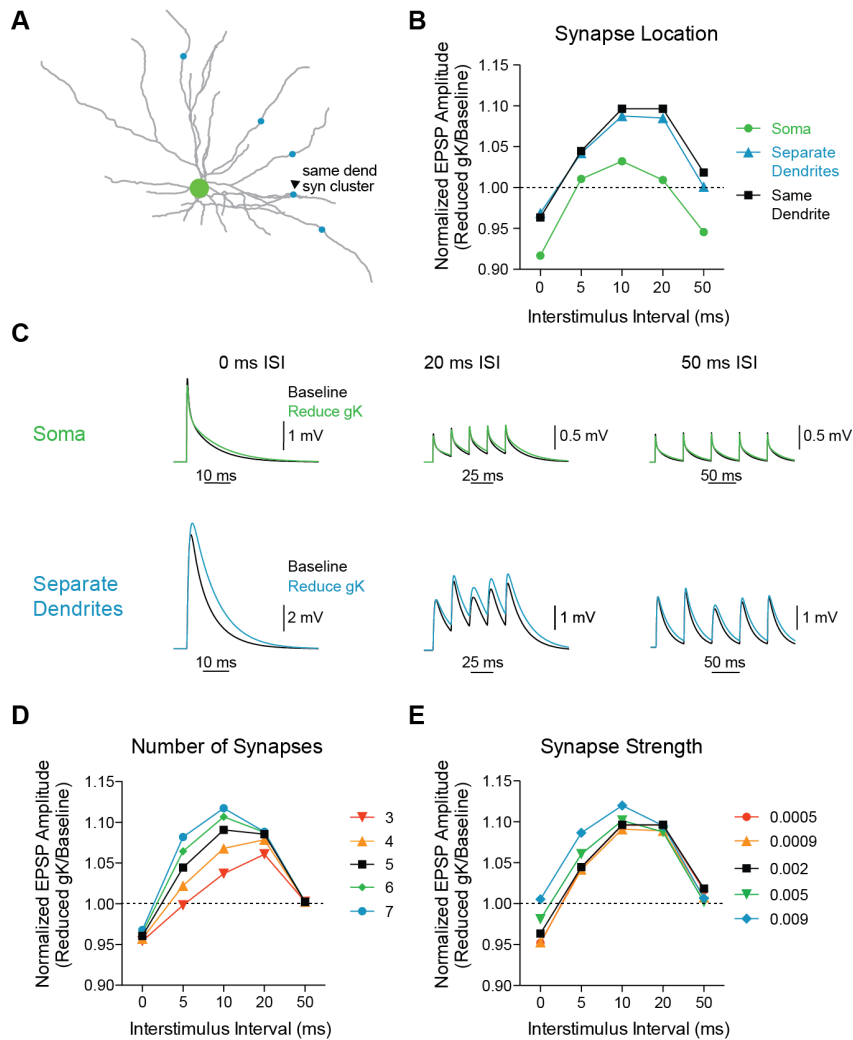


Figure 2.15 – Supplement to Figure 6. Model is robust to changes in synaptic parameters.

A) Experimental design: Five synapses were placed either on the same dendrite (1 μm apart, arrowhead, black), separate dendrites (blue), or soma (green). The synapses were stimulated at varying interstimulus intervals (0, 5, 10, 20, 50 ms) and voltage responses at the soma were recorded.

B) The ratio of amplitude of the 5th EPSP (Reduced gK / Baseline) as a function of interval for different synapse locations.

C) Example traces for compound EPSPs with 0 ms, 20 ms, and 50 ms ISIs at baseline (black) and after reducing gK by 70% (blue) with synapses placed either on the soma (green) or separate dendrites (blue).

D) The ratio of amplitude of the 5th EPSP (Reduced gK / Baseline) as a function of interval for different numbers of synapses (on same dendrite) activated.

E) The ratio of amplitude of the 5th EPSP (Reduced gK / Baseline) as a function of interval for varying synapse weights.

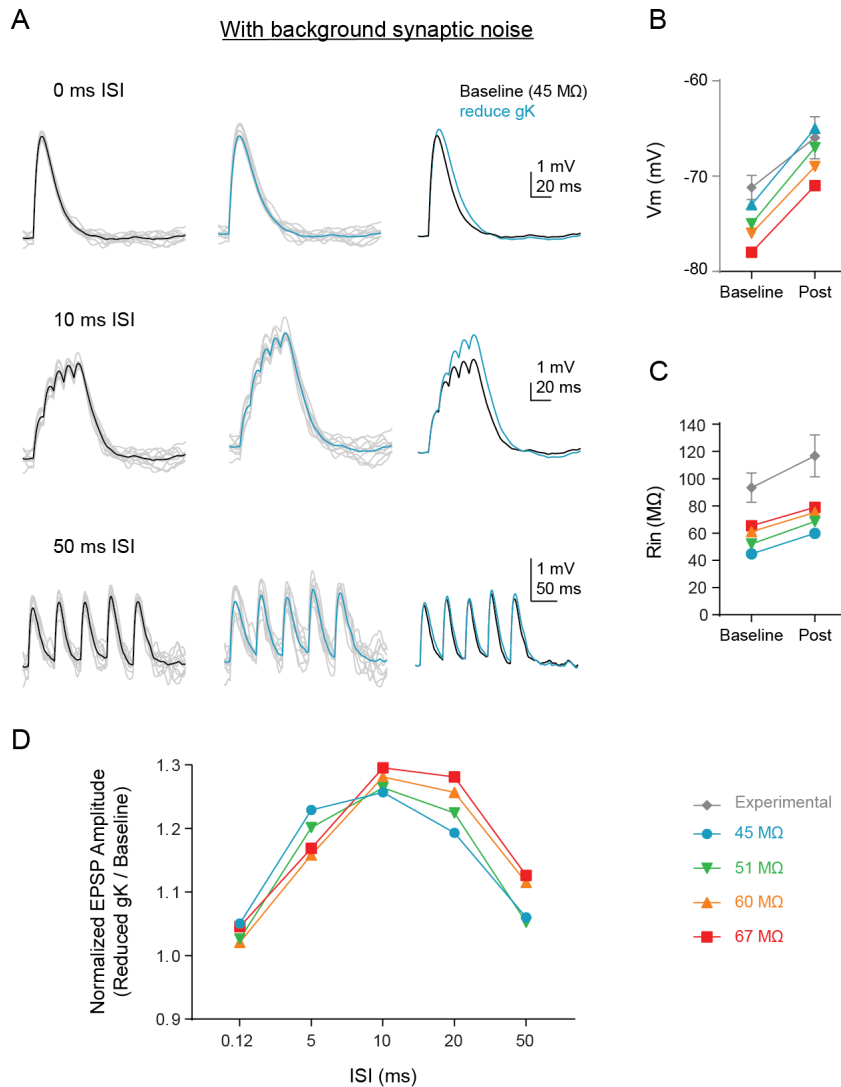


Figure 2.16 – Supplement to Figure 6. Background synaptic noise does not change summation enhancement.

A) Experimental design: Synaptic noise was included at various levels in a subset of dendrites of the compartmental model and synapses in model (Figure 6C) were stimulated at variable ISIs. Example traces for compound EPSPs at baseline (black, left) and after reducing gK by 70% (blue, middle) when initial input resistance was 45 MΩ to closely match in vivo conditions. Gray traces are single example trials. B-C) Comparisons of model (colored) and experimental (gray) intrinsic properties at baseline (circles) and after manipulations (colored = model: reducing gK by 70%, black = experimental: application of 5HT). D) The ratio of amplitude of the 5th EPSP (Reduced gK / Baseline) as a function of interval for different levels of synaptic noise to change baseline R_{in}.

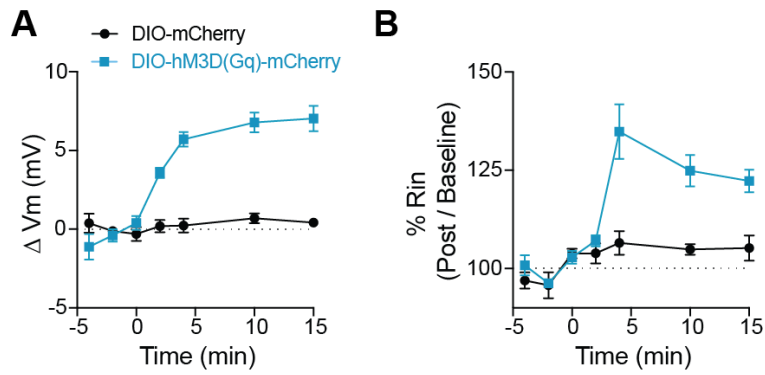


Figure 2.17 – Supplement to Figure 7. CNO has no effect on FSIs not expressing DREADD.

A-B) Change in membrane potential (A) and input resistance (B) over time with application of CNO in FSIs that either express the Gq-coupled DREADD, hM3D(Gq)-mCherry (blue) or a control fluorophore, mCherry (black). CNO application begins at time 0.

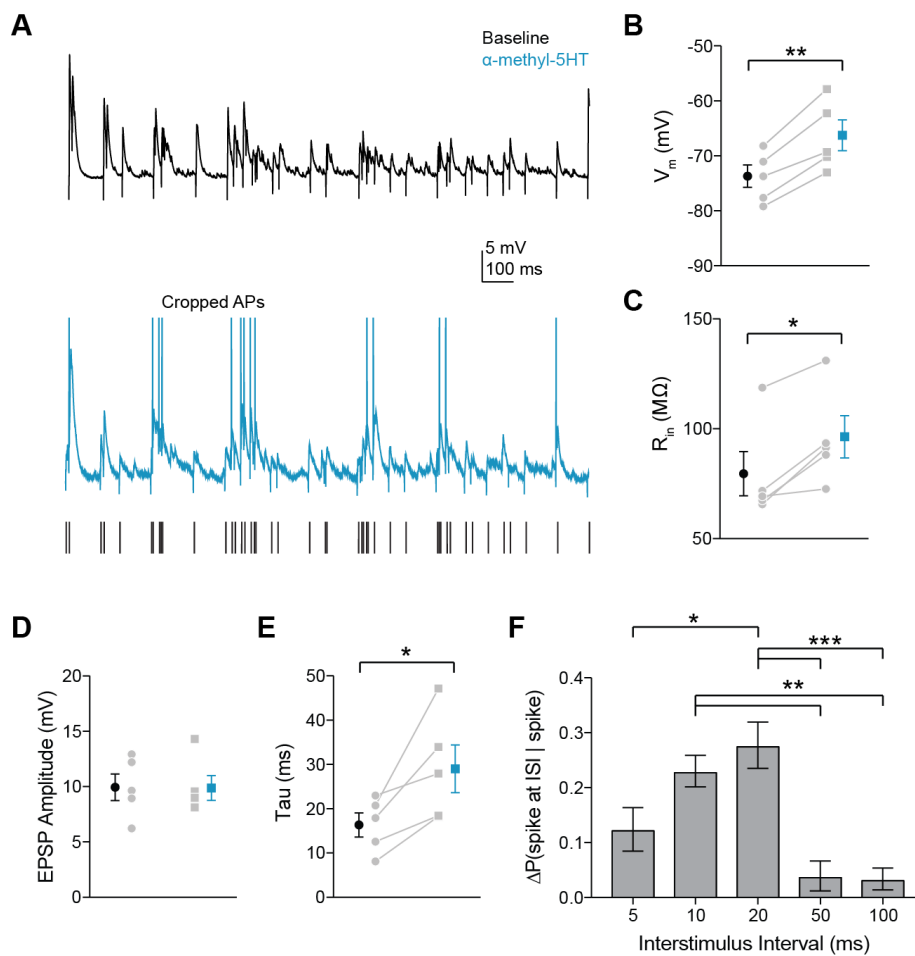


Figure 2.18 – Supplement to Figure 7. 5HT2A agonist increases probability of FSI firing in response to gamma frequency inputs.

A) Experimental design: A stimulating electrode was placed in the tissue within 100 μm of the recorded FSI and a 2 second train of randomly distributed stimulating current pulses (200 μs) with varied interstimulus intervals (ISIs = 5, 10, 20, 50, 100 ms) was delivered. Example FSI responses to stimulus train at baseline (black) and after application of the 5HT2A agonist α -methyl-5HT (blue). B-C) Change in membrane potential (B) and input resistance (C) with application of α -methyl-5HT. D-E) Change in amplitude (B) and tau (C) for subthreshold events with application of α -methyl-5HT. F) Change in the percentage of all spikes occurring at each ISI after CNO. * $p < 0.05$, ** $p < 0.01$ *** $p < 0.005$

2.7 REFERENCES

- Abrahamsson, T., Cathala, L., Matsui, K., Shigemoto, R., Digregorio, D.A., 2012. Thin dendrites of cerebellar interneurons confer sublinear synaptic integration and a gradient of short-term plasticity. *Neuron* 73, 1159–72.
- Alagem, Dvir, and Reuveny, 2001. Mechanism of Ba(2+) block of a mouse inwardly rectifying K⁺ channel: differential contribution by two discrete residues. *J Physiology* 534, 381–93.
- Araneda, Andrade, 1991. 5-Hydroxytryptamine₂ and 5-hydroxytryptamine_{1A} receptors mediate opposing responses on membrane excitability in rat association cortex. *Neuroscience* 40, 399–412.
- Arora, Meltzer, 1991. Serotonin₂ (5-HT₂) receptor binding in the frontal cortex of schizophrenic patients. *J Neural Transm* 85, 19–29.
- Avesar, D., Gullledge, A.T., 2012. Selective serotonergic excitation of callosal projection neurons. *Front Neural Circuits* 6, 12.
- Baker, P.M., Thompson, J.L., Sweeney, J.A., Ragozzino, M.E., 2011. Differential effects of 5-HT(2A) and 5-HT(2C) receptor blockade on strategy-switching. *Behav. Brain Res.* 219, 123–31.
- Bartos, M., Vida, I., Frotscher, M., Meyer, A., Monyer, H., Geiger, J., Jonas, P., 2002. Fast synaptic inhibition promotes synchronized gamma oscillations in hippocampal interneuron networks. *Proceedings of the National Academy of Sciences* 99, 13222–13227.
- Bartos, M., Vida, I., Jonas, P., 2007. Synaptic mechanisms of synchronized gamma oscillations in inhibitory interneuron networks. *Nat Rev Neurosci* 8, 45–56.
- Bracci, E., Centonze, D., Bernardi, G., Calabresi, P., 2003. Voltage-dependent membrane potential oscillations of rat striatal fast-spiking interneurons. *J. Physiol. (Lond.)* 549, 121–30.
- Buzsáki, G., Chrobak, J.J., 1995. Temporal structure in spatially organized neuronal ensembles: a role for interneuronal networks. *Curr. Opin. Neurobiol.* 5, 504–10.
- Buzsáki, G., Wang, X.-J., 2012. Mechanisms of Gamma Oscillations. *Annu. Rev. Neurosci.*
- Cardin, J., Carlén, M., Meletis, K., Knoblich, U., Zhang, F., Deisseroth, K., Tsai, L.-H., Moore, C., 2009. Driving fast-spiking cells induces gamma rhythm and controls sensory responses. *Nature* 459, 663–7.

Carli, M., Baviera, M., Invernizzi, R.W., Balducci, C., 2006. Dissociable contribution of 5-HT_{1A} and 5-HT_{2A} receptors in the medial prefrontal cortex to different aspects of executive control such as impulsivity and compulsive perseveration in rats. *Neuropsychopharmacology* 31, 757–67.

Cho, K.K.A., Hoch, R., Lee, A.T., Patel, T., Rubenstein, J.L.R., Sohal, V.S., 2015. Gamma Rhythms Link Prefrontal Interneuron Dysfunction with Cognitive Inflexibility in *Dlx5/6*^{+/-} Mice. *Neuron* 85, 1332–1343.

Clarke, H.F., Dalley, J.W., Crofts, H.S., Robbins, T.W., Roberts, A.C., 2004. Cognitive inflexibility after prefrontal serotonin depletion. *Science* 304, 878–80.

Clarke, H.F., Walker, S.C., Dalley, J.W., Robbins, T.W., Roberts, A.C., 2007. Cognitive inflexibility after prefrontal serotonin depletion is behaviorally and neurochemically specific. *Cereb. Cortex* 17, 18–27.

Dias, R., Robbins, T.W., Roberts, A.C., 1996. Primate analogue of the Wisconsin Card Sorting Test: effects of excitotoxic lesions of the prefrontal cortex in the marmoset. *Behav. Neurosci.* 110, 872–86.

Euston, D., Gruber, A., McNaughton, B., 2012. The Role of Medial Prefrontal Cortex in Memory and Decision Making. *Neuron* 76.

Drevets, W., Price, J., and Furey, M., 2008. Brain structural and functional abnormalities in mood disorders: implications for neurocircuitry models of depression. *Brain Struct Funct* 213, 93–118.

Fellous, J.M., Houweling, A.R., Modi, R.H., Rao, R.P., Tiesinga, P.H., Sejnowski, T.J., 2001. Frequency dependence of spike timing reliability in cortical pyramidal cells and interneurons. *J. Neurophysiol.* 85, 1782–7.

Freund, T.F., Katona, I., 2007. Perisomatic inhibition. *Neuron* 56, 33–42.

Galarreta, Hestrin, 2001. Spike transmission and synchrony detection in networks of GABAergic interneurons. *Science (New York, N.Y.)* 292, 2295–9.

Gonzalez-Burgos, G., Cho, R.Y., Lewis, D.A., 2015. Alterations in Cortical Network Oscillations and Parvalbumin Neurons in Schizophrenia. *Biol. Psychiatry*.

Gonzalez-Burgos, G., Hashimoto, T., Lewis, D., 2010. Alterations of cortical GABA neurons and network oscillations in schizophrenia. *Current psychiatry reports* 12, 335–44.

Gulyás, A.I., Megías, M., Emri, Z., Freund, T.F., 1999. Total number and ratio of excitatory and inhibitory synapses converging onto single interneurons of different types in the CA1 area of the rat hippocampus. *J. Neurosci.* 19, 10082–97.

- Hu, H., Martina, M., and Jonas, P., 2010. Dendritic Mechanisms Underlying Rapid Synaptic Activation of Fast-Spiking Hippocampal Interneurons. *Science* 327, 52–58.
- Kim, H., Ährlund-Richter, S., Wang, X., Deisseroth, K., and Carlén, M., 2016. Prefrontal Parvalbumin Neurons in Control of Attention. *Cell* 164, 208–218.
- Koot, S., Zoratto, F., Cassano, T., Colangeli, R., Laviola, G., Bos, R. van den, Adriani, W., 2012. Compromised decision-making and increased gambling proneness following dietary serotonin depletion in rats. *Neuropharmacology* 62, 1640–50.
- Lee, S., Hjerling-Leffler, J., Zaghera, E., Fishell, G., and Rudy, B., 2010. The largest group of superficial neocortical GABAergic interneurons expresses ionotropic serotonin receptors. *J. Neurosci.* 30, 16796–808.
- Lewis, D., Hashimoto, T., Volk, D., 2005. Cortical inhibitory neurons and schizophrenia. *Nature Reviews Neuroscience* 6, 312–324.
- McBain, Fisahn, 2001. Interneurons unbound.
- Meltzer, H.Y., Li, Z., Kaneda, Y., Ichikawa, J., 2003. Serotonin receptors: their key role in drugs to treat schizophrenia. *Prog. Neuropsychopharmacol. Biol. Psychiatry* 27, 1159–72.
- Meltzer, Massey, 2011. The role of serotonin receptors in the action of atypical antipsychotic drugs. *Current Opinion in Pharmacology*.
- Michalikova M, Remme MWH, Kempter R., 2016. Spikelets in Pyramidal Neurons: Action Potentials Initiated in the Axon Initial Segment that do not Activate the Soma *PLOS Comp Biol*, 13.
- Mintz, Gotow, Triller, and Korn, 1989. Effect of serotonergic afferents on quantal release at central inhibitory synapses. *Science* 245, 190–192
- Moca, V.V., Nikolic, D., Singer, W., Mureşan, R.C., 2014. Membrane resonance enables stable and robust gamma oscillations. *Cereb. Cortex* 24, 119–42.
- Nörenberg, A., Hu, H., Vida, I., Bartos, M., Jonas, P., 2010. Distinct nonuniform cable properties optimize rapid and efficient activation of fast-spiking GABAergic interneurons. *Proc. Natl. Acad. Sci. U.S.A.* 107, 894–9.
- Pala, A., and Petersen, C., 2015. In Vivo Measurement of Cell-Type-Specific Synaptic Connectivity and Synaptic Transmission in Layer 2/3 Mouse Barrel Cortex. *Neuron* 85, 68–75.

- Passamonti, L., Crockett, M., Apergis-Schoute, A., Clark, L., Rowe, J., Calder, A., and Robbins, T., 2012. Effects of Acute Tryptophan Depletion on Prefrontal-Amygdala Connectivity While Viewing Facial Signals of Aggression. *Biol Psychiat* 71, 36–43.
- Pike, F.G., Goddard, R.S., Suckling, J.M., Ganter, P., Kasthuri, N., Paulsen, O., 2000. Distinct frequency preferences of different types of rat hippocampal neurones in response to oscillatory input currents. *J. Physiol. (Lond.)* 529 Pt 1, 205–13.
- Puig, M.V., Watakabe, A., Ushimaru, M., Yamamori, T., Kawaguchi, Y., 2010. Serotonin modulates fast-spiking interneuron and synchronous activity in the rat prefrontal cortex through 5-HT1A and 5-HT2A receptors. *J. Neurosci* 30, 2211-22.
- Puig, M.V., Gullledge, A.T., 2011. Serotonin and prefrontal cortex function: neurons, networks, and circuits. *Mol. Neurobiol.* 44, 449–64.
- Ray, R.D., Zald, D.H., 2012. Anatomical insights into the interaction of emotion and cognition in the prefrontal cortex. *Neurosci Biobehav Rev* 36, 479–501.
- Risch, S.C., Nemeroff, C.B., 1992. Neurochemical alterations of serotonergic neuronal systems in depression. *J Clin Psychiatry* 53 Suppl, 3–7.
- Rudy, B., Fishell, G., Lee, S., Hjerling-Leffler, J., 2011. Three groups of interneurons account for nearly 100% of neocortical GABAergic neurons. *Dev Neurobiol* 71, 45–61.
- Schulz, S., Heidmann, K., Mike, A., Klafz, Z., Heinemann, U., Gerevich, Z., 2012. First and second generation antipsychotics influence hippocampal gamma oscillations by interactions with 5-HT3 and D3 receptors. *British Journal of Pharmacology* 167, 1480–91.
- Selvaraj, S., Arnone, D., Cappai, A., Howes, O., 2014. Alterations in the serotonin system in schizophrenia: a systematic review and meta-analysis of postmortem and molecular imaging studies. *Neurosci Biobehav Rev* 45, 233–45.
- Sohal, V.S., Zhang, F., Yizhar, O., Deisseroth, K., 2009. Parvalbumin neurons and gamma rhythms enhance cortical circuit performance. *Nature* 459, 698–702.
- Stuart, G., Spruston, N., 2015. Dendritic integration: 60 years of progress. *Nature Neuroscience* 18, 1713-21.
- Tamás, G., Buhl, E.H., Lörincz, A., Somogyi, P., 2000. Proximally targeted GABAergic synapses and gap junctions synchronize cortical interneurons. *Nature neuroscience* 3, 366–371.
- Titeler, M., Lyon, R.A., Glennon, R.A., 1988. Radioligand binding evidence implicates the brain 5-HT2 receptor as a site of action for LSD and phenylisopropylamine hallucinogens. *Psychopharmacology (Berl.)* 94, 213–6.

- Uhlhaas, P., Singer, W., 2010. Abnormal neural oscillations and synchrony in schizophrenia. *Nature reviews. Neuroscience* 11, 100–113.
- Weber, E., Andrade, R., 2010. Htr2a Gene and 5-HT2A Receptor Expression in the Cerebral Cortex Studied Using Genetically Modified Mice. *Frontiers in Neuroscience* 4.
- Williams, GV, Rao, SG, 2002. The physiological role of 5-HT2A receptors in working memory. *The Journal of ...*
- Willner, P., 1985. Antidepressants and serotonergic neurotransmission: an integrative review. *Psychopharmacology (Berl.)* 85, 387–404.
- Zhong, P., Yan, Z., 2011. Differential Regulation of the Excitability of Prefrontal Cortical Fast-Spiking Interneurons and Pyramidal Neurons by Serotonin and Fluoxetine. *PLoS ONE* 6, e16970.
- Zhou, F.M., Hablitz, J.J., 1999. Activation of serotonin receptors modulates synaptic transmission in rat cerebral cortex. *J. Neurophysiol.* 82, 2989–99.

CHAPTER 3

SEROTONIN 1B RECEPTORS REGULATE PREFRONTAL FUNCTION BY GATING CALLOSAL AND HIPPOCAMPAL INPUTS

3.1 ABSTRACT

Both the medial prefrontal cortex (mPFC) and serotonin play key roles in anxiety, however, specific mechanisms through which serotonin might act on the mPFC to modulate anxiety-related behavior remain unknown. Here, we use a combination of optogenetics and synaptic physiology to show that serotonin acts presynaptically via 5-HT1B receptors to selectively suppress inputs from the contralateral mPFC and ventral hippocampus (vHPC), while sparing those from mediodorsal thalamus. To elucidate how these actions could potentially regulate prefrontal circuit function, we infused a 5-HT1B agonist into the mPFC of freely behaving mice. Consistent with previous studies that have optogenetically inhibited vHPC-mPFC projections, activating prefrontal 5-HT1B receptors suppressed theta-frequency (4-12 Hz) mPFC activity, and also reduced avoidance of anxiogenic regions in the elevated plus maze. These findings suggest a potential mechanism, linking specific receptors, synapses, patterns of circuit activity, and behavior, through which serotonin may regulate prefrontal circuit function including anxiety-related behaviors.

3.2 INTRODUCTION

The medial prefrontal cortex (mPFC) is an associational cortical region receiving a wide range of inputs from sensory cortices as well as contralateral mPFC, and is connected to limbic areas such as thalamus, hippocampus, and amygdala (Ishikawa and Nakamura, 2006; Miller and Cohen, 2001; Vertes, 2004; Verwer et al., 1997).

Serotonin is believed to play an important role in regulating prefrontal function, since mPFC receives dense serotonergic innervation from the raphe nuclei (Groenewegen and Uylings, 2000; Hajós et al., 1998). Nevertheless, specific mechanisms through which serotonin might act on the mPFC to regulate network function remain largely unknown. In mPFC, as well as other forebrain regions, serotonin is generally believed to modulate circuit function through postsynaptic effects (Crino et al., 1990; de Almeida and Mengod, 2008; Santana et al., 2004). The postsynaptic effects of serotonin are mediated in large part by 5-HT_{1A} receptors, such that most prefrontal neurons are inhibited by serotonin (Araneda and Andrade, 1991; Béique et al., 2004; Zhong and Yan, 2011). However, serotonin can also regulate presynaptic neurotransmitter release. The identity of presynaptically located serotonin receptors remains largely unknown, but has been suggested to comprise 5-HT_{1A}, 5-HT_{1B}, and/or 5-HT_{2A} receptors (Murakoshi et al., 2001; Tanaka and North, 1993; Troca-Marín and Geijo-Barrientos, 2010; Zhou and Hablitz, 1999).

Recent studies suggest that the mPFC may guide anxiety-related behaviors through interactions with the ventral hippocampus (vHPC) (Ciocchi et al., 2015). Specifically, theta-frequency synchronization between these two regions increases in aversive environments (Adhikari et al., 2010). At the level of single neurons, mPFC neurons that encode aspects of anxiety-related behavior tend to phase-lock to ongoing theta-frequency activity in the hippocampus (Adhikari et al., 2011). This suggests that vHPC inputs to mPFC may transmit theta-frequency activity that encodes anxiety-related signals, and indeed, theta frequency activity in the mPFC seems to actively inhibit the exploration of anxiogenic regions (Adhikari et al., 2010). Conversely,

optogenetically suppressing vHPC inputs to mPFC elicits anxiolytic effects by suppressing theta-frequency synchronization between the vHPC and mPFC (Padilla-Coreano et al., 2016). Thus, if serotonin does act presynaptically to control transmitter release, it could potentially gate afferent inputs from limbic regions such as the vHPC to mPFC and thereby regulate behavior.

To explore such a role for serotonin, we first investigated the effects of serotonin receptor activation on callosal, hippocampal, and MD thalamic projections to the mPFC, then explored how these synaptic effects might impact circuit physiology and anxiety-related behavior. We found that by activating presynaptic 5-HT_{1B} receptors, serotonin selectively inhibits callosal and hippocampal inputs to mPFC, and that prefrontal infusion of a 5-HT_{1B} receptor agonist suppresses prefrontal theta oscillations and elicits anxiolytic effects. These findings define – at the levels of synaptic function, in vivo electrophysiology, and behavior – a circuit mechanism through which prefrontal 5-HT_{1B} receptors can acutely suppress ventral hippocampal inputs and thereby potentially regulate theta-frequency activity and anxiety-related behavior.

The medial prefrontal cortex (mPFC) is an associational cortical region receiving a wide range of inputs from sensory cortices as well as contralateral mPFC, and is connected to limbic areas such as thalamus, hippocampus, and amygdala (Ishikawa and Nakamura, 2006; Miller and Cohen, 2001; Vertes, 2004; Verwer et al., 1997). Serotonin is believed to play an important role in regulating prefrontal function, since mPFC receives dense serotonergic innervation from the raphe nuclei (Groenewegen and Uylings, 2000; Hajós et al., 1998). Nevertheless, specific mechanisms through which serotonin might act on the mPFC to regulate network function remain largely

unknown. In mPFC, as well as other forebrain regions, serotonin is generally believed to modulate circuit function through postsynaptic effects (Crino et al., 1990; de Almeida and Mengod, 2008; Santana et al., 2004). The postsynaptic effects of serotonin are mediated in large part by 5-HT_{1A} receptors, such that most prefrontal neurons are inhibited by serotonin (Araneda and Andrade, 1991; Béique et al., 2004; Zhong and Yan, 2011). However, serotonin can also regulate presynaptic neurotransmitter release. The identity of presynaptically located serotonin receptors remains largely unknown, but has been suggested to comprise 5-HT_{1A}, 5-HT_{1B}, and/or 5-HT_{2A} receptors (Murakoshi et al., 2001; Tanaka and North, 1993; Troca-Marín and Geijo-Barrientos, 2010; Zhou and Hablitz, 1999).

Recent studies suggest that the mPFC may guide anxiety-related behaviors through interactions with the ventral hippocampus (vHPC) (Ciocchi et al., 2015). Specifically, theta-frequency synchronization between these two regions increases in aversive environments (Adhikari et al., 2010). At the level of single neurons, mPFC neurons that encode aspects of anxiety-related behavior tend to phase-lock to ongoing theta-frequency activity in the hippocampus (Adhikari et al., 2011). This suggests that vHPC inputs to mPFC may transmit theta-frequency activity that encodes anxiety-related signals, and indeed, theta frequency activity in the mPFC seems to actively inhibit the exploration of anxiogenic regions (Adhikari et al., 2010). Conversely, optogenetically suppressing vHPC inputs to mPFC elicits anxiolytic effects by suppressing theta-frequency synchronization between the vHPC and mPFC (Padilla-Coreano et al., 2016). Thus, if serotonin does act presynaptically to control transmitter

release, it could potentially gate afferent inputs from limbic regions such as the vHPC to mPFC and thereby regulate behavior.

To explore such a role for serotonin, we first investigated the effects of serotonin receptor activation on callosal, hippocampal, and MD thalamic projections to the mPFC, then explored how these synaptic effects might impact circuit physiology and anxiety-related behavior. We found that by activating presynaptic 5-HT_{1B} receptors, serotonin selectively inhibits callosal and hippocampal inputs to mPFC, and that prefrontal infusion of a 5-HT_{1B} receptor agonist suppresses prefrontal theta oscillations and elicits anxiolytic effects. These findings define – at the levels of synaptic function, in vivo electrophysiology, and behavior – a circuit mechanism through which prefrontal 5-HT_{1B} receptors can acutely suppress ventral hippocampal inputs and thereby potentially regulate theta-frequency activity and anxiety-related behavior.

3.3 METHODS

All experiments were conducted in accordance with protocols approved by the Administrative Panels on Laboratory Animal Care at the University of California, San Francisco.

3.31 Slice electrophysiology and optogenetics

We expressed hChR2-eYFP in neurons within mPFC, MD thalamus, and vHPC using a previously described AAV5 vector encoding hChR2-eYFP under control of the CaMKII α promoter (37). After waiting at least 4-6 weeks, we prepared 250 μ m coronal slices from 8-12 week-old wild-type C57BL/6 male mice, and made whole cell

recordings using patch pipettes filled with a Cs-methanesulfonate based solution from pyramidal neurons in layer V of infralimbic or prelimbic cortex (contralateral to the site of virus injection). We stimulated ChR2 in axon terminals using flashes of 470 nm light delivered to the slice through a 40x objective.

3.32 Drug infusion

We implanted stainless steel dual guide cannulas bilaterally into mPFC. One week later, we infused drug through a stainless steel internal cannula projecting 1.5 mm beyond the tip of the guide cannula in a volume of 0.5 μ L saline at a rate of 150 nL/min (EPM experiments) or 50 nL/min (LFP recording).

3.33 Local field potential recording

50 k Ω impedance tungsten electrodes were attached to the right arm of a dual guide cannula and implanted in mPFC. Two stainless steel screws acting as reference and ground were implanted above cerebellum. The electrode and screws were attached to a head mount using conductive wire and the set-up was cemented down. Mice recovered for one week before recording/infusion sessions, and signal was acquired using an EEG monitoring and acquisition system (Pinnacle Technology).

3.34 Behavior

C57BL/6 male mice were kept in a 12-h light/12-h dark cycle with ad libitum access to food and water. The elevated plus maze (EPM) consisted of two open and two closed arms (arm length: 50 cm; width: 6 cm) extending from a central platform, and the open

field was 50 x 50 cm. Mice were infused with drug and placed in the center of the EPM and the head and body of the mouse was tracked (ANYmaze software) for 15 min.

3.4 RESULTS

3.41 Serotonin suppresses synaptic input to prefrontal pyramidal neurons in a projection-specific manner

To investigate how serotonin affects various inputs to pyramidal neurons in prefrontal cortex, we made whole-cell recordings (voltage-clamped at -70 mV) from layer V pyramidal neurons and examined how serotonin wash-in affected EPSCs elicited by optogenetic stimulation of terminals from the contralateral mPFC, vHPC, or MD thalamus (Figure 3.1A). We expressed ChR2 in one hemisphere of the mPFC, vHPC, or MD thalamus, and used light flashes (470 nm; light intensity adjusted to yield an EPSC three times the size of the smallest possible evoked EPSC) to stimulate the terminals. To minimize possible contamination from polysynaptic responses, we measured the EPSC amplitude 1.5 ms after light stimulation (zoomed trace, Figure 3.1B). Evoked EPSCs were blocked by application of 1 μ M of the voltage-sensitive sodium channel blocker, TTX (Supplementary Figure 3.5).

We found that 5 min after wash-in, 30 μ M serotonin reduced the initial amplitude of EPSCs evoked by optogenetic stimulation of terminals from contralateral mPFC by almost half ($46 \pm 9\%$ reduction; $p < 0.01$; Figure 3.1B). Input from vHPC was similarly reduced by $36 \pm 7\%$ ($p < 0.01$; Figure 3.1C). However, no effect of serotonin application was observed for EPSCs evoked by stimulation of MD thalamic terminals ($p > 0.05$; Figure 3.1D). Thus, serotonin suppresses specific inputs to PFC (Figure 3.1E). As a

control, we confirmed that this reduction in EPSC amplitude (induced by activation of callosal terminals) was not simply an artifact due to time-dependent effects (Figure 3.1F). The suppressing effect of serotonin was also dose dependent: 1 μ M reduced callosal EPSCs by $23 \pm 7\%$, 3 μ M serotonin elicited a near-maximal effect ($44 \pm 7\%$ suppression), and the effect saturated at 10 and 30 μ M, which reduced EPSCs by $51 \pm 8\%$ and $53 \pm 12\%$, respectively (Figure 3.1G).

3.42 Serotonin suppresses synaptic input through the 5-HT1B receptor

Next, we sought to understand which 5-HT receptors mediate this synaptic suppression. We specifically studied the effects of agonists for 5-HT1A (100 nM 8-OH DPAT), 5-HT1B (300 nM CP 93129), and 5-HT7 (10 nM LP-44) receptors on callosal or vHPC EPSCs. Importantly, we also performed control recordings with no drug wash-in. This allowed us to confirm that drug-induced changes in EPSC amplitude were not simply artifacts of time-dependent rundown. For each experiment, Figure 3.2 shows the EPSC amplitude (normalized to the baseline EPSC amplitude at the beginning of each experiment) as a function of time; the time course observed during drug application is superimposed over the time course observed during control experiments (no drug). To determine whether drug application was associated with a statistically significant change in EPSC amplitude, we compared the EPSC amplitude during drug application to the average of the amplitude measured before and after drug application. For callosal inputs, the normalized EPSC amplitude during application of the 5-HT1B agonist, CP 93129, was $58 \pm 5\%$ of the baseline amplitude. This was significantly smaller than the average of the amplitudes during the pre- and post-drug periods, which was $87 \pm 6\%$ of

baseline ($p < 0.01$; Figure 3.2B). Notably, the reduction observed during CP 93129 application was almost identical to the one observed during application of $3 \mu\text{M}$ serotonin (pre/post amplitude: $85 \pm 4\%$; amplitude during 5-HT application: $57 \pm 6\%$; $p < 0.05$; Figure 3.2A). For vHPC input, the amount of EPSC suppression was again very similar for $3 \mu\text{M}$ 5-HT (pre/post: $77 \pm 4\%$; 5-HT: $56 \pm 8\%$; $p < 0.05$; Figure 3.2E) and the 5-HT_{1B} receptor agonist, CP 93129 (pre/post: $84 \pm 3\%$; CP 93129: $50 \pm 4\%$; $p < 0.001$; Figure 3.2F). Notably, the reductions in EPSC amplitude observed during application of CP 93129 and 5-HT were not observed during control recordings (no drug). Specifically, for both callosal and vHPC EPSCs, we observed 40-50% reductions in EPSC amplitude immediately following drug application, whereas at the same time points in control recordings, we observed only minimal amounts of rundown. In control recordings, normalized EPSC amplitudes were $86 \pm 4\%$ and $88 \pm 7\%$ of baseline for callosal and vHPC EPSCs, respectively (amplitude of callosal EPSCs: $p < 0.001$ for CP 93129 vs. control and $p < 0.01$ for 5-HT vs. control; Figure 3.2D and Figure 3.6E; amplitude of vHPC EPSCs: $p < 0.001$ for CP 93129 vs. control and $p < 0.05$ for 5-HT vs. control; Figure 3.2H and Figure 3.6E). Importantly, as can be seen by comparing the time course of EPSC amplitudes in control conditions vs. during drug application, in every case, the suppression of callosal or hippocampal EPSCs by 5-HT or CP 93129 was reversible, and the EPSC amplitudes returned to control levels after 4-5 min of drug washout.

To confirm that the effects of CP 93129 reflect specific actions on 5-HT_{1B} receptors, we carried out additional experiments in which we first applied $10 \mu\text{M}$ of the 5-HT_{1B} receptor antagonist, SB 216641, for 20 min. Applying CP 93129 in the

presence of SB 216641 blocked the CP 93129-induced suppression of callosal input (EPSC amplitude in SB 216641, pre/post: $83 \pm 6\%$; CP 93129 + SB 216641: $78 \pm 3\%$; n.s.; Figure 3.2C). For vHPC input, CP 93129 still caused a slight reduction in EPSC amplitude (SB 216641, pre/post: $73 \pm 3\%$; CP 93129 + SB 216641: $64 \pm 5\%$; $p < 0.01$; Figure 3.2G). However, for both callosal and vHPC input, the EPSC suppression induced by CP 93129 alone was significantly larger than that elicited by CP 93129 in the presence of SB 216641 ($p < 0.01$ for callosal input, Figure 3.2D; $p < 0.05$ for vHPC input, Figure 3.2H), confirming that the EPSC suppression was mediated largely by 5-HT_{1B} receptors.

In contrast to the effects of the 5-HT_{1B} receptor agonist CP 93129, the 5-HT_{1A} and 5-HT₇ receptor agonists, 8-OH DPAT and LP-44, respectively, had no consistent reversible effects on EPSC amplitudes elicited by either callosal (8-OH DPAT, pre/post: $72 \pm 8\%$; drug: $82 \pm 2\%$; n.s.. LP-44, pre/post: $80 \pm 10\%$; drug: $82 \pm 4\%$; n.s., Figure 3.2D, Figure 3.6A,B) or vHPC terminal stimulation (8-OH DPAT, pre/post: $75 \pm 4\%$; drug: $76 \pm 4\%$; n.s.. LP-44, pre/post: $84 \pm 4\%$; drug: $86 \pm 4\%$; n.s.. Figure 3.2H, Figure 3.6C,D).

3.43 Serotonin suppresses synaptic input via presynaptic inhibition

To investigate whether this 5-HT_{1B} receptor-mediated EPSC suppression reflects presynaptic mechanisms, we first measured the paired pulse ratio (PPR) for pairs of EPSCs evoked via optogenetic stimulation of callosal or vHPC terminals using interflash intervals (IFI) of 50 ms (Figure 3.3A and F). We measured the PPR during 3-

min wash-in of 5-HT (3 μ M), CP 93129 (300 nM), and CP 93129 in combination with the 5-HT_{1B} receptor antagonist SB 216641 (10 μ M).

For callosal terminals, 5-HT and CP 93129 increased PPR to $118 \pm 2\%$ and $117 \pm 4\%$ of control, respectively ($p < 0.01$; Figure 3.3B and C). This effect could be washed out for CP 93129 (drug versus post-drug: $p < 0.05$). Pre-application of the 5-HT_{1B} receptor antagonist, SB 216641, blocked the PPR increase induced by CP 93129 ($p < 0.05$; Figure 3.3D and E). For vHPC terminals, there was a no effect of 3 μ M 5-HT application on PPR (Figure 3.3G). CP 93129 did significantly increase the PPR compared to the pre-drug period ($114 \pm 4\%$; $p < 0.05$; Figure 3.3H) and this effect was reversed during drug wash-out (drug versus post-drug: $p < 0.01$). The CP 93129 induced increase in PPR was blocked by pre-application of SB 216641 (Figure 3.3I and J).

Of course, measurements of PPR may be imperfect in optogenetic experiments, because PPR in this setting is an amalgamation of short-term synaptic dynamics, i.e., depression/facilitation, and ChR2 inactivation. Therefore, to more strongly establish a presynaptic locus for the effects of serotonin, we also performed a quantal analysis of synaptic responses by recording asynchronous unitary EPSCs (uEPSC) elicited by optogenetic stimulation of either callosal or vHPC terminals after replacing calcium in the external solution with strontium (Sr^{2+} , 2 mM) (Figure 3.3K). Light intensity was adjusted to produce an EPSC of ~ 200 pA, and analysis of uEPSCs started 50 ms after each flash. uEPSCs from each recorded cell were collected following 120 light stimulations (delivered with a 3 second inter-stimulus interval), both before and following serotonin and CP 93129 wash-in. After washing in serotonin, we observed a reduction

in the frequency of uEPSCs following each stimulus delivered to callosal terminals ($p < 0.05$; Figure 3.3M), with no change in uEPSC amplitude, rise time, or decay time (Figure 3.3L and Figure 3.7). We observed a similar effect when stimulating terminals from vHPC: serotonin reduced uEPSC frequency ($p < 0.05$; Figure 3.3O), but had no effect on uEPSC amplitude or kinetics (Figure 3.3N and Figure 3.7). We confirmed that the selective 5-HT_{1B} receptor agonist CP 93129 (300 nM) elicits a similar, selective reduction in uEPSC frequency, without affecting the amplitude or kinetics of uEPSCs evoked by vHPC terminal stimulation (Figure 3.7).

3.44 Local infusion of a 5-HT_{1B} receptor agonist into mPFC reduces innate anxiety

To determine whether this 5-HT_{1B} receptor-mediated inhibition of callosal and hippocampal inputs to mPFC could regulate anxiety-related behavior, we infused the 5-HT_{1B} receptor agonist, CP 93129, into the mPFC of freely moving mice while measuring anxiety-related behavior using the EPM. The EPM consists of two open and two closed arms. The open arms are exposed to the external environment so increased time spent in the open arms is commonly interpreted as reflecting reduced levels of innate anxiety (Figure 3.4A). CP 93129 (4.3 ng in 0.5 μ L, 150 nL/min) or saline (0.5 μ L) was infused bilaterally into the mPFC through an implanted guide cannula. 1 min after the internal infusion cannula was removed, the animal was placed in the EPM for 15 min. Compared to saline, CP 93129 increased the time mice spent in open arms during the first 5-min of the EPM (the period during which most open arm exploration occurs). There was no difference during the two subsequent 5-min bins, during which both

groups of animals spent much less time exploring the open arms (Figure 3.4A). We also tested the effect of CP 93129 infusion on behavior in the open field (10 min), and no difference in the distance moved was evident for the first 6 min of the test (Figure 3.4B). In addition, CP 93129 had a slight tendency to increase time spent in the center of the open field for the first 2 min of the test ($p = 0.14$; Figure 3.8A).

3.45 Local infusion of a 5-HT1B receptor agonist suppresses mPFC theta power

To investigate possible circuit mechanisms that might link the 5-HT1B receptor-mediated suppression of hippocampal input to this ability of 5-HT1B agonists to reduce anxiety-related avoidance in the EPM, we implanted animals with integrated guide cannulas/tungsten electrodes and recorded local field potentials (LFP) in mPFC continuously during 10 min infusion of the 5-HT1B receptor agonist, CP 93129 (4.3 ng in 0.5 μ L, 50 nL/min) or saline (Figure 3.4C), while the animal was in a resting cage. We compared the LFP power at various frequencies for the 4 min periods leading up to the start of infusion, and following the end of infusion, for both saline and CP 93129 infusions (Figure 3.4D and E). Compared to saline infusion, infusion of CP 93129 was associated with reduced power (ANOVA on the log-transformed power post-infusion/pre-infusion: treatment: $p < 0.01$; treatment x frequency band interaction: $p < 0.01$). A selective reduction in theta (4-12 Hz) as well as alpha and beta (12-30 Hz) power was evident (Figure 3.4D and E; $p < 0.05$). There was no significant change in power at lower (1-4 Hz) or higher frequencies (30-100 Hz).

Of course, it is possible that the behavioral and electrophysiological effects of 5-HT1B receptor agonist infusion reflects actions other than the 5-HT1B receptor-

mediated suppression of synaptic input that we have described. To address this possible concern we confirmed that in contrast to serotonin itself, 5-HT1B receptor agonist application does not alter the intrinsic properties of layer V pyramidal neurons in mPFC (Figure 3.8A).

3.5 DISCUSSION

We investigated whether serotonin modulates specific inputs to the mPFC, and if so, whether this might enable specific prefrontal serotonin receptors to regulate anxiety-related behavior. We found that serotonin acts presynaptically via 5-HT1B receptors to suppress callosal and hippocampal inputs, but not those from the MD thalamus. Then we found that activating 5-HT1B receptors within the mPFC increased the exploration of anxiogenic regions of the EPM, while also suppressing mPFC power in the theta, alpha, and beta frequency bands.

3.51 Serotonin acts presynaptically through 5-HT1B receptors

For callosal projections, both serotonin and the 5-HT1B receptor agonist, CP 93129, increased the PPR and reduced the frequency of uEPSCs observed in Sr2+, without affecting their amplitude or kinetics, all of which is consistent with a presynaptic site of action. For vHPC terminals, the 5-HT1B receptor agonist, CP 93129, elicited a statistically significant increase in PPR. The effect of serotonin on the PPR of vHPC inputs was not statistically significant, but both serotonin and CP 93129 reduced the frequency of uEPSCs elicited by vHCP inputs in Sr2+, without affecting their amplitude

or kinetics. Taken together, these effects are consistent with a presynaptic locus for the actions of serotonin.

Serotonin has been shown to reduce excitatory input to layer V visual neurons elicited by local electrical stimulation while increasing the PPR and reducing the frequency of spontaneous excitatory events (Murakoshi et al., 2001). A similar presynaptic effect of serotonin has been observed for excitatory inputs to prefrontal pyramidal neurons elicited via electrical stimulation of the corpus callosum or subcortical white matter (Tanaka and North, 1993; Troca-Marín and Geijo-Barrientos, 2010). Using optogenetics to overcome the limitations of electrical stimulation, which can activate fibers from multiple sources in both anterograde and retrograde directions, we found that serotonin acts presynaptically to suppress callosal and hippocampal inputs to layer V pyramidal neurons, but not those from MD thalamus. The absence of an effect of serotonin on inputs from MD thalamus is in contrast to a study in somatosensory cortex of neonatal (postnatal day 5-9) mice showing that serotonin reduces excitatory synaptic input elicited by electrical stimulation of internal capsule (Laurent et al., 2002). However, differences in optogenetic vs. electrical stimulation, brain regions being studied, and developmental stage may explain these discrepancies.

3.52 Serotonin targets specific cells and synapses within the mPFC

Our finding that serotonin acts with specificity at the level of inputs to the mPFC fits well with earlier studies showing that serotonin acts with a similar specificity with respect to its postsynaptic actions on mPFC neurons. In the mPFC, postsynaptic serotonin receptors are differentially expressed by various subtypes of layer V

pyramidal neurons that project to different targets (Avesar and Gullledge, 2012; Stephens et al., 2014). Thus, serotonin is well poised to dynamically regulate the flow of information both into and out of the mPFC, thereby coordinating its participation in distributed brain networks. Notably, we found that serotonin modulates presynaptic terminals in the mPFC via 5-HT1B receptors, but that these receptors fail to elicit obvious postsynaptic effects, which instead appear to be mediated by 5-HT1A and 5-HT2A receptors. This makes it possible to selectively target these various pre- and postsynaptic effects using specific serotonin receptor agonists or antagonists.

3.53 Serotonin regulates the flow of anxiety-related information through the mPFC

As described in the Introduction, the mPFC receives input from many sources including the hippocampus (Hoover and Vertes, 2007) and is reciprocally connected with the amygdala and other limbic areas (Vertes, 2004). Thus the mPFC is well positioned to connect contextual information with appropriate anxiety behavior. A recent study that recorded from mPFC neurons found firing patterns consistent with a model in which these neurons utilize vHPC inputs to guide avoidance behaviors in the EPM (Adhikari et al., 2011). In particular, vHPC projections to the mPFC appear regulate anxiety-related behavior by transmitting theta-frequency (4-12 Hz) activity, since 1) both the firing of mPFC-projecting cells within the vHPC and theta-frequency synchronization between the vHPC and mPFC increase in anxiogenic environments (Adhikari et al., 2010; Ciochi et al., 2015), and 2) optogenetically suppressing mPFC inputs from vHPC (but not from MD thalamus) decreases open arm avoidance by desynchronizing vHPC

and mPFC theta activity (Padilla-Coreano et al., 2016). In this context, our findings that 5-HT1B receptors suppress vHPC input to mPFC, theta-frequency (4-12 Hz) activity in mPFC, and avoidance behaviors in the EPM, suggest that serotonin may suppress the ability of vHPC input in order to drive theta-frequency activity in mPFC and thereby elicit avoidance behaviors. This model, in which serotonin suppresses long-range inputs to the mPFC, is also consistent with a recent study showing enhanced functional connectivity between the mPFC and subcortical networks in a mouse model of serotonin deficiency (Dzirasa et al., 2013).

Of course, the intra-mPFC infusion of CP 93129 may target other 5-HT1B receptors, e.g., possible autoreceptors on serotonergic fibers, in addition to 5-HT1B receptors on the presynaptic terminals of fibers from the vHPC or contralateral mPFC. We do know that 5-HT1B receptor activation is sufficient to suppress vHPC inputs to mPFC, and that such suppression elicits anxiolytic effects, but we cannot rule out the possibility that other, possibly unknown effects of prefrontal 5-HT1B receptors, contribute as well.

3.6 CONCLUSION

Elucidating the role of prefrontal serotonin in brain network function requires connecting specific serotonin receptors with their cellular and synaptic effects, then understanding how these shape circuit physiology in ways that could impact behavior. Here, we have described a mechanism through which 5-HT1B receptors can presynaptically suppress specific sources of input to the mPFC, as well as a known

circuit-level electrophysiological correlate of anxiety (mPFC theta oscillations). Our results are consistent with a model in which the mPFC integrates inputs from various limbic sources in order to direct affective behavior, and suggest that by acting as a gatekeeper, serotonin may be able to powerfully modulate this process.

3.7 FIGURES

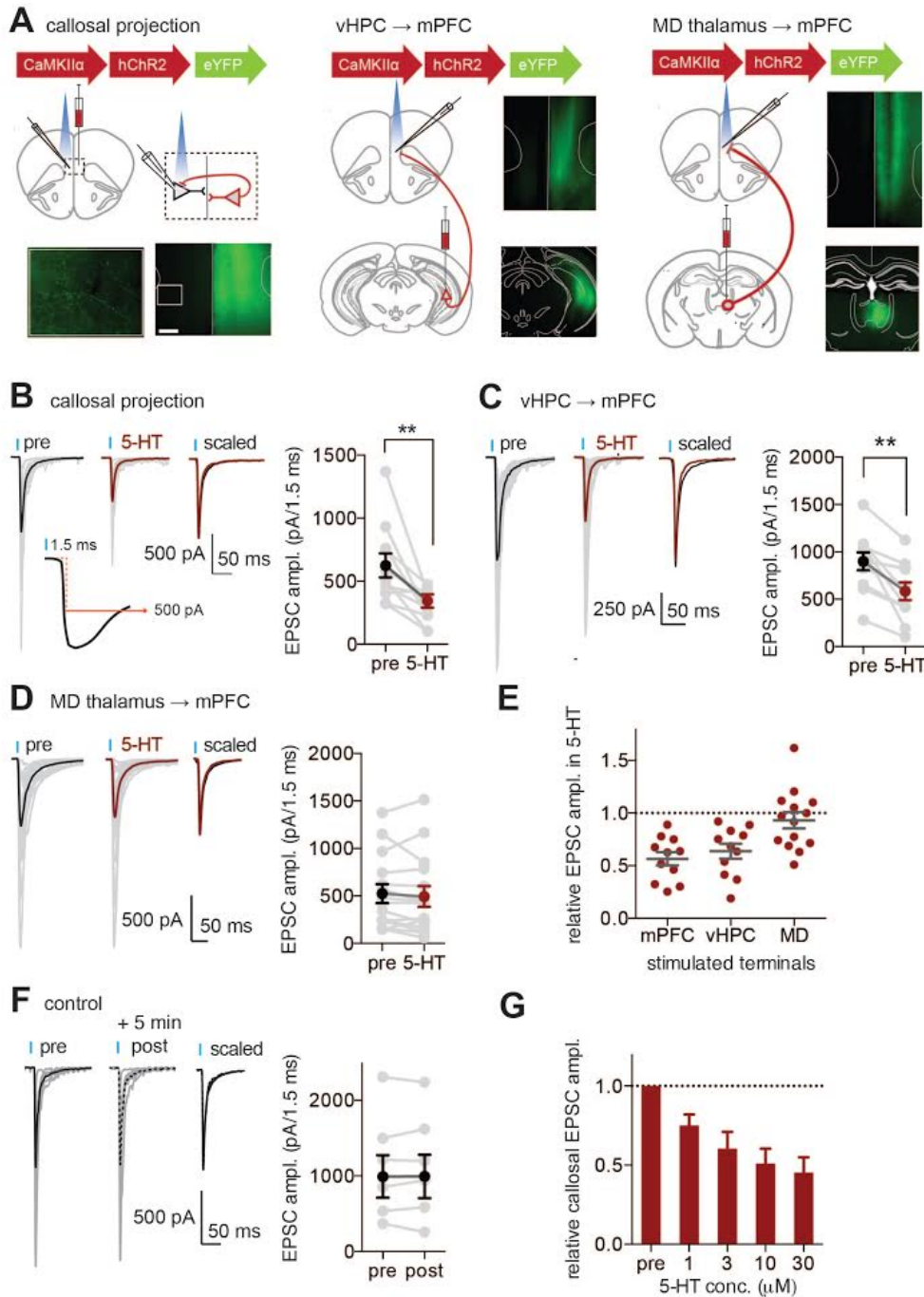


Figure 3.1. Serotonin suppresses afferent input to mPFC layer V pyramidal neurons from the contralateral mPFC and vHPC, but not MD thalamus. a. Experimental design: AAV5-CaMKIIα-hChR2-eYFP was injected unilaterally into medial prefrontal cortex (mPFC), ventral hippocampus (vHPC), or mediodorsal (MD) thalamus. Whole cell voltage clamp recordings were obtained from layer V pyramidal neurons in mPFC. Postsynaptic currents were evoked by 470 nm light flashes activating ChR2

expressing terminals (red). Low-power images show ChR2-eYFP expression at the injection site, and the high-power images show ChR2-eYFP within axon terminals in mPFC (scale bar: 50 μ m). b. Postsynaptic responses of layer V pyramidal neurons to activation of callosal terminals by single light flashes in voltage clamp. Below, a magnified example trace shows how we measure EPSC amplitude 1.5 ms after EPSC initiation to minimize possible contamination from polysynaptic responses. Wash-in of 30 μ M serotonin (5-HT) reduces the amplitude of evoked excitatory postsynaptic currents (EPSCs). Gray traces represent data from individual experiments and black / red traces represent averages across experiments. Scaled responses at baseline (pre) and following 5 min of serotonin wash-in are shown at the right. c. 30 μ M serotonin (5-HT) reduced the amplitude of EPSCs evoked by vHPC terminal stimulation. d. There was no effect of 5-HT on the responses of layer V pyramidal neurons to activation of MD thalamic terminals. e. The relative amplitudes of optogenetically evoked EPSCs following 5-HT wash-in for projections from the mPFC, vHPC, or MD thalamus. f. Responses to callosal stimulation did not change simply as a function of time. g. The relative EPSC amplitude as a function of serotonin concentration (EPSCs evoked by callosal stimulation). Data are represented as mean \pm SEM. * $p < 0.05$; ** $p < 0.01$. $n = 11$ for callosal stimulation; $n = 14$ for MD thalamus; $n = 11$ for vHPC; $n = 6$ for time control; $n = 4$ for dose-response.

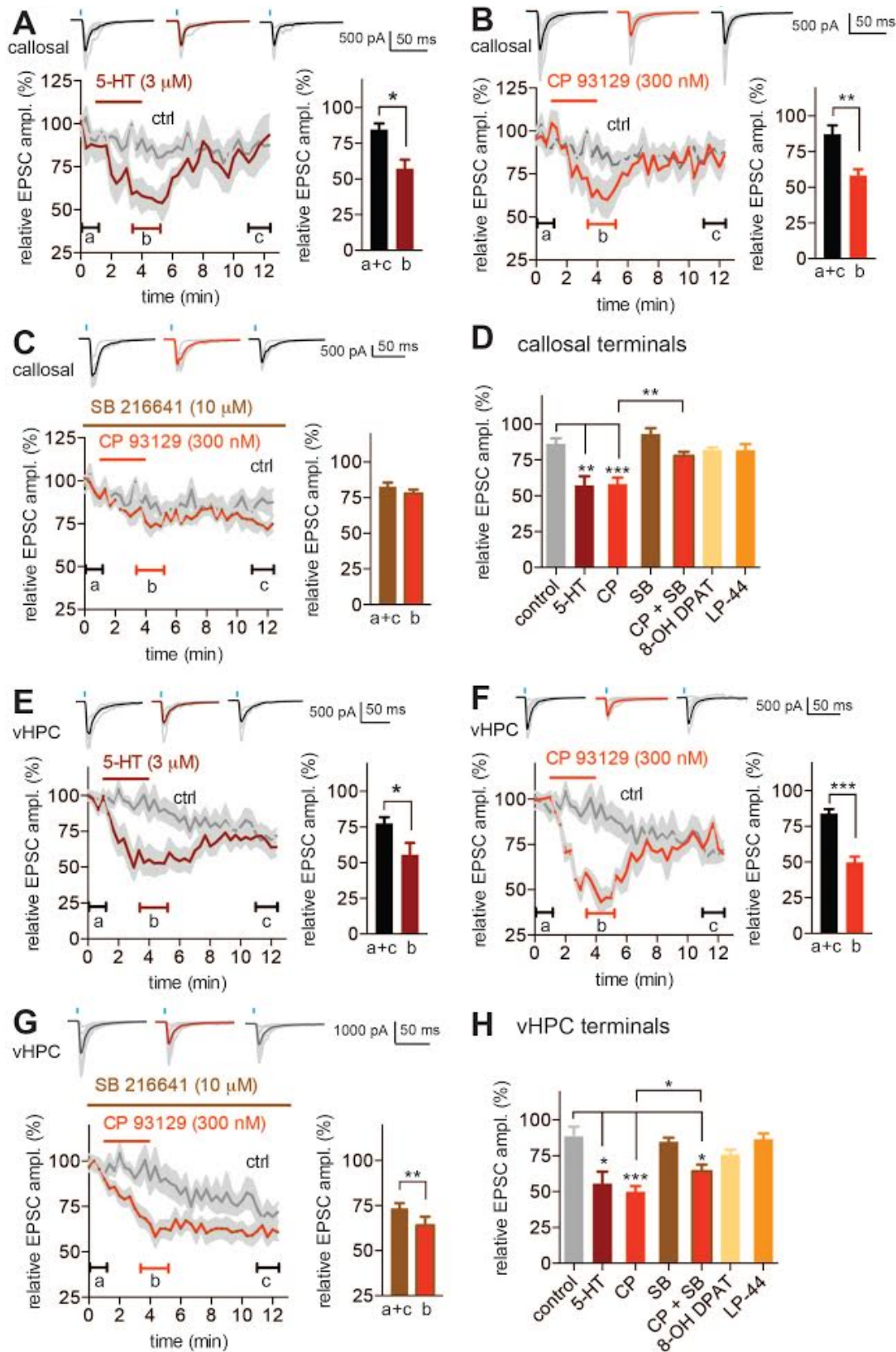


Figure 3.2. Serotonin suppresses callosal and ventral hippocampal input to mPFC through the 5-HT_{1B} receptor. a. Excitatory postsynaptic currents (EPSCs) in mPFC

layer V pyramidal cells were recorded in response to optogenetic stimulation of callosal terminals and during 3-min wash-in followed by wash-out of 3 μ M 5-HT. Relative EPSC amplitude (normalized by the initial amplitude) is plotted as a function of time (red line). The dark red bar above the trace shows the time of 5-HT application. The labels 'a', 'b' and 'c' below the trace indicate the periods used to calculate EPSC amplitude during the pre-drug period ('a'), immediately following 5-HT application ('b'), and the post-drug period ('c'). The timecourse of EPSC amplitudes during control recordings (no drug) is superimposed for comparison (gray line, 'ctrl'). The summary graph (right) shows the average EPSC amplitude during the pre- and post-drug periods ('a+c') compared to the period immediately following 5-HT application ('b'). Top: individual (gray) and mean (black/dark red) traces are shown for pre-drug, drug, and post-drug periods. b. Similar to a, but shows effects of the 5-HT_{1B} receptor agonist, CP 93129 (300 nM) on callosal EPSC amplitude. c. Similar to a, but shows that the effect of the 5-HT_{1B} receptor agonist, CP 93129 (300 nM), on EPSC amplitude is blocked in the presence of the 5-HT_{1B} receptor antagonist, SB 216641 (10 μ M). d. Summary graph comparing callosal EPSC amplitudes during application of each drug combination. Callosal EPSCs were suppressed (relative to control recordings) by 5-HT and CP 93129 (CP), and the effect of CP 93129 was blocked by pre-application of SB 216641 (SB). e-g. Similar to a-c, but shows effects of 5-HT (e), CP 93129 (f), and CP 93129 + SB 216641 on EPSCs evoked by optogenetic stimulation of vHPC terminals. h. Summary graph comparing the effects of various drugs on vHPC EPSC amplitude. 5-HT and CP 93129 (CP) suppressed EPSC amplitude (relative to control recordings). CP 93129 alone suppressed EPSCs to a larger extent than CP 93129 + SB 216641 (SB). Data are represented as mean \pm SEM. * p < 0.05; ** p < 0.01; *** p < 0.001. Callosal input: n = 5 for 5-HT; n = 4 for control; n = 8 for CP 93129; n = 5 for CP 93129 + SB 216641; n = 7 for 8-OH DPAT; n = 5 for LP-44. vHPC input: n = 6 for 5-HT; n = 8 for control; n = 6 for CP 93129; n = 9 for CP 93129 + SB 216641; n = 8 for 8-OH DPAT; n = 11 for LP-44.

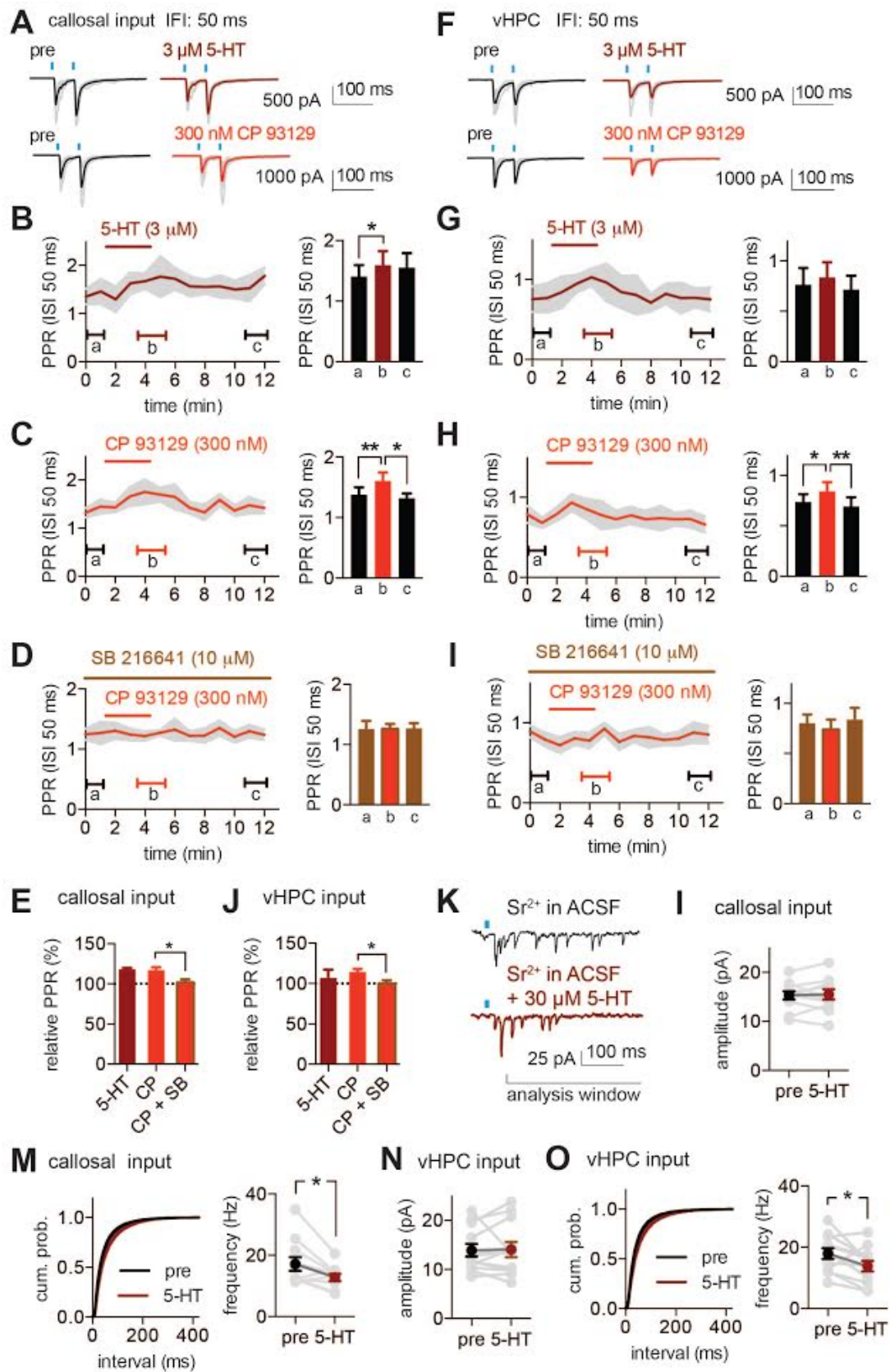


Figure 3.3. 5-HT_{1B} receptors increase the paired pulse ratio and reduce the frequency of asynchronous unitary events elicited by stimulation of callosal or vHPC terminals. a. mPFC pyramidal cell responses to pairs of light flashes activating callosal terminals with interflash intervals (IFI) of 50 ms before and after wash-in of serotonin (5-HT) or the 5-HT_{1B} receptor agonist, CP 93129. Gray traces represent data from individual cells and black / red traces represent averages across experiments. b. 3 μ M 5-HT increased the PPR of EPSCs evoked by activation of callosal terminals with (IFI: 50 ms). c. For callosal terminals, PPR was also increased in response to wash-in of CP 93129 (300 nM), and returned to baseline levels following wash-out. d. There was no effect on PPR when CP 93129 application was preceded by application of SB 216641 (10 μ M). e. Summary graph showing the drug-induced change in PPR of EPSCs evoked by optogenetic stimulation of callosal projections (relative to the pre-drug period). The PPR increase following CP 93129 (CP) wash-in was blocked following pre-application of SB 216641 (SB). f. Example of pyramidal cell responses to pairs of light flashes (IFI: 50 ms) activating vHPC input in response to serotonin (5-HT) and CP 93129. g. For vHPC input, 5-HT (3 μ M) elicited a non-significant increase in the PPR (IFI: 50ms). h. For vHPC input, CP 93129 reversibly increased PPR. i. Pre-application of SB 216641 blocked the effect of CP 93129 on the PPR of responses to vHPC input. j. Summary plot for vHPC terminals: the CP 93129-induced increase in PPR was blocked by pre-application of SB 216641. k. Example traces showing asynchronous unitary EPSCs (uEPSC) induced by photostimulation of callosal terminals in ACSF in which Ca²⁺ has been replaced with 2 mM Sr²⁺. l. There was no difference in callosally induced uEPSC amplitude following wash-in of 5-HT. m. For uEPSCs elicited by callosal terminal stimulation, the cumulative probability plot of inter-event intervals is shifted to the right following serotonin application. The summary plots show that the frequency of uEPSCs is lower in 5-HT. n. vHPC stimulation-induced uEPSCs did not show a change in amplitude following 5-HT application. o. The frequency of uEPSCs evoked by vHPC terminal stimulation is reduced following 5-HT wash-in as shown in the cumulative probability and summary plot. Data are represented as mean \pm SEM. * $p < 0.05$, ** $p < 0.01$; PPR: $n = 6/8/5$ for callosal terminals; $n = 5/6/8$ for vHPC terminals. uEPSC: $n = 11$ for callosal terminals; $n = 12$ for vHPC.

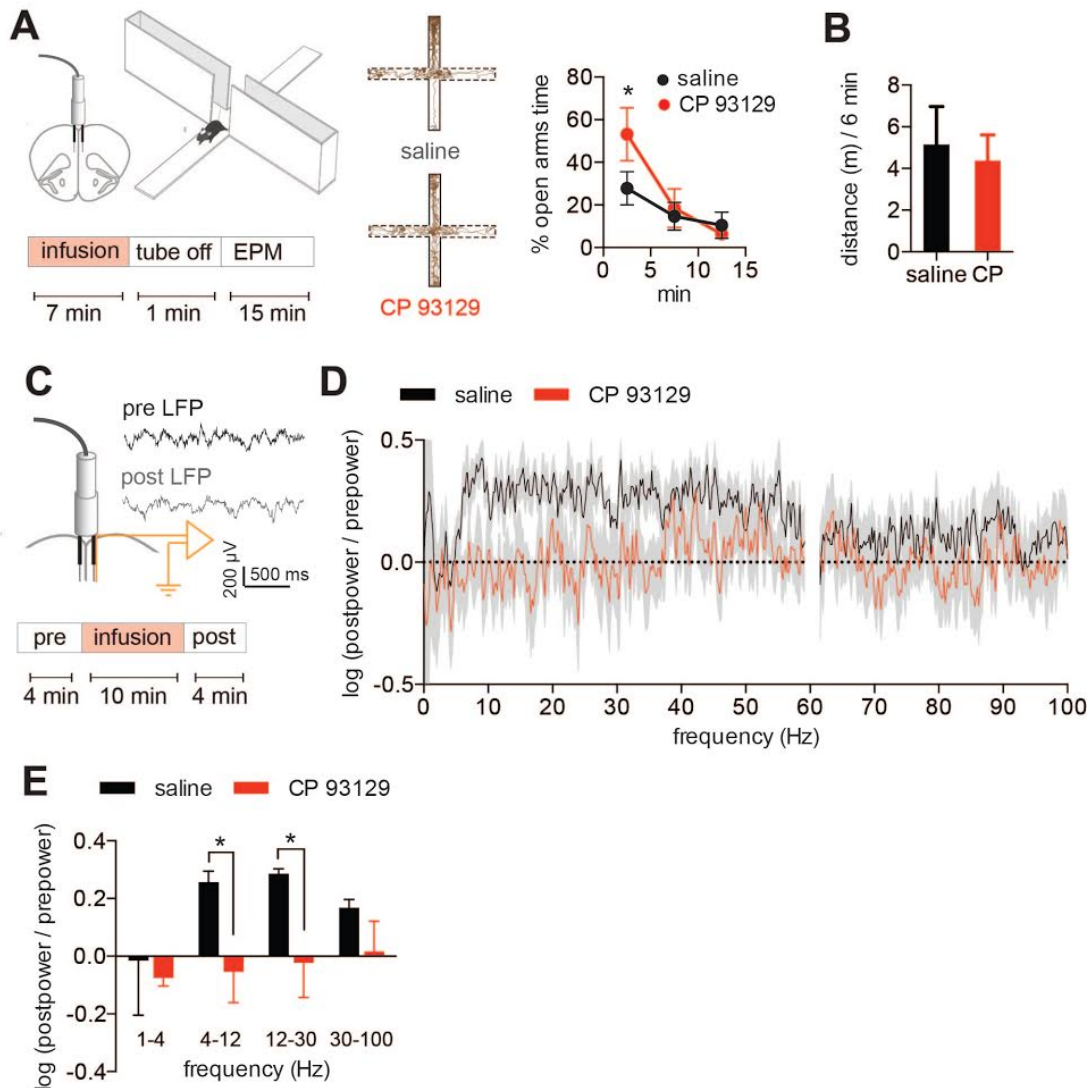


Figure 3.4. Intra-mPFC infusion of a 5-HT1B receptor agonist reduces innate anxiety and mPFC theta power. a. Left: experimental set-up. Freely moving mice were infused with saline +/- a 5-HT1B receptor agonist through a guide cannula implanted bilaterally in the mPFC. Following infusion, the animal was placed in an elevated plus maze (EPM) for 15 min. Right: infusion of the 5-HT1B receptor agonist, CP93129 (4.3 ng in 0.5 μ L), increased time spent in the open arms of the EPM compared to saline infused mice. b. There was no effect of CP 93129 infusion in distance moved in the first 6 min of the open field test. c. Experimental set-up. A tungsten electrode was attached to a bilateral guide cannula and implanted within the mPFC. Local field potentials (LFP) were recorded continuously during infusion and power spectra for 4-min pre- and post-infusion periods were compared. Example traces showing recordings before and after infusions of saline are shown. d. The logarithm of the ratio between the pre- and post-drug power spectra for saline (black) and CP 93129 (red) infusion are shown. e. The summary plot shows the mean log ratio power for saline and CP 93129 infusions in different frequency bands. Theta (4-12 Hz) and beta (12-30 Hz) are selectively reduced

following CP 93129 infusion. Data are represented as mean \pm SEM. * $p < 0.05$. EPM: $n = 4$ for saline and $n = 5$ for CP 93129; LFP: $n = 11$ for saline and $n = 8$ for CP 93129.

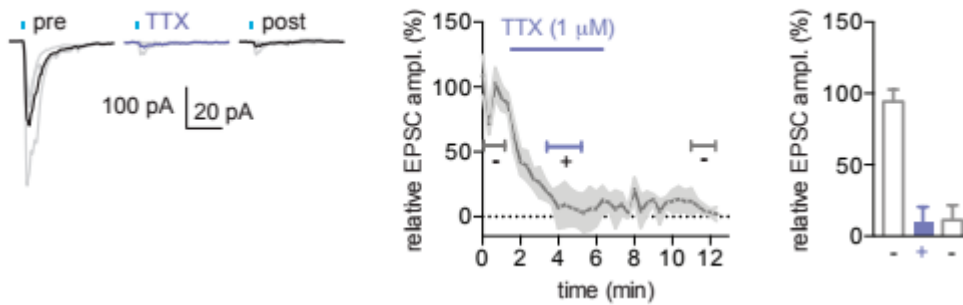


Figure 3.5 - Supplemental Figure. Tetrodotoxin blocks EPSCs induced by ChR2-expressing terminals. 5 min wash-in of the voltage-sensitive sodium channel blocker, tetrodotoxin (TTX, 1 μ M) blocks excitatory postsynaptic currents (EPSCs) in mPFC pyramidal neurons induced by activation of channelrhodopsin (ChR2) expressed in ventral hippocampal terminals. Data are shown as mean \pm SEM. $n = 3$.

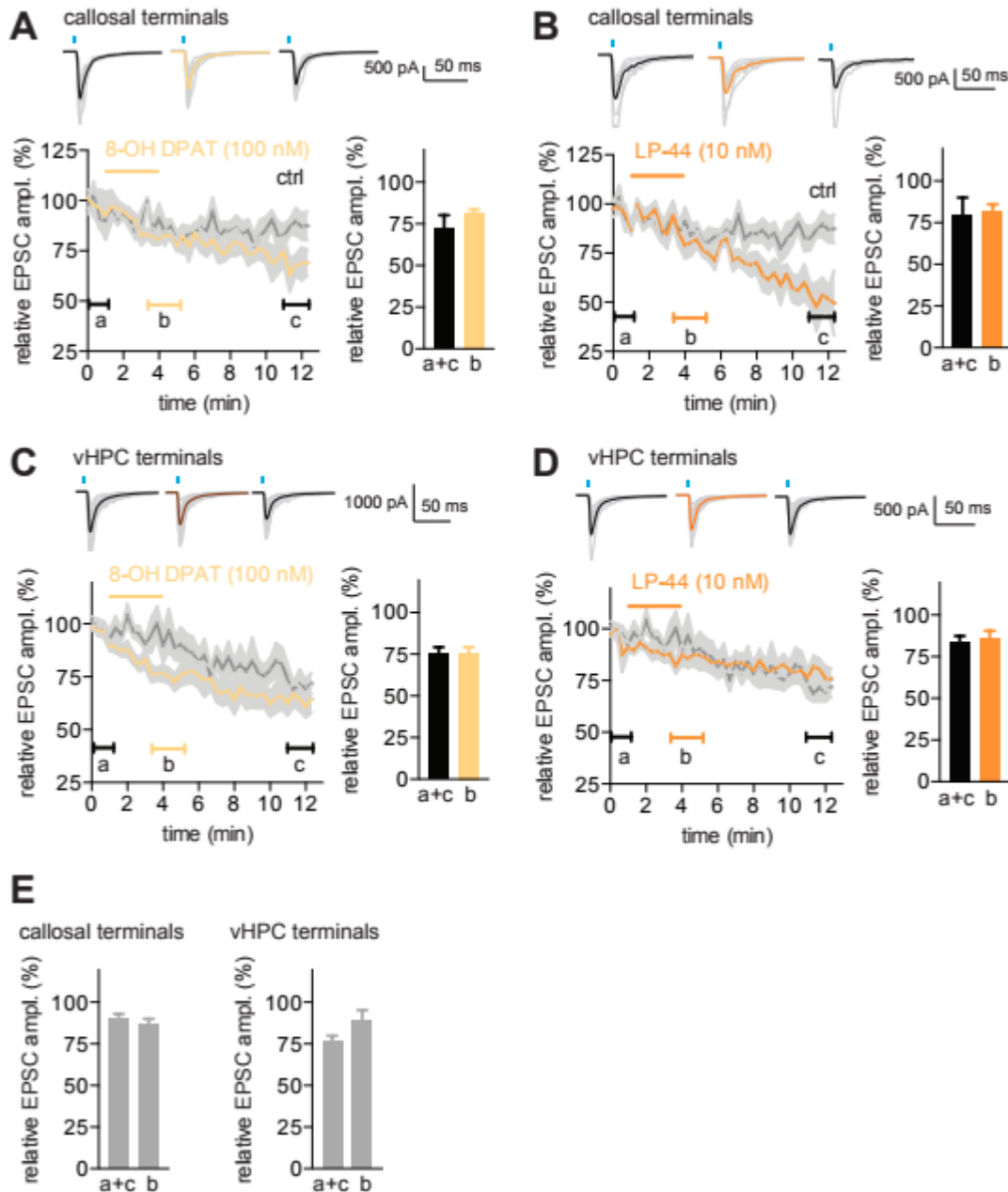


Figure 3.6 - Supplemental Figure. No effect of 5-HT_{1A} or 5-HT₇ receptor activation on evoked callosal or ventral hippocampal EPSCs. Excitatory postsynaptic currents (EPSCs) in mPFC layer V pyramidal cells were recorded in response to optogenetic stimulation of callosal (A, B, E) or ventral hippocampal (C, D, E) terminals. In addition to each experimental condition, we also made recordings in control conditions to assay for possible time-dependent drift in the baseline, and these measurements of control responses (gray traces) have been superimposed on the experimental traces in each panel (A-D). A. The yellow trace shows callosal EPSC amplitudes before, during, and after application of the selective 5-HT_{1A} receptor agonist 8-OH DPAT (100 nM). As shown by the bar graph to the right, there was no difference between the average EPSC amplitude during the period immediately following

application of 8-OH DPAT ('b'), and the average of the pre and post-applications periods ('a+c'). B. The brown trace shows callosal EPSC amplitudes before, during, and after application of the selective 5-HT7 receptor agonist LP-44 (10 nM). As shown by the bar graph to the right, there was no difference between the average EPSC amplitude during the period immediately following application of LP-44 ('b'), and the average of the pre and post-applications periods ('a+c'). C. The yellow trace shows ventral hippocampal EPSC amplitudes before, during, and after application of the selective 5-HT1A receptor agonist 8-OH DPAT (100 nM). As shown by the bar graph to the right, there was no difference between the average EPSC amplitude during the period immediately following application of 8-OH DPAT ('b'), and the average of the pre and post-applications periods ('a+c'). D. The brown trace shows ventral hippocampal EPSC amplitudes before, during, and after application of the selective 5-HT7 receptor agonist LP-44 (10 nM). As shown by the bar graph to the right, there was no difference between the average EPSC amplitude during the period immediately following application of LP-44 ('b'), and the average of the pre and post-applications periods ('a+c'). E. Bar graphs comparing control (no drug) responses to optogenetic stimulation of callosal (left) or ventral hippocampal (right) terminals during the period when drug would have been washed in ('b') to the average of the pre / post-drug application periods ('a+c'). In each case, data is based on control recordings in the absence of any actual drug application. Data are represented as mean \pm SEM. Callosal input: n = 4 for control; n = 7 for 8-OH DPAT; n = 5 for LP-44. vHPC input: n = 8 for control; n = 8 for 8-OH DPAT; n = 11 for LP-44.

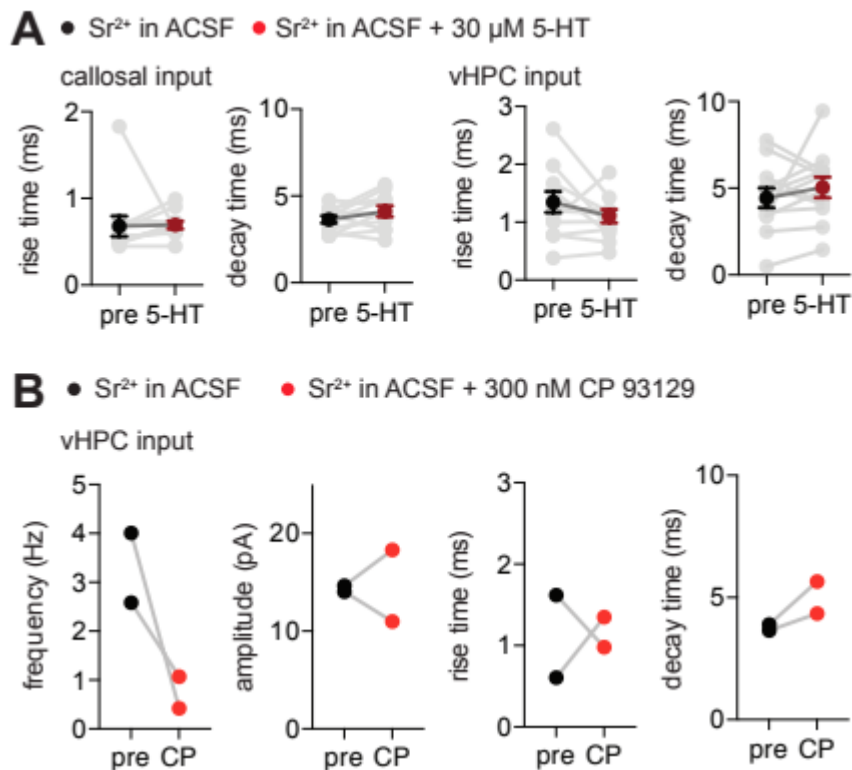


Figure 3.7 - Supplemental Figure. 5-HT and the 5-HT1B receptor agonist, CP 93129, reduces the frequency of asynchronous unitary events without affecting

amplitude, rise time or decay time. A. Asynchronous unitary EPSCs (uEPSC) induced by photostimulation of callosal and ventral hippocampal (vHPC) terminals in ACSF containing Sr²⁺ instead of Ca²⁺ was recorded. No change in rise time or decay time was observed following wash-in of 30 μ M 5-HT. B. uEPSC induced by photostimulation of vHPC terminals was recorded in two cells before and after wash-in of 300 nM CP 93129. The frequency of uEPSCs responded with a pronounced reduction with no apparent effect on amplitude and kinetics. Data are represented as mean \pm SEM. 5-HT: n = 11 for callosal terminals; n = 12 for vHPC; CP 93129: n = 2 for vHPC.

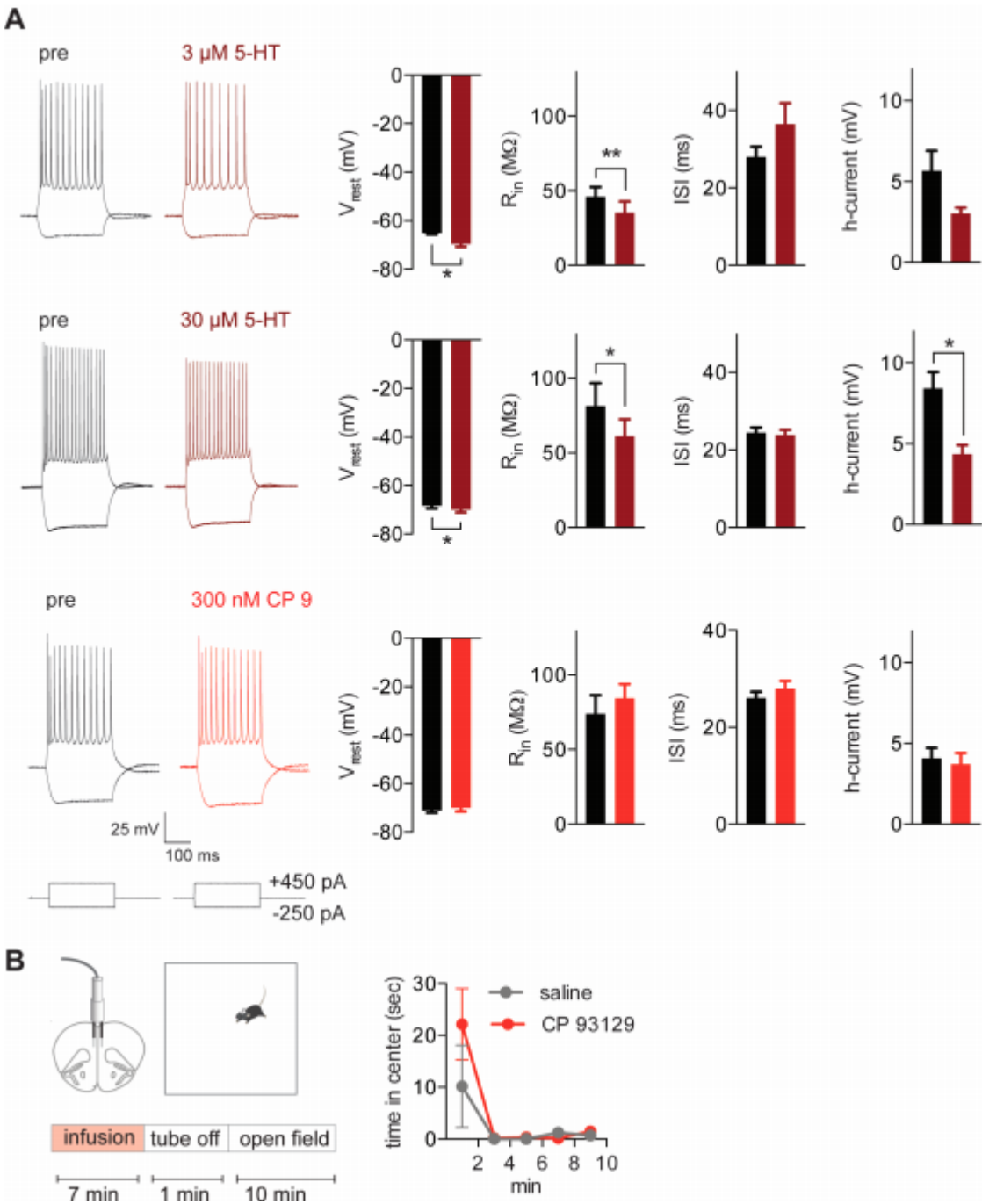


Figure 3.8 - Supplemental Figure. Effect of 5-HT_{1B} receptors on intrinsic properties in layer V pyramidal neurons and on open field enter zone exploration.

A. Top: Example traces showing the responses of a layer V pyramidal neuron to current injections (-250 pA and 450 pA). Application of 3 μ M serotonin hyperpolarizes the resting membrane potential (V_{rest}) and reduces the input resistance (R_{in}) of layer V pyramidal neurons in prefrontal cortex. In addition, there is a trend towards a reduction in the size of the h-current induced sag and rebound during/following a hyperpolarizing current pulse. The interspike-interval (ISI) did not change. Middle panel: More

pronounced effects are evident after applying 30 μ M serotonin. The resting membrane potential, input resistance, and size of the h-current-induced sag/rebound are all reduced. Bottom panel: Application of the 5-HT_{1B} receptor agonist CP 93129 (300 nM) did not disrupt any of the intrinsic effects elicited by serotonin. B. Freely moving mice were infused with saline +/- a 5-HT_{1B} receptor agonist through a guide cannula implanted bilaterally in the mPFC. Following infusion, the animal was placed in an open field for 10 min. Infusion of the 5-HT_{1B} receptor agonist, CP93129 (4.3 ng in 0.5 μ L), had a tendency to increase time spent in the center of the open field during the first two minutes compared to saline infused mice ($p = 0.14$). Data are represented as mean \pm SEM. * $p < 0.05$, ** $p < 0.01$. 3 μ M serotonin: $n = 4$; 30 μ M serotonin: $n = 7$; CP 93129: $n = 7$. Open field: saline: $n = 5$; CP 93129: $n = 3$.

3.8 REFERENCES

- Adhikari, A., Topiwala, M.A., Gordon, J.A., 2011. Single Units in the Medial Prefrontal Cortex with Anxiety-Related Firing Patterns Are Preferentially Influenced by Ventral Hippocampal Activity. *Neuron* 71, 898–910. doi:10.1016/j.neuron.2011.07.027
- Adhikari, A., Topiwala, M.A., Gordon, J.A., 2010. Synchronized activity between the ventral hippocampus and the medial prefrontal cortex during anxiety. *Neuron* 65, 257–69. doi:10.1016/j.neuron.2009.12.002
- Araneda, R., Andrade, R., 1991. 5-Hydroxytryptamine₂ and 5-hydroxytryptamine 1A receptors mediate opposing responses on membrane excitability in rat association cortex. *Neuroscience* 40, 399–412.
- Avesar, D., Gullledge, A.T., 2012. Selective serotonergic excitation of callosal projection neurons. *Front. Neural Circuits* 6, 12. doi:10.3389/fncir.2012.00012
- Béïque, J.-C., Campbell, B., Perring, P., Hamblin, M.W., Walker, P., Mladenovic, L., Andrade, R., 2004. Serotonergic regulation of membrane potential in developing rat prefrontal cortex: coordinated expression of 5-hydroxytryptamine (5-HT)_{1A}, 5-HT_{2A}, and 5-HT₇ receptors. *J. Neurosci.* 24, 4807–17. doi:10.1523/JNEUROSCI.5113-03.2004
- Ciocchi, S., Passecker, J., Malagon-Vina, H., Mikus, N., Klausberger, T., Fanselow, M.S., Dong, H.W., Cenquizca, L.A., Swanson, L.W., Jennings, J.H., Sparta, D.R., Stamatakis, A.M., Ung, R.L., Pleil, K.E., Kash, T.L., Stuber, G.D., Adhikari, A., Topiwala, M.A., Gordon, J.A., Jung, M.W., Wiener, S.I., McNaughton, B.L., Kjelstrup, K.B., Solstad, T., Brun, V.H., Hafting, T., Leutgeb, S., Witter, M.P., Moser, E.I., Moser, M.B., Girardeau, G., Zugaro, M., Tye, K.M., Prakash, R., Kim, S.Y., Fenno, L.E., Grosebeck, L., Zarabi, H., Thompson, K.R., Gradinaru, V., Ramakrishnan, C., Deisseroth, K., Adhikari, A., Topiwala, M.A., Gordon, J.A., Likhtik, E., Stujenske, J.M., Topiwala, M.A., Harris, A.Z., Gordon, J.A., Vertes, R.P., Orsini, C.A., Kim, J.H., Knapska, E., Maren, S., Royer, S., Sirota, A., Patel, J., Buzsáki, G., Bannerman, D.M., Sprengel, R., Sanderson,

D.J., McHugh, S.B., Rawlins, J.N., Monyer, H., Seeburg, P.H., Kjelstrup, K.G., Tuvnes, F.A., Steffenach, H.A., Murison, R., Moser, E.I., Moser, M.B., Felix-Ortiz, A.C., Beyeler, A., Seo, C., Leppla, C.A., Wildes, C.P., Tye, K.M., Groen, T. van, Miettinen, P., Kadish, I., Zhang, S.J., Ye, J., Miao, C., Tsao, A., Cerniauskas, I., Ledergerber, D., Moser, M.B., Moser, E.I., Lee, S.H., Marchionni, I., Bezaire, M., Varga, C., Danielson, N., Lovett-Barron, M., Losonczy, A., Soltesz, I., Hussaini, S.A., Kempadoo, K.A., Thuault, S.J., Siegelbaum, S.A., Kandel, E.R., Kim, C.S., Chang, P.Y., Johnston, D., Arszovszki, A., Borhegyi, Z., Klausberger, T., Graves, A.R., Moore, S.J., Bloss, E.B., Mensh, B.D., Kath, W.L., Spruston, N., Maren, S., Hobin, J.A., Carr, G.D., White, N.M., Jones, M.W., Wilson, M.A., Komorowski, R.W., Garcia, C.G., Wilson, A., Hattori, S., Howard, M.W., Eichenbaum, H., Keinath, A.T., Wang, M.E., Wann, E.G., Yuan, R.K., Dudman, J.T., Muzzio, I.A., Lisman, J.E., Grace, A.A., Ruediger, S., Spirig, D., Donato, F., Caroni, P., Csicsvari, J., Hirase, H., Czurko, A., Buzsáki, G., Hazan, L., Zugaro, M., Buzsáki, G., Rich, E.L., Shapiro, M., Walf, A.A., Frye, C.A., Gallistel, C.R., Fairhurst, S., Balsam, P., Smith, A.C., Frank, L.M., Wirth, S., Yanike, M., Hu, D., Kubota, Y., Graybiel, A.M., Suzuki, W.A., Brown, E.N., Pi, H.J., Hangya, B., Kvitsiani, D., Sanders, J.I., Huang, Z.J., Kepecs, A., 2015. Brain computation. Selective information routing by ventral hippocampal CA1 projection neurons. *Science* 348, 560–3. doi:10.1126/science.aaa3245

Covington, H.E., Lobo, M.K., Maze, I., Vialou, V., Hyman, J.M., Zaman, S., LaPlant, Q., Mouzon, E., Ghose, S., Tamminga, C.A., Neve, R.L., Deisseroth, K., Nestler, E.J., 2010. Antidepressant effect of optogenetic stimulation of the medial prefrontal cortex. *J. Neurosci.* 30, 16082–90. doi:10.1523/JNEUROSCI.1731-10.2010

Crino, P.B., Vogt, B.A., Volicer, L., Wiley, R.G., 1990. Cellular localization of serotonin 1A, 1B and uptake sites in cingulate cortex of the rat. *J. Pharmacol. Exp. Ther.* 252, 651–6.

de Almeida, J., Mengod, G., 2008. Serotonin 1A receptors in human and monkey prefrontal cortex are mainly expressed in pyramidal neurons and in a GABAergic interneuron subpopulation: implications for schizophrenia and its treatment. *J. Neurochem.* 107, 488–96. doi:10.1111/j.1471-4159.2008.05649.x

Dzirasa, K., Kumar, S., Sachs, B.D., Caron, M.G., Nicoletis, M.A.L., 2013. Cortical-amygdalar circuit dysfunction in a genetic mouse model of serotonin deficiency. *J. Neurosci.* 33, 4505–13. doi:10.1523/JNEUROSCI.4891-12.2013

Gonzalez, L.E., Rujano, M., Tucci, S., Paredes, D., Silva, E., Alba, G., Hernandez, L., 2000. Medial prefrontal transection enhances social interaction. I: behavioral studies. *Brain Res.* 887, 7–15.

Groenewegen, H.J., Uylings, H.B., 2000. The prefrontal cortex and the integration of sensory, limbic and autonomic information. *Prog. Brain Res.* 126, 3–28. doi:10.1016/S0079-6123(00)26003-2

Hajós, M., Richards, C.D., Székely, A.D., Sharp, T., 1998. An electrophysiological and neuroanatomical study of the medial prefrontal cortical projection to the midbrain raphe nuclei in the rat. *Neuroscience* 87, 95–108.

Hervás, I., Vilaró, M.T., Romero, L., Scorza, M.C., Mengod, G., Artigas, F., 2001. Desensitization of 5-HT(1A) autoreceptors by a low chronic fluoxetine dose effect of the concurrent administration of WAY-100635. *Neuropsychopharmacology* 24, 11–20. doi:10.1016/S0893-133X(00)00175-5

Hoover, W.B., Vertes, R.P., 2007. Anatomical analysis of afferent projections to the medial prefrontal cortex in the rat. *Brain Struct. Funct.* 212, 149–79. doi:10.1007/s00429-007-0150-4

Ishikawa, A., Nakamura, S., 2006. Ventral hippocampal neurons project axons simultaneously to the medial prefrontal cortex and amygdala in the rat. *J. Neurophysiol.* 96, 2134–8. doi:10.1152/jn.00069.2006

Lacroix, L., Spinelli, S., Heidbreder, C.A., Feldon, J., 2000. Differential role of the medial and lateral prefrontal cortices in fear and anxiety. *Behav. Neurosci.* 114, 1119–30.

Laurent, A., Goillard, J.-M., Cases, O., Lebrand, C., Gaspar, P., Ropert, N., 2002. Activity-dependent presynaptic effect of serotonin 1B receptors on the somatosensory thalamocortical transmission in neonatal mice. *J. Neurosci.* 22, 886–900.

Le Poul, E., Laaris, N., Doucet, E., Laporte, A.-M., Hamon, M., Lanfumey, L., 1995. Early desensitization of somato-dendritic 5-HT_{1A} autoreceptors in rats treated with fluoxetine or paroxetine. *Naunyn. Schmiedeberg's Arch. Pharmacol.* 352, 141–148. doi:10.1007/BF00176767

Li, Q., Muma, N., van de Kar, L., 1996. Chronic fluoxetine induces a gradual desensitization of 5-HT_{1A} receptors: reductions in hypothalamic and midbrain Gi and G(o) proteins and in neuroendocrine responses to a 5-HT_{1A} agonist. *J. Pharmacol. Exp. Ther.* 279, 1035–1042.

Miller, E.K., Cohen, J.D., 2001. An integrative theory of prefrontal cortex function. *Annu. Rev. Neurosci.* 24, 167–202. doi:10.1146/annurev.neuro.24.1.167

Murakoshi, T., Song, S.Y., Konishi, S., Tanabe, T., 2001. Multiple G-protein-coupled receptors mediate presynaptic inhibition at single excitatory synapses in the rat visual cortex. *Neurosci. Lett.* 309, 117–20.

Padilla-Coreano, N., Bolkan, S.S., Pierce, G.M., Blackman, D.R., Hardin, W.D., Garcia-Garcia, A.L., Spellman, T.J., Gordon, J.A., 2016. Direct Ventral Hippocampal-Prefrontal Input Is Required for Anxiety-Related Neural Activity and Behavior. *Neuron* 89, 857–66. doi:10.1016/j.neuron.2016.01.011

Santana, N., Bortolozzi, A., Serrats, J., Mengod, G., Artigas, F., 2004. Expression of serotonin1A and serotonin2A receptors in pyramidal and GABAergic neurons of the rat prefrontal cortex. *Cereb. Cortex* 14, 1100–9. doi:10.1093/cercor/bhh070

Shah, A.A., Sjovold, T., Treit, D., 2004. Inactivation of the medial prefrontal cortex with the GABAA receptor agonist muscimol increases open-arm activity in the elevated plus-maze and attenuates shock-probe burying in rats. *Brain Res.* 1028, 112–5. doi:10.1016/j.brainres.2004.08.061

Shah, A.A., Treit, D., 2003. Excitotoxic lesions of the medial prefrontal cortex attenuate fear responses in the elevated-plus maze, social interaction and shock probe burying tests. *Brain Res.* 969, 183–94.

Sohal, V.S., Zhang, F., Yizhar, O., Deisseroth, K., 2009. Parvalbumin neurons and gamma rhythms enhance cortical circuit performance. *Nature* 459, 698–702. doi:10.1038/nature07991

Stephens, E.K., Avesar, D., Gullidge, A.T., 2014. Activity-dependent serotonergic excitation of callosal projection neurons in the mouse prefrontal cortex. *Front. Neural Circuits* 8, 97. doi:10.3389/fncir.2014.00097

Tanaka, E., North, R.A., 1993. Actions of 5-hydroxytryptamine on neurons of the rat cingulate cortex. *J. Neurophysiol.* 69, 1749–57.

Troca-Marín, J.A., Geijo-Barrientos, E., 2010. Inhibition by 5-HT of the synaptic responses evoked by callosal fibers on cortical neurons in the mouse. *Pflugers Arch.* 460, 1073–85. doi:10.1007/s00424-010-0875-4

Vertes, R.P., 2004. Differential projections of the infralimbic and prelimbic cortex in the rat. *Synapse* 51, 32–58. doi:10.1002/syn.10279

Verwer, R.W., Meijer, R.J., Van Uum, H.F., Witter, M.P., 1997. Collateral projections from the rat hippocampal formation to the lateral and medial prefrontal cortex. *Hippocampus* 7, 397–402. doi:10.1002/(SICI)1098-1063(1997)7:4<397::AID-HIPO5>3.0.CO;2-G

Warden, M.R., Selimbeyoglu, A., Mirzabekov, J.J., Lo, M., Thompson, K.R., Kim, S.-Y., Adhikari, A., Tye, K.M., Frank, L.M., Deisseroth, K., 2012. A prefrontal cortex-brainstem neuronal projection that controls response to behavioural challenge. *Nature* 492, 428–32. doi:10.1038/nature11617

Zhong, P., Yan, Z., 2011. Differential regulation of the excitability of prefrontal cortical fast-spiking interneurons and pyramidal neurons by serotonin and fluoxetine. *PLoS One* 6, e16970. doi:10.1371/journal.pone.0016970

Zhou, F.-M., Hablitz, J.J., 1999. Activation of Serotonin Receptors Modulates Synaptic Transmission in Rat Cerebral Cortex. *J Neurophysiol* 82, 2989–2999.

CHAPTER 4

INPUT-SPECIFIC MODULATION OF EXCITATORY SYNAPSES ONTO PREFRONTAL FAST-SPIKING INTERNEURONS

4.1 INTRODUCTION

The firing of an individual neuron is determined by the integration of synaptic inputs from multiple different sources. In the prefrontal cortex (PFC), neurons receive inputs from a variety of cortical and subcortical structures, which are thought to potentially encode different streams of information. For example, theta-synchronized projections from the ventral hippocampus (vHPC) have been implicated in anxiety behavior (Adhikari et al., 2010, Padilla-Coreano et al., 2016), while connections between the mediodorsal thalamus (MD) and PFC are thought to play a role in working memory (Parnaudeau et al., 2013, Bolkan et al., 2017). The corpus callosum, on the other hand, carries projections from the contralateral cortex and is critical for bilateral integration of information. By regulating different types of synapses differentially, neuromodulators may be able to bias the circuit towards specific types of information during different contexts, allowing the circuit to flexibly adapt to changing environmental demands.

Serotonin (5HT) has been shown to modulate synapses both presynaptically and postsynaptically in the PFC. Presynaptic 5HT_{2A} receptors can increase NMDA transmission at thalamocortical synapses (Barre et al., 2016). Yet others have found that 5HT reduces synaptic responses from callosal inputs (Troca-Marin et al., 2014) and reduce AMPA-mediated EPSCs via the 5HT_{1A} receptor (Yuen et al., 2014). Recently, we found (Chapter 3) that 5HT differentially modulates synaptic responses from distinct brain regions, reducing callosal and hippocampal inputs via presynaptic 5HT_{1B}

receptors while sparing thalamic inputs (Kjaerby et al., 2016). However, all of these studies have limited their observations to synapses onto excitatory pyramidal neurons in prefrontal cortex. Here, I repeat experimental procedures from our previous investigation and examine serotonergic effects on projection-specific excitatory synapses in fast-spiking interneurons (FSIs). In line with our previous observations, I found that 5HT presynaptically reduced the amplitude of excitatory postsynaptic currents evoked by stimulation of callosal and hippocampal inputs without altering thalamic inputs. Despite these presynaptic changes, 5HT increased FSI firing in response to all these inputs, suggesting that postsynaptic effects play a larger role in determining FSI output.

4.2 METHODS

4.21 Electrophysiology

Coronal brain slices (250 μm) including medial prefrontal cortex were made from adult mice aging 8 weeks or older. We used the following transgenic mouse line: PV-Cre::Ai14 (RRID:MGI:2176738). All experiments were conducted in accordance with procedures established by the Institutional Animal Care and Use Committee and Laboratory Animal Resource Center at the University of California, San Francisco. Slicing solution was chilled to 4°C and contained (in mM): 234 sucrose, 26 NaHCO_3 , 11 glucose, 10 MgSO_4 , 2.5 KCl, 1.25 NaH_2PO_4 , 0.5 CaCl_2 , bubbled with 5% CO_2 / 95% O_2 . Slices were incubated in artificial cerebrospinal fluid (aCSF) at 32°C for 30 minutes and then at room temperature until recording. aCSF contained (in mM): 123 NaCl, 26

NaHCO₃, 11 glucose, 3 KCl, 2 CaCl₂, 1.25 NaH₂PO₄, 1 MgCl₂, also bubbled with 5% CO₂/ 95% O₂.

Neurons were visualized using differential interference contrast or DODT contrast microscopy on an upright microscope (Olympus). Fast-spiking interneurons were identified by fluorescent visualization of td-Tomato (PV-Cre::Ai14 mice). Recordings were made using a Multiclamp 700B (Molecular Devices) amplifier and acquired with pClamp. Patch pipettes (2-5 MΩ tip resistance) were filled with the following (in mM): 130 KGlucuronate, 10 KCl, 10 HEPES, 10 EGTA, 2 MgCl₂, 2 MgATP, 0.3 Na₃GTP. All recordings were made at 32-34°C. Series resistance was compensated in all current clamp experiments and monitored throughout recordings. Recordings were discarded if Rs changed by >25%.

5HT (Tocris) was dissolved in water (30 μM) before being diluted in aCSF and applied in the bath. The experimenter was not blind to pharmacological treatment.

4.22 Viral injection for expression of ChR2

Viral injections were performed using standard mouse stereotactical methods. Mice were anesthetized for the duration of the surgery using isoflurane gas. After cleaning, an incision was made in the scalp, the skull was leveled, and small burr holes were drilled over the brain region of interest using a dental drill. Virus was injected through the burr holes using a microinjector (WPI) at a speed of 150 nL/minute and the scalp was closed using sutures or tissue adhesive (Vetbond).

For expression of the optogenetic protein channelrhodopsin (ChR) in neurons that project to PFC, we injected a virus encoding ChR2 under the CaMKII promoter to

ensure expression in excitatory projection neurons (AAV5-CaMKII-ChR2-eYFP) into contralateral PFC (cPFC, 750 nL), mediodorsal (MD) thalamus (320 nL), or ventral hippocampus (vHPC, 500 nL) of PV-Cre::Ai14 mice and waited 4-6 weeks for trafficking of ChR2 to the axon terminals in mPFC.

Contralateral PFC coordinates were A/P = 1.7, M/L = 0.3, D/V = -2.75. MD thalamus injection coordinates were A/P = -1.7, M/L = +/- 0.3, D/V = -3.45. vHPC injection coordinates were A/P = -3.3, M/L = 3.2, D/V = -4.0.

4.23 ChR2 stimulation

We stimulated ChR2 in terminals using 5ms flashes of light generated by a Lambda DG-4 (Sutter Instruments) high-speed optical switch with a 300 W Xenon lamp delivered through a 470 nm excitation filter. For stimulation of ChR2 terminals in voltage clamp, 2 light flashes were delivered with an interstimulus interval of 50 ms. For stimulation of ChR2 terminals in current clamp, 10 light flashes were delivered at varying frequencies (5, 10, 20, 30, 40 Hz) through a 40x objective.

4.3 RESULTS

4.31 5HT suppresses callosal and hippocampal inputs to FSIs presynaptically

To study the effect of 5HT on excitatory synapses onto FSIs in prefrontal cortex, we selectively expressed channelrhodopsin (ChR2) in projections neurons from either the contralateral PFC (cPFC), mediodorsal thalamus (MD), or ventral hippocampus (vHPC) in PV-Cre::Ai14 mice (Figure 4.1A,F,K). After waiting 4-6 weeks for expression, we performed whole cell patch clamp recordings from fluorescently identified FSIs. We

stimulated ChR2-expressing axon terminals from one of the aforementioned projections and recorded excitatory postsynaptic currents (EPSCs) at baseline and after application of 5HT (30 μ M, Figure 4.1B,G,L). Consistent with our previously work in Chapter 2, we found that 5HT depolarized all neurons recorded, indicated by an increase in the negative holding current required to keep the cells at -70 mV ($p < 0.001$ for cPFC, MD, and vHPC, paired t-test baseline vs. 5HT, Figure 4.1E,J,O). We also found that 5HT suppressed the amplitude of EPSCs in cPFC ($p = 0.0312$, paired t-test baseline vs. 5HT, $n=6$, Figure 4.1C) and vHPC ($p = 0.0769$, same test, $n=5$, Figure 4.1M) but not MD thalamus ($p = 0.4609$, same test, $n=8$, Figure 4.1H). We next calculated the paired-pulse ratio (EPSC2 amplitude / EPSC1 amplitude), which is often used as an indicator of changes in presynaptic release probability, and found an increase in paired-pulse ratio (PPR) for both cPFC ($p = 0.0307$, paired t-test baseline vs. 5HT, $n=6$, Figure 4.1D) and vHPC ($p = 0.0391$, same test, $n=5$, Figure 4.1N) inputs, suggesting that presynaptic release probability is decreased at these synapses.

4.32 5HT increases FSI firing in response to all inputs

Next, we switched to current clamp to investigate how the cumulative effects of 5HT (presynaptic and postsynaptic) would influence FSI action potential generation in response to synaptic inputs. We optogenetically stimulated presynaptic terminals from cPFC, MD, and vHPC with 10 light flashes at five different frequencies (5, 10, 20, 30, 40 Hz) at baseline and after 5HT application (Figure 4.2A,C,E). Regardless of projection, we observed an increase in FSI firing in response to presynaptic stimulation, with higher frequency stimulation eliciting higher firing rates (Figure 4.2 B,D,F).

4.4 DISCUSSION

Here, we described how serotonin is able to modulate specific types of inputs onto prefrontal fast-spiking interneurons without altering the overall output of these neurons. Specifically, we found that serotonin suppresses the amplitude of synaptic responses to stimulation of callosal and hippocampal inputs, findings that are consistent with previous studies in pyramidal neurons (Troca Marin et al., Kjaerby et al., 2016). Due to the observed increase in paired-pulse ratio, we conclude that this suppression is due to a presynaptic reduction in release probability. Furthermore, we would expect this effect to be a result of presynaptic activation of 5HT1B receptors, consistent with our previous findings (Kjaerby et al., 2016). Also consistent with previous work, we found that serotonin did not have an effect on projections from the mediodorsal thalamus.

However, despite this projection-specific modulation of synaptic responses, we also found that serotonin increased the firing of FSIs regardless of input. Previously (Chapter 2), we characterized intrinsic changes to FSI passive membrane properties that resulted in increased excitability of these neurons (Athilingam et al., 2017). Specifically, serotonin reduces conductance of inward-rectifying potassium channels to increase input resistance and membrane potential. In the experiments described here, it seems that this postsynaptic increase in excitability wins out over any presynaptic changes. In our earlier study (Chapter 2), we additionally found that increases in FSI firing were more enhanced for gamma frequency inputs (Athilingam et al., 2017). We were unable to stimulate at high gamma frequencies due to the kinetic limitations of channelrhodopsin here. However, consistent with our earlier findings, we observed that higher frequency stimulation does indeed elicit a larger change in firing rate. Therefore,

we conclude that serotonin functions to tune FSIs to gamma frequency inputs, regardless of source.

4.5 FIGURES

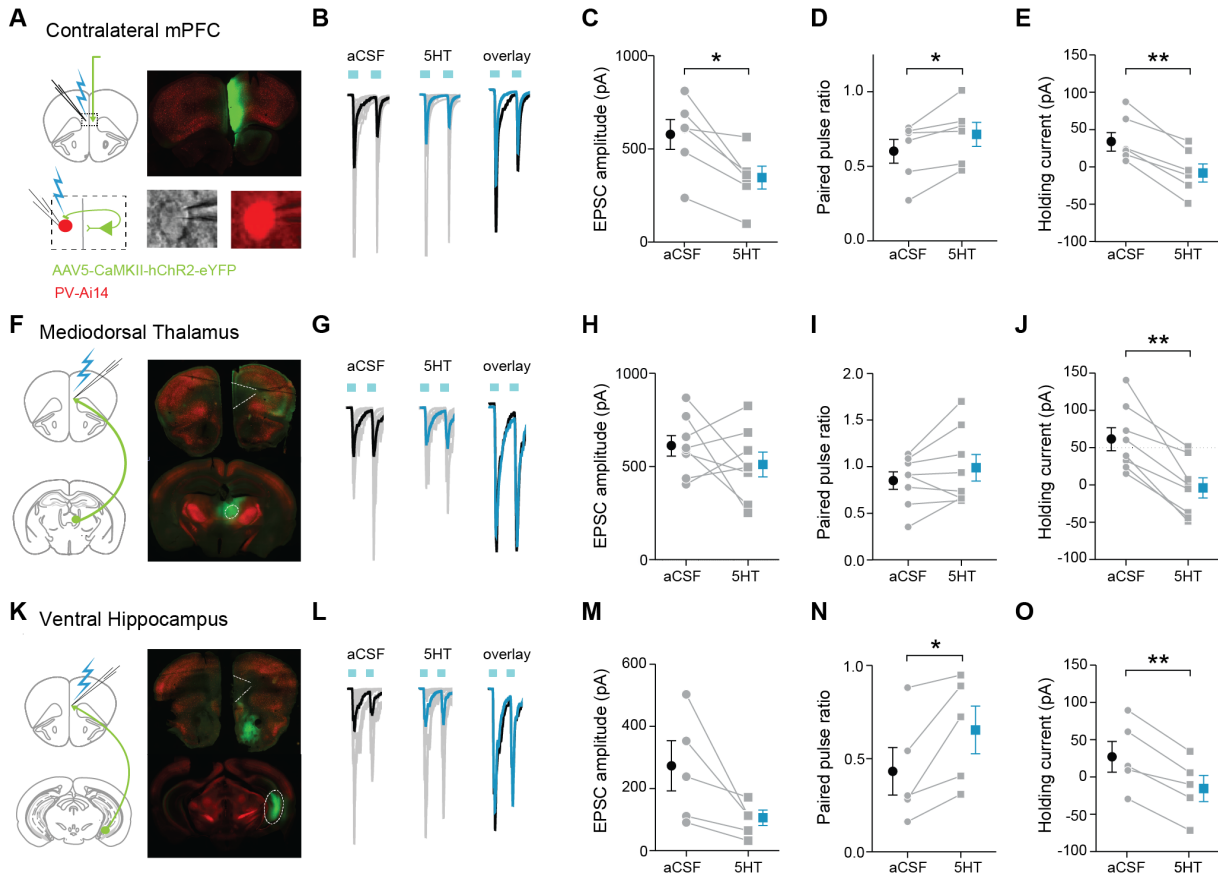


Figure 4.1. Serotonin modulates excitatory synapses in a projection-specific manner. A,F,K) Experimental design: AAV-CaMKII-ChR2-eYFP was injected into one contralateral prefrontal cortex (A), ipsilateral mediodorsal thalamus (F), or ipsilateral ventral hippocampus (K) in PV-Cre :: Ai14 mice. After waiting for expression, slices of PFC were taken and PV+ neurons were patched in the opposite hemisphere. Confocal image of injection sites and prefrontal slices. B,G,L) Example EPSCs in response to stimulation of ChR2-expressing afferents with blue light pulses (5 ms) at baseline in aCSF and after application of 30 μ M 5HT. Gray traces are individual examples. Colored traces are average. Overlay displays traces overlaid. C,H,M) Quantification of evoked EPSC amplitude at baseline in aCSF and after 5HT application for each projection. D,I,N) Quantification of paired-pulse ratio in aCSF and after 5HT application for each projection. Paired-pulse ratio was quantified by dividing the amplitude of the second EPSC by the amplitude of the first EPSC. E,J,O) Quantification of holding current required to hold neurons at -70 mV at baseline and after application of 5HT.

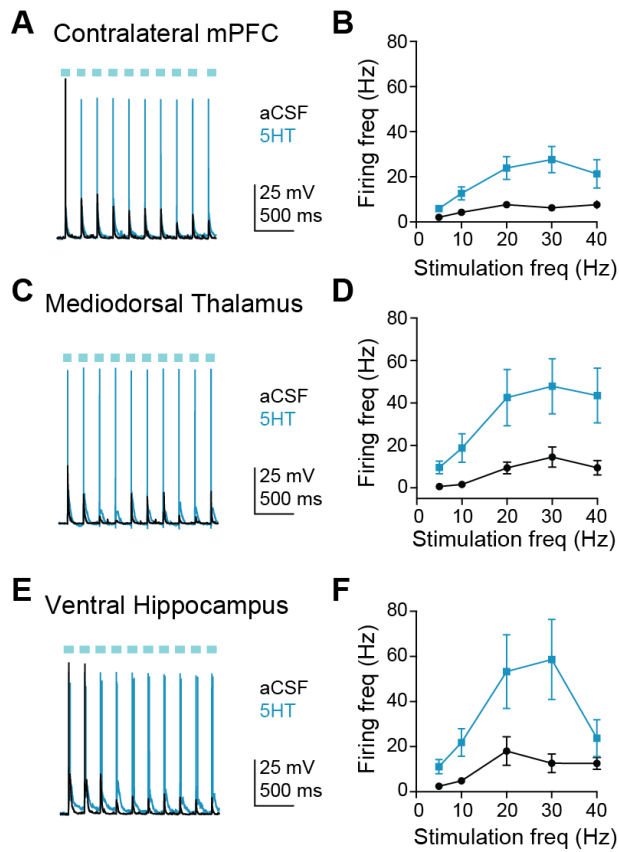


Figure 4.2 5HT increases FSI firing in response to synaptic stimulation regardless of input. A,C,E) Experimental design: FSI membrane potential fluctuations were recorded in current clamp during stimulation of ChR2 afferents from contralateral PFC (A), mediodorsal thalamus (C), or ventral hippocampus (E). Afferents were stimulated with 10 light pulses (5 ms) at 5 different frequencies (5, 10, 20, 30, 40 Hz). Black traces are baseline in aCSF and blue traces are in the presence of 30 μ M 5HT. B,D,F) Quantification of FSI firing rate in response to synaptic stimulation of different projections at different frequencies.

4.6 REFERENCES

- Adhikari, A., Topiwala, M.A., Gordon, J.A., 2011. Single Units in the Medial Prefrontal Cortex with Anxiety-Related Firing Patterns Are Preferentially Influenced by Ventral Hippocampal Activity. *Neuron* 71, 898–910. doi:10.1016/j.neuron.2011.07.027
- Athilingam, J., Ben-Shalom, R., Keeshen, C., Sohal, V.S., Bender, K.J. 2017. Serotonin enhances excitability and gamma frequency temporal integration in prefrontal fast-spiking interneurons. *eLife*.
- Barre, A., Berthoux, C., De Bundel, D., Valjent, E., Bockaert, J., Marin, P., Bécamel, C., 2016. Presynaptic serotonin 2A receptors modulate thalamocortical plasticity and associative learning. *PNAS* 113, 1382-91. doi:10.1073/pnas.1525586113
- Bolkan, S.S., Stujenske, J.M., Parnaudeau, S., Spellman, T.J., Rauffenbart, C., Abbas, A.I., Harris, A.Z., Gordon, J.A., Kellendonk, C., 2017. Thalamic projections sustain prefrontal activity during working memory maintenance. *Nature Neuroscience* 20, 987-996. doi:10.1038/nn.4568
- Kjaerby, C., Athilingam, J., Robinson, S. E., lafrati, J., & Sohal, V. S. (2016). Serotonin 1B receptors regulate prefrontal function by gating callosal and hippocampal inputs. *Cell Reports*, 17(11), 2882-2890.
- Padilla-Coreano, N., Bolkan, S.S., Pierce, G.M., Blackman, D.R., Hardin, W.D., Garcia-Garcia, A.L., Spellman, T.J., Gordon, J.A., 2016. Direct Ventral Hippocampal-Prefrontal Input Is Required for Anxiety-Related Neural Activity and Behavior. *Neuron* 89, 857-866. doi:10.1016/j.neuron.2016.01.011
- Parnaudeau, S., O'Neill, P.K., Bolkan, S.S., Ward, R.D., Abbas, A.I., Roth, B.L., Balsam, P.D., Gordon, J.A., Kellendonk, C., 2013. Inhibition of mediodorsal thalamus disrupts thalamofrontal connectivity and cognition. *Neuron* 77, 1151-1162. doi:10.1016/j.neuron.2013.01.038
- Troca-Marín, J.A., Geijo-Barrientos, E., 2010. Inhibition by 5-HT of the synaptic responses evoked by callosal fibers on cortical neurons in the mouse. *Pflugers Arch.* 460, 1073–85. doi:10.1007/s00424-010-0875-4
- Yuen, E.Y., Qin, L., Wei, J., Liu, W., Liu, A., Yan, Z., 2014. Synergistic Regulation of Glutamatergic Transmission by Serotonin and Norepinephrine Reuptake Inhibitors in Prefrontal Cortical Neurons. *J Biol Chem* 289, 25177-85. doi:10.1074/jbc.M114.567610

CHAPTER 5

SEROTONERGIC MODULATION OF PREFRONTAL OSCILLATIONS AND BEHAVIOR

5.1 INTRODUCTION

Fast-spiking interneurons (FSIs) are critical for the coordination of network oscillatory activity, specifically in the gamma frequency range (Buzsáki and Chrobak, 1995). These oscillations have been shown to enhance information transfer (Sohal et al., 2009) and may play a role in orchestrating prefrontal-dependent behaviors such as cognitive flexibility (Cho et al., 2015; Kim et al., 2016). Specifically, optogenetic activation of FSIs has been shown to rescue deficits in gamma oscillations and rule-shifting behavior in a mouse model that mimics some symptoms of schizophrenia (Cho et al., 2015). Therefore, modulation of FSIs and gamma oscillations could represent a mechanism by which circuits flexibly regulate behavioral output.

I previously found that serotonin (5HT) preferentially enhances the summation of gamma frequency input in FSIs, leading to spiking and downstream inhibition in the gamma frequency range (Athilingam et al., 2017, Chapter 2). Therefore, it is possible that 5HT could regulate the power of network oscillations by modulating FSI intrinsic excitability and responses to gamma frequency inputs.

Furthermore, 5HT has been implicated in a wide range of prefrontal-dependent behaviors (Baker et al., 2011, Carli et al., 2006, Clarke et al., 2004, Clarke et al., 2005, Koot et al., 2012, Robinson et al., 2013, Williams et al., 2002). Since most antidepressant drugs increase 5HT levels by blocking reuptake, it may also be involved in the etiology of depression (Risch & Nemeroff, 1992). Interestingly, drugs that increase GABAergic transmission are commonly used to treat anxiety. The line between

anxiety and depression is blurry; often drugs meant to treat one can also be used to treat the other. Therefore, the intersection of 5HT and inhibition could present valuable insight into the etiology of these disorders.

In Chapter 2, I thoroughly dissected the cellular effects of serotonin (5HT) in fast-spiking interneurons (FSIs), demonstrating that serotonin increases gamma frequency temporal summation due to changes to passive membrane properties. Furthermore, I showed that eliciting Gq-signaling using a Gq-coupled DREADD is able to perfectly replicate serotonergic effects. Here, I use this tool to explore the consequences of these effects *in vivo*. I found that Gq-activation in FSIs increases FSI activity *in vivo* and results in an attenuation of low-frequency oscillations while leaving gamma-frequency oscillations in tact. Interesting, I found preliminary evidence suggesting that this manipulation may be able to rescue cognitive flexibility deficits in a mouse model that presents symptoms of schizophrenia. Furthermore, I find that this manipulation increases novel object exploration time and reduces immobility time in the forced swim test, suggesting that these effects may also play a role in anxiety behavior.

5.2 METHODS

5.21 Stereotaxic surgery for viral injections and implants

Viral injections were performed using standard mouse stereotactical methods. Mice were anesthetized for the duration of the surgery using isofluorane gas. After cleaning, an incision was made in the scalp, the skull was leveled, and small burr holes were drilled over the brain region of interest using a dental drill. Virus was injected through the burr holes using a microinjector (WPI) at a speed of 150 nL/minute and the

scalp was closed using sutures or tissue adhesive (Vetbond). All experiments were conducted in accordance with procedures established by the Institutional Animal Care and Use Committee and Laboratory Animal Resource Center at the University of California, San Francisco.

For DREADD activation of fast-spiking interneurons, we injected a Cre-dependent virus expressing the Gq-DREADD (AAV-DJ-Ef1a-DIO-hM3D(Gq)- mCherry, 200 nL at 5 depths = 1000 nL total) or a control fluorophore (AAV-DJ-Ef1a-DIO-mCherry, 200 nL at 5 depths = 1000 nL total) into PV-Cre mice. mPFC injection coordinates were A/P = 1.7, M/L = +/- 0.3, D/V = -2.00, -2.25, -2.50, -2.75, -3.00. For these experiments, we waited 5 weeks for expression of the DREADD.

For *in vivo* calcium imaging (fiber photometry) experiments, we injected a cre-dependent virus expressing the genetically-encoded calcium indicator gCamp6f (AAV5-hSyn-FLEX-gCamp6f) into the same PV-Cre mice. For these experiments, we injected gCamp6f 2 weeks after DREADD injection so that gCamp would express for 3 weeks before testing.

For photometry and local field potential (LFP) recordings, we attached a tungsten electrode (50 k Ω impedance) to a photometry light fiber (400/430 μ m inner/outer diameter, 0.48 NA, 2.75 mm length, Doric Lenses) using heat-shrink wrap and super glue and inserted the unilateral implant into the right mPFC after injection of gCamp6f. An additional reference tungsten electrode was placed into the left mPFC. A conductive stainless steel screw was inserted into the skull over the cerebellum (A/P = -4.5, M/L = 1.0) to serve as a ground. The electrodes and ground screw were attached to a headstage using silver wire and silver paint and the whole implant was secured to the

mouse's skull with Metabond adhesive and dental cement. The surgery was performed at the same time as gCamp6f injection and the mice were allowed to recover for 3 weeks before testing.

5.22 *In vivo* DREADD activation

Mice were administered 1 mg/kg clozapine-N-oxide (CNO, Tocris) at a volume of 10 mL/kg or an equivalent volume of saline. Mice were handled and habituated to the injection for three days prior to any testing. Behavioral tests or recordings were performed 25 - 30 minutes following injection to allow time for DREADD activation.

5.23 *In vivo* calcium imaging and analysis

We recorded *in vivo* calcium signals using an integrated fiber photometry system (Doric Lenses, Quebec City, QC, Canada) which emits 405 nm (to measure control background autofluorescence of gCamp) and 465 nm (to measure gCamp fluorescence) via a single 400 μ m optical fiber (Doric) that is coupled to the implanted optical fibers. Fluorescence signals were collected and focused onto a visible femtowatt silicon photoreceiver (Newport, Irvine, CA). The output was directed to RZ5P Processor (Tucker Davis Technologies, Alachua, FL) and recorded with Synapse (TDT) software on a PC.

The 465 nm fluorescence signal was normalized to the 405 nm signal. The first 5 minutes of the recording were categorized as the "Baseline" period. A 5 minute period after 30 minutes was characterized as the "Post" period. The average normalized signal was computed for each period using custom MATLAB code.

5.23 Local field potential recording and analysis

Differential EEG was recorded at 2 kHz (and later downsampled to 1 kHz) from mice using a time-locked video EEG monitoring system (Pinnacle Technology). The PFC signal was recorded as the difference between left and right prefrontal electrodes. The first 5 minutes of the recording were categorized as the “Baseline” period. A 5 minute period after 30 minutes was characterized as the “Post” period. The power spectra of the two periods were computed and the power for frequency values within defined frequency bands (Theta 4-8 Hz, Alpha 9-12 Hz, Beta 13-30 Hz, Low Gamma 31-59 Hz, High Gamma 61-100 Hz) was summed for comparison. Analysis was performed with custom MATLAB (Mathworks, Natick, MA) code.

5.25 Behavioral assays

Novel object exploration. A novel object (50 mL blue falcon tube cap) was dropped into their home cage and mice were allowed to freely explore their home cage and the novel object for 5 minutes. Novel object interaction time was scored manually as the number of seconds a mouse spent directly interacting with the object using its nose.

Forced swim test. A 10 cm diameter beaker was filled with water (32 degrees celsius) 15 cm high (2 cm from the top). Mice were slowly lowered into the beaker and video recorded for 10 minutes. Only minutes 2 thru 6 were analyzed. Immobility time was scored manually as the number of seconds a mouse was not actively swimming,

defined by lack of movement of the hind limbs. Small movements of single limbs required for floatation were included in immobility time.

Elevated Plus Maze. Mice were placed into an elevated plus maze for 10 minutes. Two arms of the maze were enclosed with walls while the other two were open. Time spent in the open arms, closed arms, and center zones were computed using a custom MATLAB script.

Open Field. Mice were placed into an open arena measuring 50 cm x 50 cm for 10 minutes. Distance travelled and time spent in the perimeter zone and center zone were computed using a custom MATLAB script. The center zone was defined as a square measuring 30 cm x 30 cm in the middle of the field.

Social 3 chamber assay. The apparatus used for this task consists of 3 chambers. During the habituation stage, the mouse is contained in the middle chamber for 10 minutes with no access to the other chambers. During stage 1, an juvenile mouse of the same gender as the test mouse is placed under a wire cage in one side chamber and an empty wire cage is placed in the other chamber. The test mouse is allowed to explore all three chambers of the apparatus for 10 minutes. Time spent in the empty cage chamber versus the mouse chamber was computed using custom MATLAB script. During stage 2, a new juvenile mouse of the same gender as the test mouse is introduced into the empty wire cage and the test mouse is again allowed to explore all

three chambers for 10 minutes. Time spent with the familiar mouse versus the novel mouse was computed.

Rule-shifting task. Rule shifting assay was performed as previously described (Cho et al, 2015). Briefly, mice are shaped to dig to the bottom of a cup filled with odored (garlic or coriander) digging medium (kitty litter or sand) to find a small peanut butter chip. During the initial association phase, mice must learn to associate a stimulus from one of the modalities (e.g. garlic) with a reward. After reaching an 80% criterion, the rule is changed (rule shift phase) so a stimulus from the other modality (e.g. sand) is rewarded. Mice must complete trials until they again reach 80% criterion. Perseverative errors are characterized as errors during the rule shift where the mouse digs in the previously rewarded cup. Random errors are errors that were never previously rewarded.

5.3 RESULTS

5.31 Gq activation in FSIs increases FSI activity

To confirm that serotonin increases the activity of FSIs *in vivo*, we performed calcium imaging and utilized a Gq-coupled DREADD that I previously validated as perfectly mimicking the effects of 5HT in FSIs (Chapter 2). This technique limits activation exclusively to FSIs and prevents off-target effects at other loci within the prefrontal microcircuit. We injected cre-dependent viruses encoding for the Gq-DREADD (AAV-DJ-Ef1a-DIO-hM3D(Gq)-mCherry) and calcium indicator gCamp6f (AAV5-hSyn-FLEX-gCamp6f) and implanted a photometry light fiber into the medial

PFC of PV-Cre mice (Figure 5.1A). Consistent with our *in vitro* work (Chapter 2), we found that activation of the Gq-DREADD with CNO (1 mg/kg) increased gCamp6f fluorescence compared to saline controls (Figure 5.1B, $p = 0.0268$ t-test SAL vs. CNO), suggesting that Gq-signaling increases the activity of FSIs *in vivo*.

5.32 Gq activation in FSIs attenuates power of low-frequency oscillations

Our previous work showed that 5HT and Gq-signaling in FSIs increased gamma frequency temporal summation and FSI spiking in response to gamma frequency inputs. Since FSIs control the power of gamma oscillations *in vivo*, we recorded local field potentials (LFP) to examine if Gq-activation altered the power of network oscillatory power. We observed a trend (Figure 5.1C-D) suggesting that CNO reduces the power of low frequency oscillations (Theta 4-8 Hz, Alpha 8-12Hz) without changing the power of higher frequencies (Beta 13-30 Hz, Low Gamma 31-59 Hz, High Gamma 61-100 Hz).

5.33 Gq activation in FSIs rescues cognitive flexibility deficits in mice that model key aspects of schizophrenia

Previous work from our lab showed that deficits in FSI function in *Dlx5/6*^{+/-} mice are correlated with reduced gamma oscillation power and reduced performance in a rule-shifting task (Cho et al., 2015). In that study, optogenetic activation of FSIs at gamma frequency was able to rescue both oscillatory and behavioral deficits. I previously demonstrated that 5HT increased gamma frequency temporal summation and led to increased gamma frequency inhibition in downstream neurons (Athilingam et al., 2017, Chapter 2). Therefore, we hypothesized that serotonergic effects in FSIs may

also rescue cognitive inflexibility. We bilaterally injected $Dlx5/6^{+/-}$ mice or littermate controls with the Gq-DREADD (AAV5-Ef1a-DIO-hM3D(Gq)-mCherry) and tested them on a rule-shifting task 5 weeks later (Figure 5.2A). Consistent with previous work, saline-injected $Dlx5/6^{+/-}$ mice trended toward learning the rule-shift slower than CNO-injected littermate controls, due to increased perseverative errors (Figure 5.2B). Interestingly, CNO seemed to rescue the deficit in $Dlx5/6^{+/-}$ mice, bringing their performance to the level of their wild-type littermates. All groups performed similarly on the initial association.

5.34 Gq activation in FSIs increases novel object exploration time and reduces immobility in forced swim test

Lastly, we asked whether increasing FSI activity via Gq-activation could change the behavior of wild-type mice. We performed a battery of assays to test behaviors associated with anxiety, depression, locomotion, and social interaction. We first found that CNO increased the amount of time that mice spent exploring a novel object in their homecage (Figure 5.3A, $p = 0.03$ t-test SAL vs. CNO). Next, we found that CNO reduced immobility time in the forced swim test, a common assay of depression (Figure 5.3B, $p = 0.006$ t-test SAL vs. CNO). We also observed a trend for increased open-arm exploration time in the elevated plus maze (Figure 5.3C), though this did not reach significance. These three assays suggest that serotonergic effects in FSIs could potentially mediate anxiety behavior. We did not observe any changes in locomotion as measured by distance travelled in the open field (Figure 5.4A, $p = 0.32$ t-test CNO vs. SAL) or social behavior (Figure 5.4B).

5.4 DISCUSSION

Here, we examined the effects of serotonergic signaling in prefrontal FSIs on network oscillations and behavior *in vivo*. We found that eliciting serotonergic signaling in FSIs increases FSI activity and reduces the power of low frequency network oscillations *in vivo*. Furthermore, we found suggestive evidence that these effects may rescue cognitive deficits in mice that model key aspects of schizophrenia and reduce anxiety behaviors in wild-type mice.

5.41 Serotonergic effects increase FSI activity *in vivo* and reduce the power of low-frequency oscillations while leaving gamma power intact

We show for the first time using fiber photometry calcium imaging that the downstream signaling effects of 5HT increase FSI activity *in vivo*. This is consistent with our previous work *in vitro* demonstrating that serotonin depolarizes and increases the excitability of FSIs (Athilingam et al., 2017 - Chapter 2) and increases the frequency of inhibitory events in downstream pyramidal neurons (Athilingam et al., 2017 - Chapter 2, Weber and Andrade, 2010; Zhou and Hablitz, 1999).

Since gamma-frequency optogenetic activation of FSIs *in vivo* increases the power of gamma oscillations (Sohal et al., 2006), we predicted that chemogenetic activation would elicit a similar effect. Instead, we found that Gq-activation reduced low-frequency oscillatory power while leaving gamma power intact. Increasing inhibitory signaling via administration of benzodiazepine has been shown to decrease the power of oscillatory power across all frequency bands (Scheffzük et al., 2013). Here, it is interesting to note that gamma oscillatory power is conserved while the power in other

frequency bands is reduced. We previously found that Gq-activation preferentially enhanced the summation of gamma frequency inputs in FSIs and promoted gamma frequency inhibition in downstream pyramidal cells. Therefore, it is possible that this 5HT-mediated gamma enhancement in FSIs leads to selective filtering of gamma frequency information in the prefrontal network. This is consistent with evidence suggesting that serotonin receptors may be involved in prefrontal-mediated behaviors (Clarke et al., 2004, Baker et al., 2011), which often require gamma oscillations (Cho et al., 2015).

5.42 Serotonergic effects in FSIs may rescue cognitive flexibility deficits in a mouse model of schizophrenia

We found evidence to suggest that eliciting serotonergic signaling in FSIs may rescue cognitive flexibility deficits. Previous work showed that mice heterozygous for *Dlx5/6*, transcription factors that regulate FSI development, exhibited poor performance in a rule-shifting task that was rescued by gamma-frequency optogenetic stimulation of FSIs (Cho et al., 2015). We found that Gq-DREADD activation of FSIs in these same mice was also able to rescue these behavioral deficits. This manipulation is an interesting extension of previous work because it points to a chemical manipulation that is capable of rescuing cognitive inflexibility behavior. Designing a drug that selectively targets 5HT receptors on FSIs may be a more tractable avenue for therapy than performing optogenetics in humans.

5.43 Serotonergic effects in FSIs may mediate anxiety behavior

In our battery of behavioral assays, we found consistent evidence that activating serotonergic signaling in FSIs may reduce anxiety behavior in mice. We first found that mice injected with CNO to activate Gq-signaling to mimic serotonergic effects in FSIs spent more time interacting and investigating a novel object in their home cage. We next found that mice spent less time immobile during the forced swim test. Immobility during the forced swim test is often thought to be an indication of helplessness. And lastly, we observed a trend that mice spent more time in the open arms of an elevated plus maze, a commonly used measure of anxiety. Taken together, these results point to a potential anxiolytic effect of 5HT acting on prefrontal FSIs. Furthermore, this is consistent with our previous knowledge about the roles of serotonin and inhibition in anxiety and depressive behaviors. Selective serotonin reuptake inhibitors (SSRIs), which increase serotonin levels in the brain, are the most efficacious and commonly used treatment for depression. Furthermore, GABAergic agonists are the most commonly prescribed anxiolytics. Considering this and the hypothesized functions of the mPFC in anxiety and depression, it is logical that serotonergic activation of prefrontal inhibition could elicit anxiolytic effects. We also previously showed (Kjaerby et al., 2016, Chapter 3) that prefrontal 5HT1B receptors reduce ventral hippocampal inputs to the mPFC which are thought to carry anxiety information. In that same study, we found that 5HT1B receptor activation reduce the frequency of theta oscillations, a biomarker of anxiety. Here, we also found a reduction of prefrontal theta-frequency oscillations. Together, this suggests that serotonin may act at many loci within the mPFC microcircuit to elicit anxiolytic effects.

5.5 FIGURES

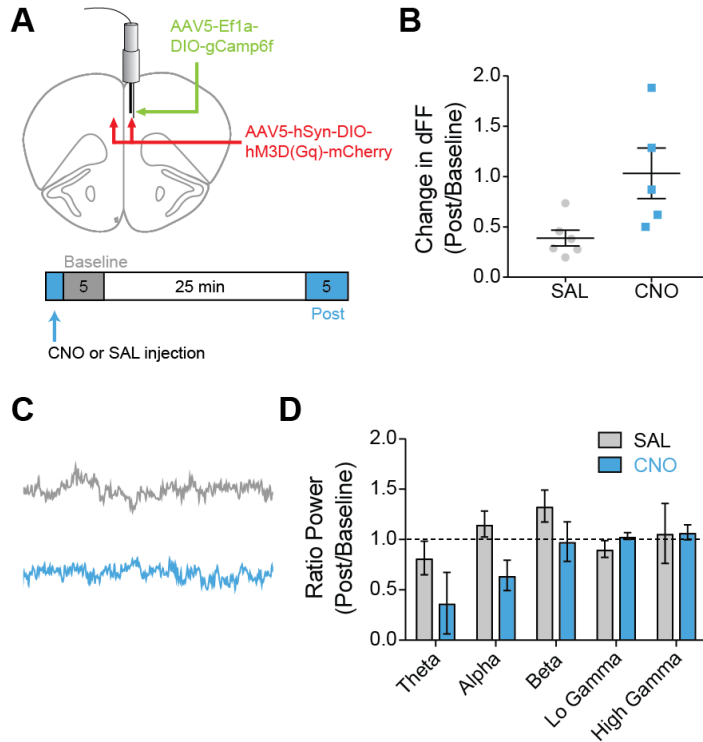


Figure 5.1. Chemogenetic activation of Gq-coupled receptors in FSIs increases FSI activity and reduces low frequency oscillations.

A) Experimental design: A Cre-dependent virus encoding the Gq-DREADD was injected bilaterally into mPFC of PV-Cre mice. Two weeks later, a Cre-dependent calcium indicator virus (AAV5-Ef1a-DIO-gCamp6f) was injected into the right mPFC and an LFP electrode coupled to an optical fiber was implanted. After 3 weeks, photometry and LFP recordings were performed with administration of saline (gray) or CNO (blue). B) Baseline-normalized change in calcium fluorescence in saline versus CNO injected mice. C) Example LFP recordings. D) Baseline-normalized change in power in different frequency bands: theta 4-8 Hz, alpha 9-12 Hz, beta 13-30Hz, low gamma 31-59 Hz, high gamma 61-100 Hz.

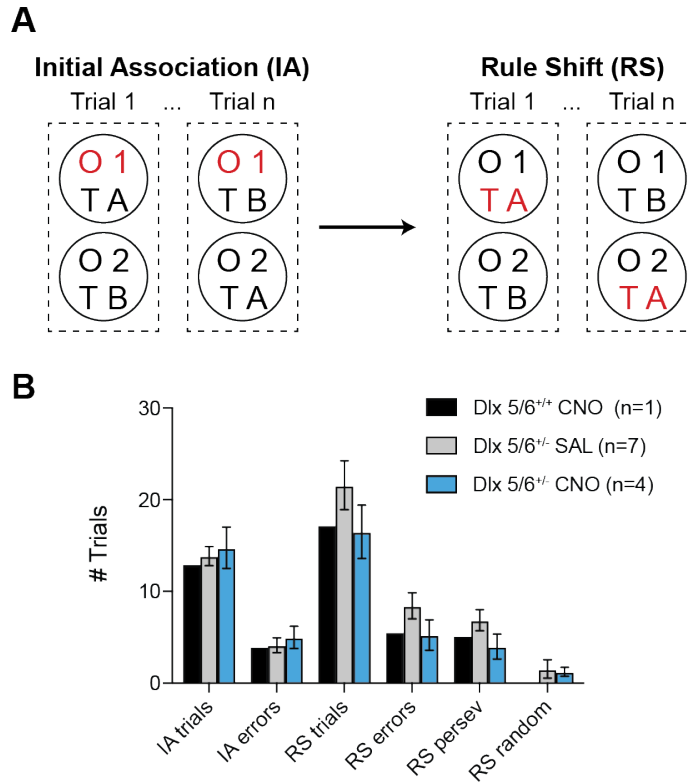


Figure 5.2. Gq-DREADD activation could attenuate cognitive flexibility deficits in a mouse model of schizophrenia.

A) Experimental design: Mice perform a rule-shifting task where they first learn to associate one modality (odor or texture) with reward (initial association, IA). After reaching 80% criterion, the reward modality is switched (rule shift, RS).

B) Number of trials needed to reach criterion during the initial association (IA trials) or rule shift (RS). Number of errors during IA and RS, the latter also split into type of error: perseverative and random.

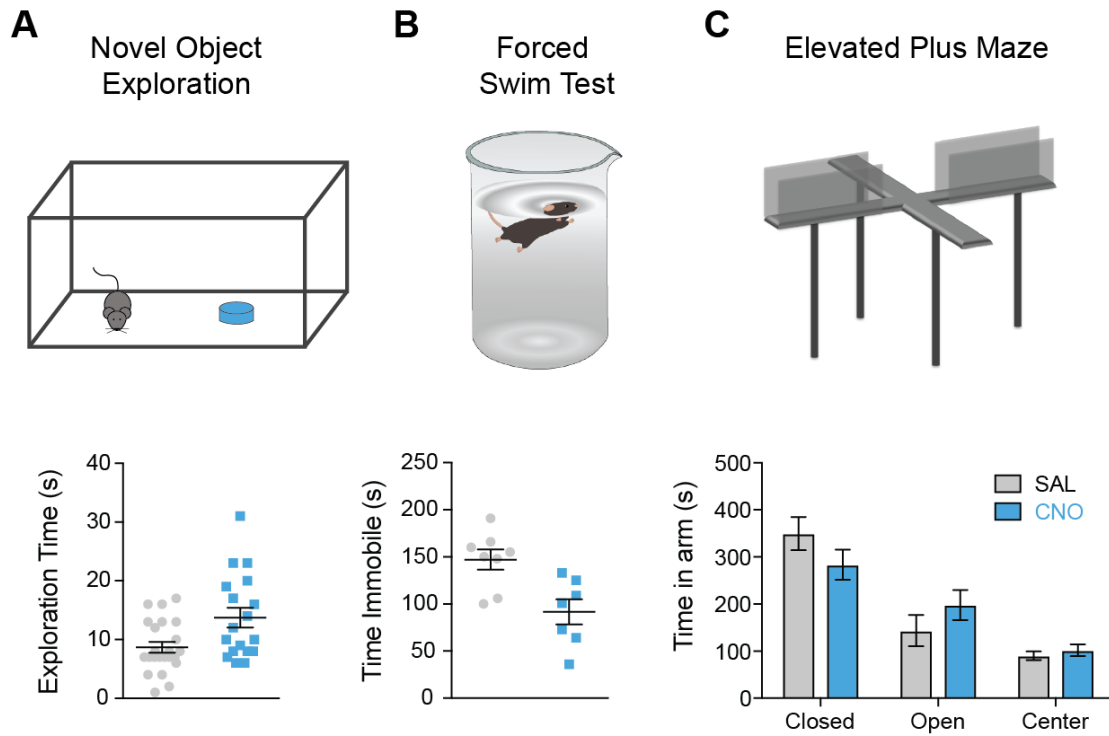


Figure 5.3. Gq-DREADD activation of prefrontal FSIs may reduce anxiety behavior.

A) Top: Experimental design: Mice were allowed to explore their homecage and a novel object (blue 50 mL falcon tube cap) was placed in their cage for 5 minutes. Bottom: Time spent exploring by novel object by saline (gray) and CNO (blue) injected mice.

B) Top: Experimental design: Mice were placed in large beaker of water and immobility time was measured. Bottom: Time spent immobile in saline versus CNO injected mice.

C) Top: Experimental design: Mice spent 10 minutes exploring an elevated plus maze. Bottom: Time spent in center area and closed/open arms by mice injected with saline or CNO.

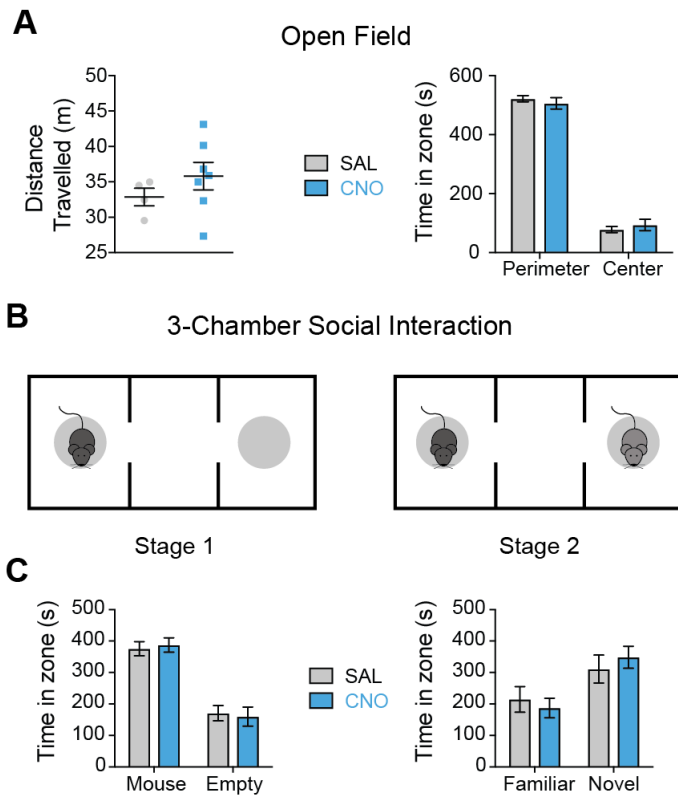


Figure 5.4. Gq-DREADD activation of FSIs has no effect on locomotion or social interaction.

A) Left: Distance travelled in 10 minutes in open field by saline versus CNO injected mice. Right: Time spent in center versus perimeter zones of open field in 10 minutes.

B) Experimental design: Mice are allowed to explore a three-chamber box for 10 minutes. In stage 1, one side has an empty cage and the other side has a juvenile mouse in a cage. In stage 2, the empty cage contains a novel juvenile.

C) Time that mice spend in respective chambers of the three chamber box during stage 1 (mouse, empty) and stage 2 (familiar, novel).

5.6 REFERENCES

- Athilingam, J., Ben-Shalom, R., Keeshen, C., Sohal, V.S., Bender, K.J. 2017. Serotonin enhances excitability and gamma frequency temporal integration in prefrontal fast-spiking interneurons. *eLife*.
- Baker, P.M., Thompson, J.L., Sweeney, J.A., Ragozzino, M.E., 2011. Differential effects of 5-HT(2A) and 5-HT(2C) receptor blockade on strategy-switching. *Behav. Brain Res.* 219, 123–31.
- Barre, A., Berthoux, C., De Bundel, D., Valjent, E., Bockaert, J., Marin, P., Bécamel, C., 2016. Presynaptic serotonin 2A receptors modulate thalamocortical plasticity and associative learning. *PNAS* 113, 1382-91. doi:10.1073/pnas.1525586113
- Buzsáki, G., Chrobak, J.J., 1995. Temporal structure in spatially organized neuronal ensembles: a role for interneuronal networks. *Curr. Opin. Neurobiol.* 5, 504–10.
- Carli, M., Baviera, M., Invernizzi, R.W., Balducci, C., 2006. Dissociable contribution of 5-HT1A and 5-HT2A receptors in the medial prefrontal cortex to different aspects of executive control such as impulsivity and compulsive perseveration in rats. *Neuropsychopharmacology* 31, 757–67.
- Cho, K.K.A., Hoch, R., Lee, A.T., Patel, T., Rubenstein, J.L.R., Sohal, V.S., 2015. Gamma Rhythms Link Prefrontal Interneuron Dysfunction with Cognitive Inflexibility in *Dlx5/6+/-* Mice. *Neuron* 85, 1332–1343.
- Clarke, H.F., Dalley, J.W., Crofts, H.S., Robbins, T.W., Roberts, A.C., 2004. Cognitive inflexibility after prefrontal serotonin depletion. *Science* 304, 878–80.
- Clarke, H.F., Walker, S.C., Dalley, J.W., Robbins, T.W., Roberts, A.C., 2007. Cognitive inflexibility after prefrontal serotonin depletion is behaviorally and neurochemically specific. *Cereb. Cortex* 17, 18–27.
- Kim, H., Åhrlund-Richter, S., Wang, X., Deisseroth, K., and Carlén, M., 2016. Prefrontal Parvalbumin Neurons in Control of Attention. *Cell* 164, 208–218.
- Koot, S., Zoratto, F., Cassano, T., Colangeli, R., Laviola, G., Bos, R. van den, Adriani, W., 2012. Compromised decision-making and increased gambling proneness following dietary serotonin depletion in rats. *Neuropharmacology* 62, 1640–50.
- Scheffzük C, Kukushka VI, Vyssotski AL, Draguhn A, Tort AB, Brankač J., 2013. Global slowing of network oscillations in mouse neocortex by diazepam. *Neuropharmacology* 65, 123-33.
- Sohal, V.S., Zhang, F., Yizhar, O., Deisseroth, K., 2009. Parvalbumin neurons and gamma rhythms enhance cortical circuit performance. *Nature* 459, 698–702.

Risch, S.C., Nemeroff, C.B., 1992. Neurochemical alterations of serotonergic neuronal systems in depression. *J Clin Psychiatry* 53 Suppl, 3–7.

Williams, GV, Rao, SG, 2002. The physiological role of 5-HT_{2A} receptors in working memory. *The Journal of*

CHAPTER 6

A VISIBLE LIGHT-SENSITIVE CAGED SEROTONIN

6.1 ABSTRACT

Serotonin, or 5-hydroxytryptamine (5HT), is an important neurotransmitter in the nervous system of both vertebrates and invertebrates. Deficits in 5HT signaling are responsible for many disabling psychiatric conditions, and its molecular machinery is the target of many pharmaceuticals. We present a new 5HT phototrigger, the compound $[\text{Ru}(\text{bpy})_2(\text{PMe}_3)(5\text{HT})]^{2+}$, where PMe_3 is trimethylphosphine. As with other ruthenium-bipyridyl based caged compounds, $[\text{Ru}(\text{bpy})_2(\text{PMe}_3)(5\text{HT})]^{2+}$ presents activity in the visible region of the spectrum. We characterize and discuss the photochemical properties of the caged compound, and demonstrate its use by modulating the excitability of mouse prefrontal principal neurons.

6.2 INTRODUCTION

A caged compound, or phototrigger, is a molecule reversibly bound to or "caged within" a protecting group that restricts its interactions with cell-membrane receptors, proteins, or other molecules. Entities that have been caged include ions, [1] acids, [2] bases, [3] neurotransmitters, [4] fluorophores, [5,6] small-molecule drugs, [7] gene inducers [8,9] and even nucleic acids [10] and proteins [11,12]. Phototriggers are light-sensitive, and will release the caged molecule upon irradiation with light of the proper wavelength, [13] thus removing the restrictions for the caged entity to interact normally with its targets. As the uncaging spot size can be precisely determined by focusing a low-power laser, this technique can have very high spatial and temporal resolution, making it of great advantage in biological research, for it allows the delivery of

molecules without mechanically acting on the preparation, a problem usually associated with more invasive techniques like microinjection.

Most common caged compounds comprise an organic protecting group, usually a nitrobenzyl [14] or nitroindonyl [15] which are active in the UV region and therefore can damage the biological tissue. Therefore, new kinds of organic-based protecting groups have been developed, such as coumarine derivatives, which can extend the photoactivity to the violet region, thus reducing cell damage. [16]

As we have shown in recent years, ruthenium-bipyridyl coordination complexes yield excellent phototriggers suitable for neurophysiology studies. They present unique properties, including nanosecond photoreaction kinetics through heterolytic photocleavage with no secondary reaction products, [7,17] and sensitivity to visible light in the blue and green regions. [3,6,7,18-20] As an important advantage over other photoprotective groups, Ru-bipyridyl phototriggers can be used in a two-photon regime. [17, 21-24] Ruthenium phototriggers were also used for general delivery of drugs, toward application in therapy. Turro and Bonnet have shown the versatility of Ru(II) polypyridines for caging nitriles and thioethers.[25-27] A similar strategy using the photoredox properties of the Ru(II) polypyridyl chemistry was used by Ford and Santana da Silva to release nitric oxide (NO) by visible light, both directly or mediated by energy transfer processes from molecular antennas.[28-29]

Ruthenium phototriggers are very stable at room temperature, both as a solid or in physiological solutions when kept in the dark, minimizing dark leakage of the caged biomolecule, one of the most common drawbacks of nitrobenzyls and similar caging groups.

Serotonin is one of the most important neuromodulators in a very wide range of animal phyla. It modulates basic behaviours such as feeding and mating, [30] and imbalances in its physiology lead to debilitating psychiatric conditions in humans, such as obsessive compulsive disorder, panic disorder, or major depression. [31] For this reason, the serotonergic system is the target of many pharmaceuticals such as tricyclic antidepressants (TCAs) selective serotonin reuptake inhibitors (SSRIs) and monoamine oxidase inhibitors (MAOIs), and even many recreational drugs. [32] Discerning the effects of 5HT on its various receptor and cellular subtypes and understanding its interactions with other systems of neurotransmitters would be greatly aided by a caged 5HT. As serotonin does not exhibit a carboxylate group, most strategies used to cage neuroactive aminoacids cannot be extended directly to cage this amine. Currently, two of the commercially available caged serotonins are NPEC-5HT and BHQ-O-5HT, which use the phenol group of the 5HT for anchoring the photoremovable protecting group and are active under UV light (365 nm). While the first shows negligible absorption in two-photon regime [33] and has a very slow response time in the hundreds of milliseconds, [34] BHQ-O-5HT can also be used at 740 nm (2P) with good quantum yields. [35,36] Other caged 5HT compounds have been described, showing dissimilar performances. [36-40]

We report the synthesis and chemical properties of the complex $[\text{Ru}(\text{bpy})_2(\text{PMe}_3)(5\text{HT})]^{+2}$, which releases 5HT upon absorption of visible light, and demonstrate its use by modulating the excitability of mouse prefrontal principal cells that have previously been shown to be regulated by 5HT. [41]

6.3 METHODS

6.31 Syntheses

All chemicals were purchased from Sigma-Aldrich and used as received without further purification. Ru(bpy)₂Cl₂ was synthesized according to literature [45] and from this [Ru(bpy)₂(PMe₃)(Cl)]PF₆ was obtained as previously described. [17]

Syntheses of [Ru(bpy)₂(PMe₃)(5HT)]Cl₂: 207 mg (320 μmol) of [Ru(bpy)₂(PMe₃)(Cl)]PF₆ were dissolved in 2 ml acetone and 10 ml water. The mixture was stirred with Cl⁻-loaded Dowex ion exchange resin during 15–30 minutes. After evaporation of acetone the resultant solution of [Ru(bpy)₂(PMe₃)(Cl)]Cl was heated at 70 C to obtain the aquo complex [Ru(bpy)₂(PMe₃)(H₂O)]Cl. Then 320 mg (1500 μmol) of serotonin hydrochloride salt were introduced under N₂ atmosphere in a Schlenk flask and the pH was raised to 9-10 by adding 1400 μL of NaOH 1 M. When the formation of serotonin complex was confirmed by UV-visible spectroscopy, the mixture was cooled in an ice bath and HCl 1 M was added to lower the pH and prevent possible oxidation of serotonin by air during the subsequent procedures. The solution was filtered and after the addition of 1500 μL of KPF₆ 0.5 M the complex [Ru(bpy)₂(PMe₃)(5HT)](PF₆)₂ precipitates as an orange powder. Anal. Calcd. for C, 41.47; H, 3.90; N, 8.79. Found: C, 41.2; H, 4.1; N, 8.5. For the purification of the serotonin complex, hexafluorophosphate anion was interchanged for chloride using Dowex-22 ion exchange resin. The complex was reprecipitated with KPF₆ 0.5 M at pH 3, the anion interchanged again and pH adjusted between 7–8. The lyophilized complex [Ru(bpy)₂(PMe₃)(5HT)]Cl was characterized by NMR spectroscopy. ¹H-NMR (D₂O, K₂CO₃) δ, ppm = 8.78 (1H, d, bpy), 8.57 (1H, d, bpy), 8.36 (1H, d, bpy), 8.13 (1H, d, bpy), 8.10 (1H, t, bpy), 7.99 (1H,

d, bpy), 7.94 (1H, d, bpy), 7.83 (1H, t, bpy), 7.79 (1H, t, bpy), 7.69 (1H, t, bpy), 7.64 (1H, t, bpy), 7.36 (1H, t, bpy), 7.31 (1H, d, bpy), 7.29 (1H, d, bpy), 7.19 (1H, d, J=8.5 Hz, 5HT), 7.13 (1H, t, bpy), 6.95 (1H, t, bpy), 6.89 (1H, s, 5HT), 6.63 (1H, dd, J=8.5 Hz and J=2 Hz, 5HT), 6.21 (1H, d, J=2 Hz, 5HT), 3.57 (1H, t, 5HT), 2.65 (1H, t, 5HT), 2.61-2.47 (2H, m, 5HT), 2.42 (1H, m, 5HT), 1.76 (1H, m, 5HT), 0.92 (9H, d, PMe₃).

6.32 Spectroscopic Measurements and Photolysis

The optical bench used for UV-Vis measurements consists, briefly, of a set of collinear lasers directed towards a four-faceted cuvette, stirred and thermostated at 25 °C. The solution's absorbance is monitored perpendicularly to the laser path by an OceanOptics PC2000 diode-array spectrophotometer run by OOIChem software. Quantum yield measurements of photocaging were performed recording full absorption spectra while the photoreaction occurs. Then, the quantum yield of photolysis (PD) was adjusted as a parameter in order to fit the equation 1 to the measured spectra.

NMR spectra were obtained with a 500 MHz Bruker AM-500. The compound was photolyzed inside the unopened NMR test tube with an own-designed illuminator (see supporting information, Figure S2) using an array of high power LEDs centered at 450 nm FWHM.

6.33 Voltammetry

Cyclic voltammetry was recorded at 100 mV/s scan rate in acetonitrile solution and tetrabutylammonium salt as supporting electrolyte, using a three-electrode

potentiostat based on an operational amplifier TL071 in current-voltage configuration. A Pt wire with a diameter of 500 μm was used as a working electrode and acquisition software was written in QuickBasic 4.5. Ferrocene was used as internal reference.

6.34 Electrophysiology. Slice Preparation.

Coronal brain slices (250 μm) containing medial prefrontal cortex were made from a P45 C57BL/6 male mouse. Slicing solution was chilled to 4°C and contained (in mM): 234 sucrose, 26 NaHCO₃, 11 glucose, 10 MgSO₄, 2.5 KCl, 1.25 NaH₂PO₄, 0.5 CaCl₂, bubbled with 5% CO₂/ 95% O₂. Slices were incubated in artificial cerebrospinal fluid (aCSF) at 32°C for 30 minutes and then at room temperature until recording. ACSF contained (in mM): 123 NaCl, 26 NaHCO₃, 11 glucose, 3 KCl, 2 CaCl₂, 1.25 NaH₂PO₄, 1 MgCl₂, also bubbled with 5% CO₂/ 95% O₂.

6.35 Serotonin Uncaging & Patch Clamp Electrophysiology

[Ru(bpy)₂(PMe₃)(5HT)]Cl was applied as a powder to the aCSF bath solution (100 μM) and was photolysed by 1 photon excitation with a single 5 ms light flash of a 470 nm LED (~3.6 mW).

Neurons were visualized using DODT contrast microscopy on an upright microscope (Bruker). Recordings were made using a Multiclamp 700B (Molecular Devices) amplifier and acquired with IgorPro. Patch pipettes (2-5 M Ω tip resistance, Schott 8250) were filled with the following (in mM): 130 KGlucuronate, 10 KCl, 10 HEPES, 10mM Tris-phosphocreatine, 1.1 EGTA, 2 MgCl₂, 2 MgATP, 0.3 Na₃GTP, and 0.1

Alexa-594. All recordings were made at 32-34°C. Series resistance ranged from 10-15 MΩ and pipette capacitance was compensated.

Current pulses were applied through the somatic patch pipette for electrophysiological characterization (-300 and +150 pA in 250 ms duration). The neuron that displayed voltage sag at step onset and rebound at step offset when hyperpolarized (indicative of high expression of HCN channels) was identified as a putative corticopontine (CPn) projecting neuron [41, 42, 46]. The neuron lacking significant sag and rebound was identified as a putative commissural (COM) projecting neuron [41, 42, 47]. A 9 s positive current step was then applied to elicit spiking during uncaging trials (100 and 75 pA in CPn and COM cells, respectively). 1 μM MDL100907 (stock in DMSO), a potent 5HT_{2A} receptor antagonist, was applied before uncaging for some experiments.

6.4 RESULTS AND DISCUSSION

The complex [Ru(bpy)₂(PMe₃)(5HT)]²⁺ is yellow-orange in color. Its water solubility is well above the tens of millimolar range. No decomposition was detected in samples stored in the dark for months at room temperature either dry or in solution. Water solutions of this complex present a metal to ligand charge transfer (MLCT) band with a molar extinction coefficient (ε) of 6718 M⁻¹ cm⁻¹ and an absorption maximum in the visible range at 447 nm. Its synthesis is a simple one-pot reaction and the photolysis is fast and clean, as depicted in Scheme 1.

Figure 6.2 shows the ¹H-NMR spectra of the complex (top) and of its partial photolysis (bottom). In the first, unphotolyzed spectrum, the aromatic region shows the

expected 8 doublets and 8 triplets that are characteristic of the bipyridines in a *cis* octahedral complex of the form $[\text{Ru}(\text{bpy})_2(\text{L}_1)(\text{L}_2)]^{n+}$, and the four aromatic signals of 5HT. In the aliphatic region (Figure 6.2b), besides the PMe_3 signal at 0.92 ppm the two aliphatic signals for the amine and methylenes group of coordinated 5HT can be seen between 3.60 and 1.71 ppm. The fact that proton signals of amine group can be seen in a D_2O solution at 3.57 ppm and 2.65 ppm and the shift and splitting of the methylene signals indicates the coordination of serotonin to the metal atom through its amine nitrogen. Also visible in the first spectrum are the set of signals corresponding to the *trans* configuration of the complex, although in much smaller proportion. The subtle differences in the photochemical behaviour of the *cis* and *trans* configurations of the complex are negligible in the scope of this work, and no further distinction between these isomers will be made, although a full characterization of both isomers should be needed for any biomedical uses.

Once irradiated inside the NMR tube for 60 seconds, the photolysis progressed around 40%. The signals of the bipyridines in the original complex appear diminished, while a new set of signals corresponding to the aquo-complex are evident. In the aliphatic region, the two characteristic triplets of the methylenes of free 5HT appear at 3.17 ppm and 2.98 ppm (Figure 6.2, signals a and b). Furthermore, amine protons are rapidly exchanged for deuterium and these signals are not present in the free 5HT. The signal from PMe_3 protons is now shifted to higher fields and corresponds to that of the newly formed aquo complex.

To measure the quantum efficiency of photolysis, a water solution of the complex was irradiated with a 8.56 mW, 405 nm (violet) diode laser at pH = 7 and T = 24 °C.

Figure 6.3 shows the UV-Vis spectra during the progression of the photolysis reaction. As is deduced from the presence of an isosbestic point at 434 nm, the reaction yields just one absorbing product and proceeds to completion in around 12 minutes. The spectrum of the photoproduct corresponds to that of the aquo complex $[\text{Ru}(\text{bpy})_2(\text{PMe}_3)(\text{H}_2\text{O})]^{2+}$ accordingly with the known photochemistry of the complexes of the form $[\text{Ru}(\text{bpy})_2(\text{PMe}_3)(\text{L})]^{n+}$ in water at neutral pH. [17, 22, 23] At pH>12 a broader and red-shifted absorption spectrum is obtained, which corresponds in this case to the hydroxo complex $[\text{Ru}(\text{bpy})_2(\text{PMe}_3)(\text{OH})]^+$.

The progression of the photoreaction is shown in Figure 6.4 as the amount of photoreleased 5HT versus the total number of photons absorbed. Although the quantum efficiency of the phototrigger can be directly obtained from the initial slope of this graph, a more precise value was obtained by fitting the complete curve, as described below.

Given the power of the irradiation beam, its optical path, and the amount of complex in the solution, it is possible to calculate the differential amount of product as:

$$\frac{dn_p}{dt} = I_{\text{beam}} \cdot (1 - 10^{-\text{Abs}_T}) \cdot \frac{\text{Abs}_R}{\text{Abs}_T} \cdot \phi_{PD} \quad (1)$$

where n_p is the number of the moles of uncaged product, I_{beam} is the intensity of the incident light in Einsteins/s, Abs_T and Abs_R are the total solution's absorbance and the reactant's absorbance, respectively, and ϕ_{PD} is the quantum yield of photouncaging. The expression has nonlinear factors, and adjusting the value of ϕ_{PD} by iterating a finite differences algorithm over the entire obtained spectra converges to the unique solution for the integrated expression of equation 1.

Cyclic voltammetry was used to further characterize the synthesized complex. Figure 6.5 shows a cyclic voltammogram of $[\text{Ru}(\text{bpy})_2\text{PMe}_3(5\text{HT})]^{2+}$ recorded in

acetonitrile. Ferrocene was used as internal reference. The Ru(III)/Ru(II) couple is observed at 1.07V vs. NHE (0.67 V vs. Fc/Fc+). Other two irreversible processes are evident at higher potentials and correspond to the oxidation of the coordinated amine, a behaviour also found in all other similar compounds. [17]

To confirm the biocompatibility of this complex and evaluate its performance as a serotonin phototrigger, a series of electrophysiology experiments in acute brain slices were performed.

In the mouse prefrontal cortex, separate populations of pyramidal neurons that project either subcortically to the pons (corticopontine, CPn) or to the contralateral cortex (commissural, COM) differentially express Hyperpolarization-activated cyclic nucleotide-gated (HCN) channels. HCN channel expression can be assessed electrophysiologically by hyperpolarizing neurons in current clamp recordings. HCN channels activate slowly over 10s of ms in response to neuronal hyperpolarization. Thus, cells with high HCN expression levels (e.g., CPn neurons) respond to hyperpolarization with a characteristic “sag” during and “rebound” following current pulses as the voltage overshoots steady-state membrane potential in each direction. This overshoot is indicative of the delayed activation and closure of HCN channels. [42] COM neurons express lower levels of HCN and display little to no sag, while CPn neurons express high levels of HCN and display significant sag. 5HT has differential effects on firing properties in these pyramidal neuron classes. [41] In CPn neurons, 5HT reduces neuronal excitability through 5HT1A-dependent signaling. In COM neurons, this 5HT1A-dependent reduction in excitability is often followed by a slower, 5HT2A-

dependent increase in activity. [41] As such, 5HT uncaging should result in both reductions and delayed increases in these two cell classes.

To determine whether uncaging of [Ru(bpy)₂(PMe₃)(5HT)] could alter pyramidal cell firing rates, we made recordings from COM and CPn neurons in mouse prefrontal cortex. When the caged-5HT was added to the slice in the dark, we observed no change in electrophysiological measures including resting membrane potential and input resistance, suggesting that the RuBi-5HT is not toxic in its caged form.

Consistent with previous work, firing rate was lowered by 5HT uncaging in a CPn neuron. [41] A neighboring COM neuron exhibited a characteristic biphasic modulation of firing rate after [Ru(bpy)₂(PMe₃)(5HT)] uncaging with an initial depression of firing rate followed by a brief increase in firing (Figure 6.6E). In a subsequent experiment, we selectively blocked the delayed excitation with the 5HT_{2A} receptor antagonist (1 μM MDL 100907). This experimental design thus provided an internal control that 5HT photolysis occurred (by the generation of the initial decrease in firing rate) while also demonstrating that changes in firing rate were indeed due to activation of 5HT receptors (by blocking the increase in firing rate with MDL 100907).

6.5 CONCLUSION

We have developed [Ru(bpy)₂(PMe₃)(5HT)]²⁺, a ruthenium bipyridil-based 5HT phototrigger which has its absorption maximum well into the visible range. Due to its absorption spectrum, 5HT can be released by irradiating with readily available low-power visible wavelength laser diodes at 405, 445 and even 532 nm. The photoprocess is very clean, showing no sign of other photoproducts besides free serotonin and the

corresponding aquo complexes, as is expected from the known photochemistry of this kind of compound. Its redox potential lays into the expected values for a complex of this family, and is highly related with the position of the MLCT band [43]. However, its quantum efficiency of photorelease is somewhat lower than expected. The analog complexes $[\text{Ru}(\text{bpy})_2\text{PMe}_3(\text{Dopa})]^+$ (Dopa = dopamine)[23] and $[\text{Ru}(\text{bpy})_2\text{PMe}_3(\text{GABA})]^+$ present the same absorption [44] but three times more activity than $[\text{Ru}(\text{bpy})_2\text{PMe}_3(5\text{HT})]^+$, suggesting that some degree of recaptation after uncaging may be occurring. On the other hand, the sensitivity of this new caged serotonin is high enough to allow clean and fast uncaging in biological models, as is demonstrated by confirming neuronal characterization experiments while uncaging with a 5 ms 470nm LED light source.

This phototrigger can be used with harmless visible light instead of UV light as is needed with the more traditional organic protecting groups. The water solubility of its chloride salt $[\text{Ru}(\text{bpy})_2(\text{PMe}_3)(5\text{HT})]\text{Cl}_2$ is around 200 mM, much higher than needed for biological experiments, and the excellent stability of its solutions at neutral pH has been confirmed.

6.6 FIGURES

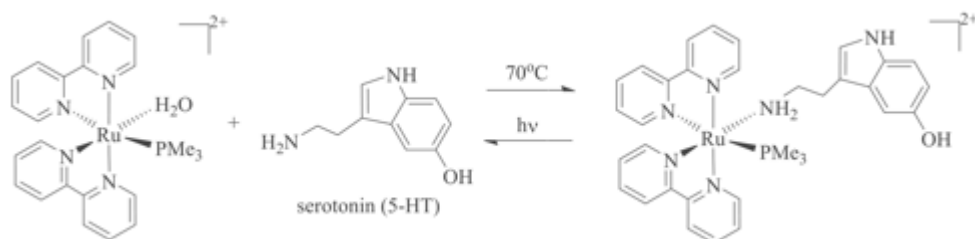


Figure 6.1. Coordination reaction schematic. Coordination reaction between serotonin and $[\text{Ru}(\text{bpy})_2(\text{PMe}_3)(\text{H}_2\text{O})]^{2+}$ (forward) and the clean, one step photorelease reaction (reverse) releasing serotonin upon light absorption.

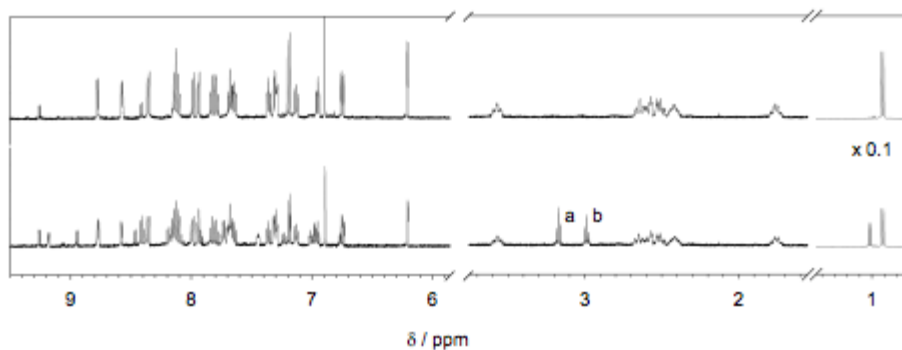


Figure 6.2. $^1\text{H-NMR}$ spectra of a 5 mg/mL solution of $[\text{Ru}(\text{bpy})_2(\text{PMe}_3)(5\text{HT})]\text{Cl}$ in D_2O before irradiation (upper trace); and after 60 s irradiation with 525 nm Green LED inside the NMR tube (lower trace). Note that after irradiation appear the triplets a and b, characteristics of free serotonin.

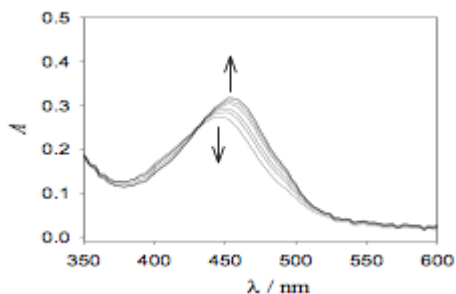


Figure 6.3. Subset of UV-Vis spectra of $[\text{Ru}(\text{bpy})_2(\text{PMe}_3)(5\text{HT})]^{2+}$ acquired in aqueous solution at $\text{pH}=7$ while irradiating with a 405 nm laser diode. The arrows indicate photolysis progress.

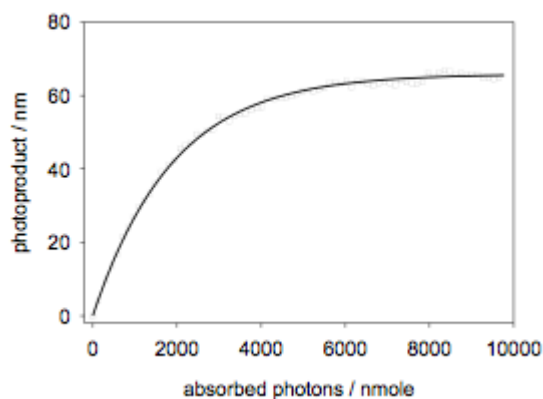


Figure 6.4 Progression of the UV-Vis spectra during a photolysis reaction against absorbed photons. The continuous line is the theoretical fit according to equation 1.

The initial slope of the curve represents the quantum yield $\text{PD} = 0.034$.

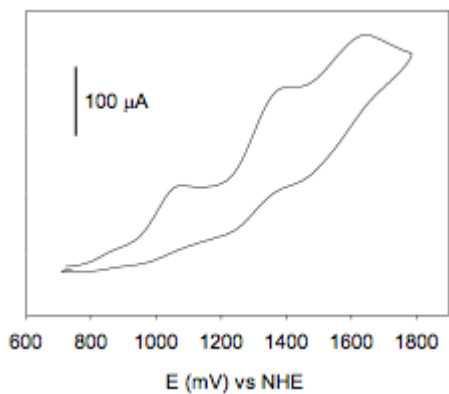


Figure 6.5. Cyclic voltammogram of $[\text{Ru}(\text{bpy})_2\text{PMe}_3(5\text{HT})]^+2$ recorded in acetonitrile at 100 mV/s on Pt wire electrode in CH_3CN containing 100 mM TBAPF6 as supporting electrolyte.

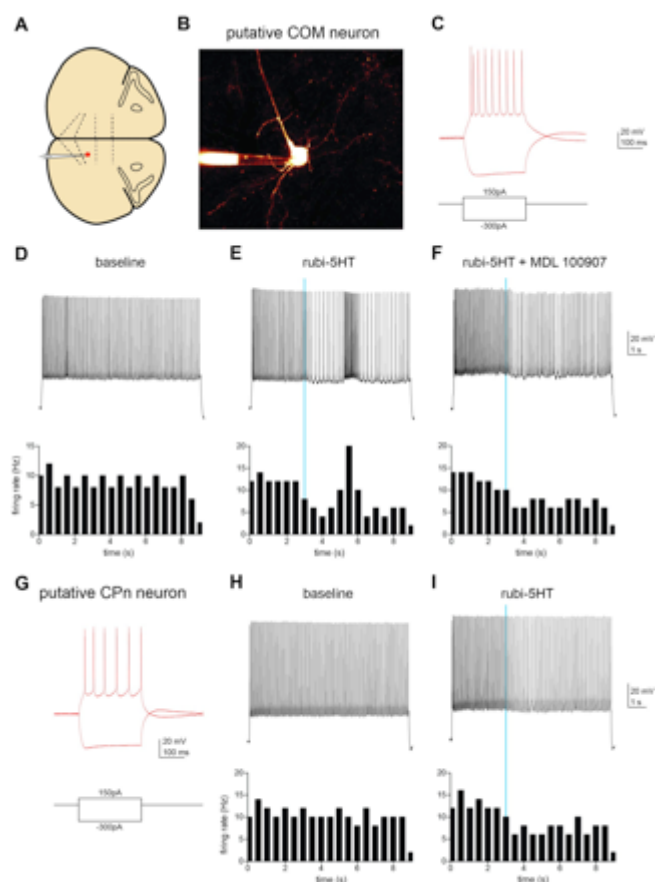


Figure 6.6. Validation of Ruby-5HT in mouse cortical neurons. A) Schematic indicating location of recorded neurons in coronal slice from mPFC of mouse. B) Two-photon z-stack image of recorded neuron filled with Alexa-594. C) Voltage responses of putative CPn neuron to hyperpolarizing and depolarizing current steps. D-F) A depolarizing current step was delivered to the CPn neuron to elicit spiking. Top: Firing of CPn neuron at baseline (D), using a pulse of blue light (470nm, 5ms, 3.6mW) to release 5HT (E), and with 5HT uncaging in the presence of a specific 5HT_{2A} receptor antagonist (1 μ M MDL100907, F). Bottom: Peristimulus time histograms of firing rate of the neuron in 200ms bins. G) Voltage responses of putative COM neuron to hyperpolarizing and depolarizing current steps. H-I) Top: Firing of COM neuron at baseline (H) and with uncaging of 5HT (I). Bottom: Peristimulus time histograms of firing rate of the neuron in 200ms bins.

6.7 REFERENCES

- [1] S.R. Adam, J.P. Kao, Y. Grynkiewicz, G.A. Minta, R.Y. Tsien, (1988) Biologically useful chelators that release Ca²⁺ upon illumination, *J. Am. Chem. Soc.* 110 3212–3220.
- [2] A. Barth, J.E. Corrie, (2002) Characterization of a new caged proton capable of inducing large pH jumps, *Biophys. J.* 83 2864–2871.
- [3] O. Filevich, G. Carrone, V. Andino Pavlovsky, R. Etchenique, (2012) Fast Optical pH Manipulation and Imaging, *Anal. Chem.* 84 5618–5624.
- [4] G.C.R. Ellis-Davies, M.Matsuzaki, M.Paukert, H.Kasai, D.E. Bergles, (2007) 4-Carboxymethoxy-5,7-Dinitroindoliny-Glu: An Improved Caged Glutamate for Expeditious Ultraviolet and Two-Photon Photolysis in Brain Slices, *J Neurosci.*, 20;27(25) 6601-6604.
- [5] V.N. Belov, C.A. Wurm, V.P. Boyarskiy, S. Jakobs, S.W. Hell, (2010) *Angew. Chem. Int. Ed.* 49 3520 –3523.

- [6] J. del Marmol, O. Filevich, R. Etchenique, (2010) A Ruthenium-Rhodamine Complex as an Activatable Fluorescent Probe, *Anal. Chem.* 82 6259–6264.
- [7] O. Filevich, M. Salierno, R. Etchenique, (2010) A caged nicotine with nanosecond range kinetics and visible light sensitivity, *J. Inorg. Biochem.* 104 1248–1251.
- [8] K. Hayashi, K. Hashimoto, N. Kusaka, A. Yamazoe, H. Fukaki, M. Tasaka, H. Nozaki, (2006) Caged gene-inducer spatially and temporally controls gene expression and plant development in transgenic Arabidopsis plant, *Bioorg. Med. Chem. Lett.* 16 2470–2474.
- [9] D.D. Young, A. Deiters, (2007) Photochemical Activation of Protein Expression in Bacterial Cells, *Angew. Chem. Int. Ed.* 46 4290–4292.
- [10] I.A. Shestopalov, S. Sinha, J.K. Chen, (2007) Light-controlled gene silencing in zebrafish embryos, *Nat. Chem. Biol.* 3 650–651.
- [11] C. Chou, A. Deiters, (2011) Light-Activated Gene Editing with a Photocaged Zinc-Finger Nuclease, *Angew. Chem. Int. Ed.* 50 6839–6842.
- [12] G. Mayer, A. Heckel, (2006) Biologically active molecules with a “light switch”, *Angew. Chem. Int. Ed.* 45 4900–4921.
- [13] A. Patchornik, B. Amit, R.B. Woodward, (1970) Photosensitive protecting groups, *J. Am. Chem. Soc.* 92 6333–6335.
- [14] R. Wieboldt, K.R. Gee, L. Niu, D. Ramesh, B.K. Carpenter, G.P. Hess, (1994) Photolabile precursors of glutamate: synthesis, photochemical properties, and activation of glutamate receptors on a microsecond time scale, *Proc. Natl Acad. Sci. U S A*, 13; 91(19) 8752–8756.
- [15] M. Canepari, L. Nelson, G. Papageorgiou, J.E.T. Corrie, D. Ogden, (2001) Photochemical and pharmacological evaluation of 7-nitroindolinyland 4-methoxy-7-nitroindolinyl-amino acids as novel, fast caged neurotransmitters, *Journal of Neuroscience Methods* 112 29–42.
- [16] N. Senda, A. Momotake, T. Arai, (2007) Synthesis and Photocleavage of 7-[[Bis(carboxymethyl)amino]coumarin-4-yl]methyl-Caged Neurotransmitters. *Bull. Chem. Soc. Jpn.* , 80, 12 , 2384-2388.
- [17] M. Salierno, E. Marceca, D.S. Peterka, R. Yuste, R. Etchenique, (2010) A fast ruthenium polypyridine cage complex photoreleases glutamate with visible or IR light in one and two photon regimes, *J. Inorg. Biochem.* 104 418-422.

- [18] E.M. Rial Verde, L. Zayat, R. Etchenique, R. Yuste, (2008) Photorelease of GABA with visible light using an inorganic caging group, *Front. Neural Circuits* 2:2.
- [19] X. Yang, D.L. Rode, D.S. Peterka, R. Yuste, S.M. Rothman, (2012) Optical control of focal epilepsy in vivo with caged γ -aminobutyric acid, *Ann Neurol.* 71,1 68-75.
- [20] J. R. Chalifoux, A. G. Carter, (2011) GABAB Receptor Modulation of Voltage-Sensitive Calcium Channels in Spines and Dendrites, *The Journal of Neuroscience*, 31, 11 4221-4232.
- [21] V. Nikolenko, R. Yuste, L. Zayat, L.M. Baraldo, R. Etchenique, (2005) Two-photon uncaging of neurochemicals using inorganic metal complexes, *Chem. Comm.* 1572–1574.
- [22] E. Fino, R. Araya, D.S. Peterka, M. Salierno, R. Etchenique, R. Yuste, (2009) RuBi-Glutamate: two-photon and visible-light photoactivation of neurons and dendritic spines, *Front. Neural Circuits* 3:2.
- [23] R. Araya, V. Andino-Pavlovsky, R. Yuste, R. Etchenique, (2013) Two-Photon Optical Interrogation of Individual Dendritic Spines with Caged Dopamine, *ACS Chem. Neurosci.*, 4,8 1163–1167.
- [24] K.E. Poskanzer, R. Yuste (2011) Astrocytic regulation of cortical UP states, *PNAS*, 108,18453–18458.
- [25] R. N. Garner, J.C. Gallucci, K. R. Dunbar and C. Turro (2011) [Ru(bpy)₂(5-cyanouracil)₂]²⁺ as a Potential Light-Activated Dual-Action Therapeutic Agent, *Inorg. Chem.* 50, 9213–9215
- [26] J. D. Knoll, C. Turro (2015) Control and Utilization of Ruthenium and Rhodium Metal Complex Excited States for Photoactivated Cancer Therapy *Coord. Chem. Rev.* 282–283, 110– 126.
- [27] A. Bahreman, J.A. Cuello-Garibo and S. Bonnet (2014) Yellow-light sensitization of a ligand photosubstitution reaction in a ruthenium polypyridyl complex covalently bound to a rhodamine dye. *Dalton Trans.* 43, 4494-4505.
- [28] Z.N. da Rocha, M.S. Marchesi, J.C. Molin, C.N. Lunardi, K.M. Miranda, L.M. Bendhack, P. C. Ford, R. S. da Silva (2008).The inducing NO-vasodilation by chemical reduction of coordinated nitrite ion in cis-[Ru(NO)₂L(bpy)₂]⁺ complex. *Dalton Trans.* 4282-7.
- [29] L.P. Franco, S.A. Cicillini, J.C. Biazotto, M.A. Schiavon, A. Mikhailovsky, P. Burks, J. Garcia P.C. Ford, R.S. da Silva (2014) Photoreactivity of a quantum dot-ruthenium nitrosyl conjugate. *J Phys Chem A.*118: 12184-91

- [30] J.E. Bundell, (1984) Serotonin and appetite, *Neuropharmacology*, 23 1537–1551.
- [31] T.A. Pigott, S.M. Seay, (1999) A review of the efficacy of selective serotonin reuptake inhibitors in obsessive-compulsive disorder, *J. Clin. Psychiatry* 60 101–106.
- [32] R. Gillette, (2006) Evolution and Function in Serotonergic Systems, *Integr. Comp. Biol.* 46 838–846.
- [33] F. Palma-Cerda, C. Auger, D.J. Crawford, A.C.C. Hodgson, S.J. Reynolds, J. K. Cowell, K.A.D. Swift, O. Cais, L. Vyklicky, J.E.T. Corrie, D. Ogden, (2012) New caged neurotransmitter analogs selective for glutamate receptor sub-types based on methoxynitroindoline and nitrophenylethoxycarbonyl caging groups, *Neuropharmacology*, 63 624-634.
- [34] J. E. T. Corrie, A. Desantis, Y. Katayama, K. Khodakhah, J. B. Messenger, D. C. Ogden And D. R. Trentham, (1993) Postsynaptic Activation At The Squid Giant Synapse By Photolytic Release Of L-Glutamate From A 'Caged' L-Glutamate, *Journal of Physiology*, 465 1-8.
- [35] Vandenberg, L. N.; Blackiston, D. J.; Rea, A. C.; Dore, T. M.; Levin, M. (2014) Left-right patterning in *Xenopus* conjoined twin embryos requires serotonin signaling and gap junctions. *Int. J. Dev. Biol.* 58, 799-809.
- [36] Rea, A. C.; Vandenberg, L. N.; Ball, R. E.; Snouffer, A. A.; Hudson, A. G.; Zhu, Y.; McLain, D. E.; Johnston, L. L.; Lauderdale, J. D.; Levin, M.; Dore, T. M. (2013) Light Activated Serotonin for Exploring Its Action in Biological Systems. *Chem. Biol.* 20, 1536-1546.
- [37] Breitingner, H.-G. A.; Wieboldt, R.; Ramesh, D.; Carpenter, B. K.; Hess, G. P. (2000) Synthesis and Characterization of Photolabile Derivatives of Serotonin for Chemical Kinetic Investigations of the Serotonin 5-HT₃ Receptor. *Biochemistry* 39, 5500-5508.
- [38] Boahen, Y. O.; MacDonald, G. M. (2005) A concise approach to caged serotonin for Fourier transform infrared (FT-IR) difference photolysis studies. *J. Ghana Sci. Assoc.* 7, 54-59.
- [39] Zayat, L.; Salierno, M.; Etchenique, R. (2006) Ruthenium(II) Bipyridyl Complexes as Photolabile Caging Groups for Amines. *Inorg. Chem.* 45, 1728-1731.
- [40] McLain, D. E.; Rea, A. C.; Widegren, M. B.; Dore, T. M. (2015) Photoactivatable, biologically-relevant phenols with sensitivity toward 2-photon excitation. *Photochem. Photobiol. Sci.*, 14, 2141-2158.
- [41] Avesar, D., Gullledge, A.T., (2012). Selective serotonergic excitation of callosal projection neurons. *Front Neural Circuits* 6, 12.

- [42] Dembrow, N.C., Chitwood, R.A., Johnston, D., (2010). Projection-specific neuromodulation of medial prefrontal cortex neurons. *J. Neurosci.* 30, 16922–37.
- [43] D.V. Pinnick, B. Durham, (1984) Photosubstitution Reactions of Ru(bpy)₂XYn⁺ Complexes. *Inorg. Chem.*, 23 1440-1445.
- [44] O. Filevich, R. Etchenique, (2013) RuBiGABA-2: a hydrophilic caged GABA with long wavelength sensitivity, *Photochem. Photobiol. Sci.*, 12 1565-1570.
- [45] C. Viala, C. Coudret, (2006) An Expeditious Route to cis-Ru(bpy)₂Cl₂ (bpy: 2,2'-bipyridine) Using Carbohydrate as Reducers, *Inorg. Chim. Acta* 359 984–989.
- [46] Gee, S., Ellwood, I., Patel, T., Luongo, F., Deisseroth, K., Sohal, V.S., (2012). Synaptic activity unmasks dopamine D2 receptor modulation of a specific class of layer V pyramidal neurons in prefrontal cortex. *J. Neurosci.* 32, 4959–71.
- [47] Seong, H.J., Carter, A.G., (2012). D1 receptor modulation of action potential firing in a subpopulation of layer 5 pyramidal neurons in the prefrontal cortex. *J. Neurosci.* 32, 10516–21.

CHAPTER 7 CONCLUDING REMARKS

The work presented here provides critical new insight into the function of serotonergic modulation in the prefrontal microcircuit. In this dissertation, I thoroughly elucidated the effects of serotonin on subclasses of interneurons derived by the medial ganglionic eminence. Specifically, I found that 5HT produces distinct excitatory effects in fast-spiking interneurons (FSIs) that express parvalbumin (PV) but not somatostatin (SOM)-expressing interneurons. By reducing conductance through inward-rectifying potassium channels, 5HT increases the input resistance and membrane potential of FSIs (Chapter 2). Furthermore, these effects result in prolonged decay of synaptic potentials that promote temporal summation of and spiking in response to gamma-frequency synaptic inputs. Overall, this increase in FSI excitability causes FSIs to fire more in response to any input, overriding serotonergic presynaptic suppression of some inputs (Chapter 4). I further found that these effects increased gamma frequency inhibition in pyramidal neurons (Chapter 2) which could explain my observation that gamma frequency power was left unchanged while lower frequencies were suppressed *in vivo* (Chapter 5). Together, these findings suggest that 5HT may tip the prefrontal circuit to prefer gamma frequency inputs.

Furthermore, gamma frequency oscillations are associated with prefrontal behaviors such as cognitive flexibility (Cho et al., 2006, Cho et al., 2015). Here, I show preliminary evidence that eliciting serotonergic signaling in FSIs is able to increase FSI activity *in vivo* and rescue cognitive flexibility deficits in a mouse model of interneuron dysfunction that mimics many symptoms of schizophrenia (Chapter 5). This lends more

evidence to the idea that modulating interneuron function can regulate behavior and specifically points to FSI 5HT receptors as a promising target for pharmaceutical development.

Lastly, I characterize a role for prefrontal serotonin in mediating anxiety behavior. In Chapter 3, I discuss how serotonergic suppression of ventral hippocampal inputs onto excitatory pyramidal neurons via presynaptic 5HT1B receptors may reduce anxiety behavior. I also provide preliminary evidence that eliciting serotonergic signaling in FSIs could also reduce anxiety behavior (Chapter 5). Moreover, in both studies I observed a reduction in prefrontal theta frequency oscillatory power, a suggested biomarker of anxiety (Adhikari et al., 2011). Together, these studies suggest that prefrontal serotonin may attenuate anxiety through actions at many loci within the circuit.

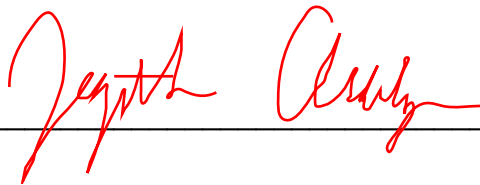
This work provides critical insight into the actions of serotonin in the prefrontal microcircuit and suggests potential roles in both behavior and disease. Many questions remain as to whether the effects discovered here are actually required for behaviors or disrupted in disease states. Future work should aim to knock out 5HT2A receptors specifically from prefrontal FSIs or 5HT1B receptors from presynaptic ventral hippocampal inputs and examine any changes in prefrontal oscillations and behavior. Furthermore, it would be interesting to study the effects described here in the context of other models of schizophrenia, depression, or anxiety. And finally, future work could examine whether psychiatric drugs (i.e. antipsychotics, antidepressants, anxiolytics) influence any of the effects described here. This work adds critical information to our knowledge of psychiatric illness and could play a role in the development of therapeutics.

Publishing Agreement

It is the policy of the University to encourage the distribution of all theses, dissertations, and manuscripts. Copies of all UCSF theses, dissertations, and manuscripts will be routed to the library via the Graduate Division. The library will make all theses, dissertations, and manuscripts accessible to the public and will preserve these to the best of their abilities, in perpetuity.

Please sign the following statement:

I hereby grant permission to the Graduate Division of the University of California, San Francisco to release copies of my thesis, dissertation, or manuscript to the Campus Library to provide access and preservation, in whole or in part, in perpetuity.



03/28/2018